10/6-14-95 OSTI

LBL-36807
UC-814

Lawrence Berkeley Laboratory
UNIVERSITY OF CALIFORNIA

EARTH SCIENCES DIVISION

Transient Dual-Porosity Simulations of Unsaturated Flow in Fractured Rocks

R.W. Zimmerman, T. Hadgu, and G.S. Bodvarsson

January 1995

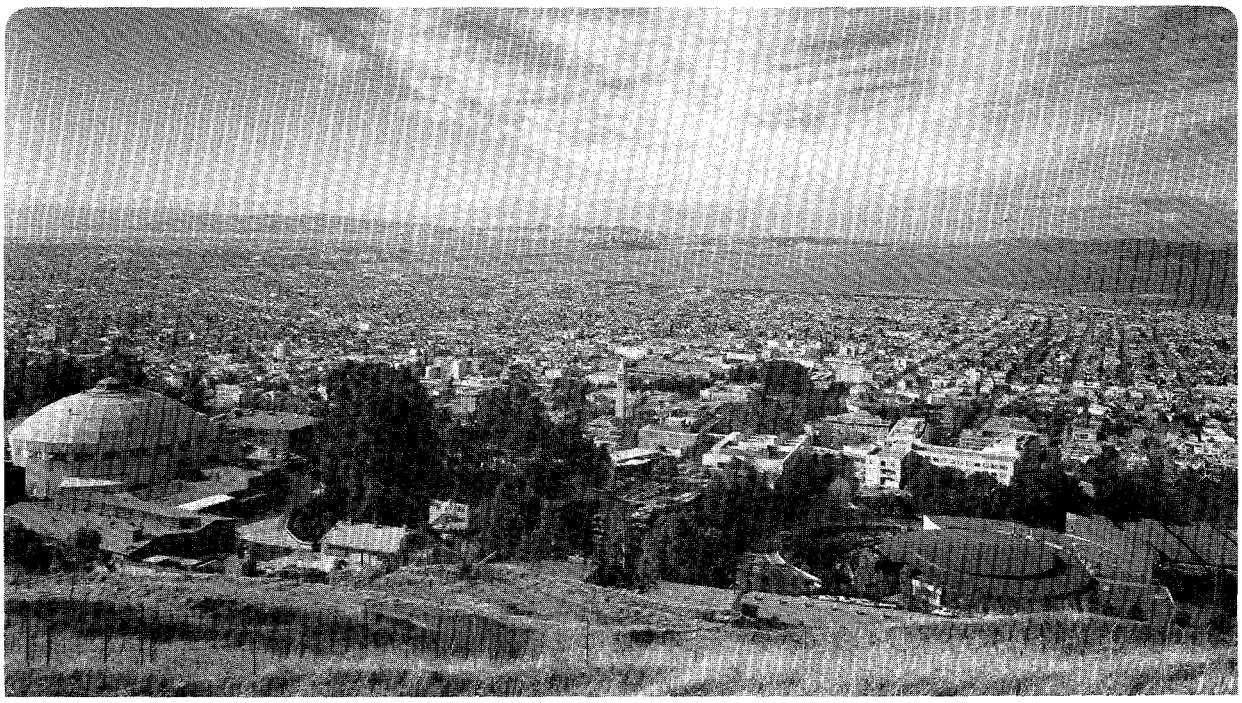

Prepared for the U.S. Department of Energy under Contract Number DE-AC03-76SF00098

Available to DOE and DOE Contractors
from the Office of Scientific and Technical Information
P.O. Box 62, Oak Ridge, TN 37831
Prices available from (615) 576-8401

Available to the public from the
National Technical Information Service
U.S. Department of Commerce
5285 Port Royal Road, Springfield, VA 22161

LBL-36807
UC-814

Transient Dual-Porosity Simulations of Unsaturated Flow in Fractured Rocks

Robert W. Zimmerman, Teklu Hadgu and Gudmundur S. Bodvarsson

Earth Sciences Division
Lawrence Berkeley Laboratory
University of California
Berkeley, CA 94720

January 1995

This work was carried out under Department of Energy Contract No. DE-AC03-76SF00098 for the Director, Office of Civilian Radioactive Waste Management, Office of Geologic Disposal, and was administered by the Nevada Operations Office, U. S. Department of Energy, in cooperation with the U. S. Geological Survey, Denver.

Transient Dual-Porosity Simulations of Unsaturated Flow in Fractured Rocks

Robert W. Zimmerman, Teklu Hadgu, and Gudmundur S. Bodvarsson

Earth Sciences Division
Lawrence Berkeley Laboratory
University of California
Berkeley, CA 94720

ABSTRACT

This report describes the development and use of a semi-analytical dual-porosity simulator for unsaturated flow in fractured rock masses. Fluid flow between the fracture network and the matrix blocks is described by a nonlinear equation that relates the imbibition rate to the local difference in liquid-phase pressure between the fractures and the matrix blocks. This equation is a generalization of the Warren-Root equation, but is accurate in both early and late time regimes. The fracture/matrix interflow equation has been incorporated into a computational module that acts as a source/sink term for fracture elements; this module is compatible with the unsaturated flow simulator TOUGH. Flow processes are then simulated using only fracture elements in the computational grid. This semi-analytical dual-porosity module has been tested with TOUGH on various problems involving transient flow in fractured/porous media, and compared with simulations performed using explicit discretization of the matrix blocks. The new semi-analytical dual-porosity model accurately simulates flow processes in unsaturated fractured rocks, and typically requires an order of magnitude less computational time than do simulations using fully-discretized matrix blocks.

Introduction

Yucca Mountain, Nevada is being studied by the U. S. Department of Energy as a potential site for an underground radioactive waste repository (U.S. DOE, 1986). The geologic setting at Yucca Mountain consists mainly of volcanic tuff, some units of which are highly-fractured. The potential repository horizon is about 300 meters below the surface, and about 300 meters above the current mean location of the water table. One part of the process of characterizing the geological and hydrological system at Yucca Mountain is the development of methods for modeling and predicting the unsaturated flow of water in fractured rock masses having low matrix permeability. Such models will also be useful in assessing the travel-times required for radionuclides from the repository to reach the saturated zone below the water table.

For the analysis of certain aspects of the long-term hydrological behavior of Yucca Mountain, it is possible to treat the rock mass as a locally homogeneous porous medium. For quasi-steady-state behavior, the fractures and matrix blocks can be assumed to be in (local) equilibrium with each other, so that a single pressure (temperature, etc.) can be assigned to both the fractures and the matrix at each point in space. In order to study the highly transient flow processes that may occur after precipitation events, however, it is necessary to account for the fact that the flow actually occurs in two intermingled networks of porosity: a relatively high-permeability, low-storativity fracture network, and low-permeability, high-storativity matrix blocks. This is due to the fact that in a transient process, the fractures and matrix blocks will not always be in local thermodynamic equilibrium with each other. Existing unsaturated-flow simulators, such as TOUGH (Pruess, 1987), are capable of treating such dual-porosity systems if both the fracture system and matrix blocks are discretized. Numerical simulations of fully-discretized systems require a large number of computational cells, and consequently a large amount of computer time. We have attempted to mitigate these problems by developing a method in which flow between the fracture

network and matrix blocks is modeled in a lumped-parameter manner, by an ordinary differential equation, eliminating the need to discretize the matrix blocks. This method has been incorporated into a computational module that is compatible with TOUGH, and which allows dual-porosity simulations to be performed in a much more computationally efficient manner than would be possible using fully-discretized grids. This new method should therefore be useful in studying transient flow processes that may be expected to occur at Yucca Mountain.

Dual-Porosity Models

When modeling processes that occur on a sufficiently slow time scale, it is often assumed that a fractured rock mass can be treated as an equivalent porous medium. Peters and Klavetter (1988) developed a numerical model for unsaturated flow at Yucca Mountain in which the fractured rock mass was treated as an equivalent porous medium. The conditions under which such an approximation would be acceptable were also studied by Pruess et al. (1988). The equivalent porous medium that would be used in a model such as that of Peters and Klavetter (1988) will have an effective permeability and an effective capillary pressure function that are some sort of appropriate weighted averages of the corresponding properties for the fractures and the matrix blocks. This approach assumes that the matrix blocks are always in local thermodynamic equilibrium with their surrounding fractures, and is therefore only capable of simulating processes that occur slowly enough so that pressure equilibrium can be achieved between the fractures and matrix blocks. However, the time required for fracture/matrix equilibration is inversely related to the permeability of the matrix blocks, and is consequently large for a hydrologic system such as the fractured tuffs at Yucca Mountain. Numerical simulations of imbibition into blocks of Topopah Spring tuff have shown (Zimmerman et al., 1990) that the equilibration time will be on the order of days to years, depending on the type of rock and the fracture spacing. A

more detailed discussion of this equilibration time, along with numerical examples for various of the geological units at Yucca Mountain, is given in Appendix C. For highly-transient processes, such as the infiltration that would occur after a precipitation event, the ''dual-porosity'' nature of the rock mass must therefore be accounted for.

In a dual-porosity medium, the fractures provide most of the permeability, whereas most of the fluid storage takes place in the relatively low-permeability matrix blocks (Duguid and Lee, 1977; Douglas and Arbogast, 1990). The complex behavior of dual-porosity systems arises from the fact that there are different time scales corresponding to diffusion of water in the fracture network and in the matrix blocks. These time regimes have been defined and delineated by Nitao and Buscheck (1989,1991) in their analytical and numerical studies of infiltration into a system consisting of parallel, periodically-spaced fractures. In principle, one way to model flow in a fractured/porous rock mass would be to explicitly account for each fracture and each matrix block in the computational mesh. In practice, however, this is rarely possible, due to the inordinately large number of gridblocks that would be needed. For example, assuming a fracture spacing of about 20 cm (Wang and Narasimhan, 1985), the total number of fractures in the vicinity of the potential repository at Yucca Mountain can readily be estimated to be on the order of 10^9. Another difficulty is that sufficient geological information concerning the locations, lengths, and other properties of the fractures would rarely be available on a large scale. On the other hand, laboratory-scale rock blocks whose lengths are on the order of 1 m may contain a manageable number of fractures, in which case explicit modeling of each fracture may be feasible.

A commonly used conceptual model of a dual-porosity system assumes the existence of two overlapping continua, the fracture continuum and the matrix continuum. Flow is assumed to take place not only through the fractures, but also between the fractures and the matrix blocks. This type of model was originated by Barenblatt

et al. (1960) for saturated flow in aquifers, and by Warren and Root (1963) for single-phase flow in oil reservoirs. Each point in space has associated with it a pair of pressures, representing the local fluid pressure in the fractures, and a mean fluid pressure in the matrix block. This is equivalent to treating the matrix block in a lumped-parameter manner. Barenblatt et al. (1960) and Warren and Root (1963) were originally interested in the development of analytical solutions to problems in dual-porosity reservoirs. Hence, in order to maintain the linearity of the equations, they assumed that the volumetric flow rate of fluid from the fractures into the matrix blocks, per unit volume of matrix block, was governed by the following linear expression, which is often referred to as the Warren-Root coupling equation:

$$q = \frac{\alpha k_m V_m}{\mu}(P_f - \bar{P}_m), \tag{1}$$

where k_m is the permeability of the matrix block, with dimensions of $[L^2]$; μ is the viscosity of the fluid, with dimensions of [PT]; P_f is the local pressure in the fractures, with dimensions of [P]; $\bar{P}_m$ is the mean pressure in the matrix block at a specified point in the fracture continuum, and also has dimensions of [P]; V_m is the volume of the matrix block, with dimensions of $[L^3]$; and α is a geometric factor with dimensions of $[L^{-2}]$. The flowrate q therefore has dimensions of $[L^3T^{-1}]$. The relationship between the numerical value of α and the size and shape of the matrix block is discussed by deSwaan (1990) and Zimmerman et al. (1993), and, for convenience, in Appendix D. (When giving the dimensions of variables, we will use M for mass, L for length, T for time, and P for pressure. Although pressure is not a fundamental dimension, but in fact has dimensions of $[ML^{-2}T^{-1}]$, its frequent occurrence makes it convenient to use M, L, T, and P when expressing the dimensions of physical variables.)

The flow of fluid into the matrix block causes the fluid pressure in the block to increase. If the fluid is a slightly-compressible liquid, this pressure increase is described by the following equation, within the context of a lumped-parameter approach:

$$\phi_m c_m V_m \frac{d\bar{P}_m}{dt} = q \,, \tag{2}$$

where ϕ_m is the (dimensionless) porosity of the matrix block, and c_m, with dimensions of $[P^{-1}]$, is the combined compressibility of the pore fluid and the pore space of the matrix blocks. If eqs. (1) and (2) are combined, they yield the following equation that governs the fluid pressure in the matrix block:

$$\frac{d\bar{P}_m}{dt} = \frac{\alpha k_m}{\phi_m \mu c_m} (P_f - \bar{P}_m). \tag{3}$$

The combination of terms $k_m/\phi_m \mu c_m$ is often referred to as the hydraulic diffusivity (Matthews and Russell, 1967). Since k_m has dimensions of $[L^2]$, c has dimensions of $[P^{-1}]$, μ has dimensions of [PT], and ϕ is dimensionless, the diffusivity has dimensions of $[L^2 T^{-1}]$. We can re-write eq. (3) in terms of the diffusivity to arrive at

$$\frac{d\bar{P}_m}{dt} = \alpha D_m (P_f - \bar{P}_m), \tag{4}$$

where $D_m = k_m/\phi_m \mu c_m$.

For saturated flow into a matrix block, eq. (4) can be interpreted as representing the most-slowly-decaying Fourier mode in the exact solution for infiltration into a

matrix block (see Zimmerman et al., 1993; also Appendix D). As such, it correctly predicts the relaxation time needed for the matrix block to equilibrate with the surrounding fractures. However, as it does not contain any of the higher modes, it is not accurate at earlier stages of imbibition. Consider the case where a step-function increase in the fracture pressure occurs at $t = 0$. The imbibition rate will initially be proportional to $t^{-1/2}$, where t is the elapsed time (Crank, 1975, p. 91). The Warren-Root equation, however, predicts that the early-time imbibition rate is constant. The cause of this error can be explained as follows. The Warren-Root approach assumes that any fluid that enters the matrix block is instantaneously distributed uniformly throughout it. Therefore, at early times, after a small amount of fluid has entered the block, the average pressure $\bar{P}_m$ is still essentially unchanged. Hence, the right-hand side of eq. (1) remains nearly constant, and so the predicted flux rate is also nearly constant. More generally, regardless of how the fracture pressure varies with time, the matrix pressure predicted by the Warren-Root equation will be grossly incorrect at early times (see deSwaan, 1990; Zimmerman et al., 1993). When incorporated into a dual-porosity model, the Warren-Root equation leads to qualitatively incorrect behavior during the transition between fracture-dominated and effective-continuum flow regimes (Najurieta, 1980; Streltsova, 1983).

One way to improve upon the poor accuracy of a Warren-Root-type fracture/matrix coupling equation would be to treat the internal flow in the matrix block numerically, by discretizing each matrix block into a nested series of gridblocks. This allows the pressure gradients inside the matrix block to be resolved on a finer scale. Since the pressure gradient at the outer boundary of the block is inversely proportional to the depth to which the pressure front has penetrated, discretization of the matrix allows the calculated penetration depth to increase with time, thereby correctly predicting that the imbibition rate decreases with t. One such dual-porosity model, in which the matrix is discretized into concentric shells, is known as the MINC method

(Multiple INteracting Continua; Pruess and Narasimhan, 1985). In practice, the computational fracture gridblocks are typically much larger than the typical matrix block. Hence, each fracture gridblock is associated with a hypothetical set of nested matrix blocks that do not have the same dimensions as the actual matrix blocks. However, the volumes, areas, and nodal point distances of the gridblocks can be scaled so as to accurately model flow in the actual matrix blocks. MINC-type simulations require many fewer computational cells than do discrete-fracture simulations that utilize actual-size matrix blocks, but still require large numbers of matrix gridblocks. For the types of problems discussed in this report, we have found that accurate treatment of transient effects with the MINC method requires that the representative matrix block associated with each fracture gridblock must be broken up into about ten nested grid blocks. MINC simulations of transient processes may therefore be expected to require about eleven times the number of computational cells needed for quasi-steady-state equivalent porous medium simulations having the same macroscopic resolution. Since the CPU time required by most numerical simulators grows at a rate at least directly proportional to the number of computational cells, MINC-type simulation of large-scale transient processes in fractured rocks can become computationally burdensome.

Our intention has been to find a method of simulating unsaturated flow in fractured rocks that combines, in a sense, the computational efficiency of a Warren-Root-type model, in which the matrix blocks do not need to be discretized, with the accuracy of the MINC method. In order to do this, the following steps had to be taken. First, it was necessary to find the unsaturated flow parameters that are analogous to the hydraulic diffusivity that appears in eq. (4). Secondly, it was necessary to find a way to modify eq. (4) so as to be applicable to all time regimes of the imbibition process. Finally, a method was needed to relate the parameter α to the geometric properties of the matrix blocks. These developments are discussed in the next section of this report. The final result of this analysis is a differential equation that predicts the rate of fluid

exchange between fractures and matrix blocks, and which can be used as a source/sink term for fracture elements in a numerical simulator.

Several other dual-porosity models have been developed in recent years for unsaturated flow, with the aim of eliminating the need for explicit fine-scale discretization of the matrix blocks. In each case, the fracture/matrix coupling equation was essentially taken to be of the Warren-Root form, in that the volumetric rate of flux depends linearly of the difference between the fracture potential and the mean potential in the matrix block. In the code DCM3D (Updegraff et al., 1991), the fracture network and matrix rock were assumed to behave as two interpenetrated continua, each governed by a macroscopic pressure diffusion equation. The source/sink terms for the two continua were assumed to be equal in magnitude, but opposite in sign. The rate of fracture/matrix interflow was assumed to be proportional to the difference in potential between the fracture and matrix continua, as in eq. (1), with the nonlinearity of the unsaturated flow process accounted for by multiplying k_m by the relative permeability function of the matrix rock. Gerke and van Genuchten (1993) also modeled the fracture/matrix interflow with a Warren-Root-type differential equation, and allowed the effective diffusivity to vary from one timestep to the next, in response to changes in saturation, etc. Their model also allows for flow between matrix blocks, which is not currently included in our model. However, due to the inherent limitations of the Warren-Root approach, their predicted fracture/matrix fluxes are not accurate at all time scales (see their Fig. 2).

A different approach to the problem of accounting for fracture/matrix leakage in a semi-analytical fashion was taken by Pruess and Wu (1993), who approximated the pressure profile in the matrix blocks by a polynomial that was damped by an exponential term. The exponential damping factor was taken to have the form $\exp(-x/\sqrt{4D_m t})$, where x is the distance from the outer boundary of the block. The coefficients of the polynomial were found, at each timestep, by requiring the approximate pressure profile

to satisfy the governing equation in an integrated sense over the entire matrix block, and point-wise at the outer boundary. The calculation of the fracture/matrix interflow is thereby reduced to a small number of algebraic calculations at each timestep. Their approach has been used successfully for saturated flow and heat conduction, but has not yet been applied to unsaturated flow.

Finally, we mention that, for mathematically linear processes such as saturated flow, the fracture/matrix interaction term can be found *exactly* by utilizing a convolution integral, as was done by Elsworth (1989). A drawback of this approach is that it at each timestep the convolution integral must be evaluated from $t=0$ to the current time t. Consequently, all previous values of $\bar{P}_m$ must be saved, in order to carry out the convolution integrals. These factors tend to be at variance with the goal of minimizing the amount of computational effort, and computer memory, required to simulate flow in a dual-porosity system.

Fracture/Matrix Flow Interaction Equation

In principle, fluid flow in a two-component air/water system would be governed by a pair of equations, representing conservation of mass for water and air, respectively (see Appendix E). However, it is common to assume that the low viscosity of the air renders it effectively ''infinitely mobile''. In this case the air pressure is always uniform (aside from gravitational gradients, which are small for air), and the two conservation equations decouple from each other. In this approach, only the water-balance equation is used. If Darcy's law, modified by a relative permeability function, is used in conjunction with the conservation of mass equation, we arrive at the Richards equation (Richards, 1931; Hillel, 1980, p. 203):

$$\frac{\partial}{\partial x}\left[\frac{k k_r(\psi)}{\mu}\,\frac{\partial \psi(x,t)}{\partial x}\right] = \phi \frac{\partial S(x,t)}{\partial t}\,. \tag{5}$$

In eq. (5), ψ represents the "capillary potential" or "matric potential" of the water in the matrix block, which has dimensions of [P]. This potential is measured relative to the pressure in the air phase, i.e., $\psi = \psi_w - \psi_a$, where the subscripts w and a denote water and air, respectively. In regions of full liquid saturation ψ is positive, but in regions of partial saturation it is negative (see Hillel, 1980, p. 141). The saturation S, which is dimensionless, represents the fraction of pore space that is filled with water. S and ψ are related through the capillary pressure relation, the precise form of which depends on rock type; forms of this function that have been used to describe the behavior of volcanic tuffs are described below. The parameter k, which has dimensions of $[L^2]$, is the permeability of the rock matrix under fully-saturated conditions; μ, with dimensions of [PT], is the viscosity of the pore water; and ϕ, which is dimensionless, is the porosity of the rock matrix. $k_r(\psi)$ is the dimensionless relative permeability function, which quantifies the decrease in the permeability to water due to the fact that some of the pores are occupied by air; it is typically a strongly increasing function of S.

Aside from assumption that the air phase is always at uniform pressure, there are various other assumptions and simplifications used in eq. (5). The porosity is assumed to be independent of the potential, which is equivalent to ignoring the compressibility of the rock matrix. For tuffs in the unsaturated zone, this assumption is acceptable (see Peters and Klavetter, 1988), since the capacitance associated with the change in saturation is much larger than that associated with expansion of the pore space. Most rocks and soils are hysteretic with regards to capillary pressure, which means that the $S(\psi)$ relationship depends on whether drainage or imbibition is occurring, and on the past saturation history of the rock (see Niemi and Bodvarsson, 1988). For many of the processes of interest with regards to the hydrological behavior of Yucca Mountain, the saturation varies monotonically, and so hysteresis can be ignored. Hence, we assume that S is a single-valued function of ψ, with no dependence on past values. Eq. (5)

also assumes that as the liquid water imbibes into the matrix, it is not impeded by the air that is initially in place. This assumption is known to be correct for flow into an unbounded medium, since the air can escape ahead of the advancing liquid front. For flow that is assumed to be entering a finite-sized matrix block, it has been thought that air might be trapped in a pocket at the center of the block, thus impeding the imbibition of water. Studies of this and related air-impedance effects have been conducted by Wilson and Luthin (1963), Youngs and Peck (1964), Adrian and Franzini (1966), Phuc and Morel-Seytoux (1972), Touma and Vauclin (1986), and Constantz et al. (1988). This issue is addressed to some extent in Appendix E.

Eq. (5) also neglects gravity, which otherwise would cause an additional potential term $\rho g z$ to be added to the pressure potential ψ. Roughly speaking, gravity can be neglected if the matrix block sizes are smaller than the so-called "sorptive length" of the rock material. If this condition holds, then the gravitational gradient will be negligible compared to the capillary pressure gradient. To understand this criterion, consider a matrix block whose characteristic length is L. The potential difference between the matrix block and the adjacent fractures will be on the order of ψ_a, which is the characteristic potential that appears in the capillary pressure function, and so the magnitude of the pressure gradient will be on the order of $|\psi_a|/L$. The gravitational gradient is always ρg, where ρ is the density of the liquid, and g is the gravitational acceleration. Hence, the criterion for the gravitational gradient to be negligible is $\rho g \ll |\psi_a|/L$, which can be written as

$$L \ll \frac{|\psi_a|}{\rho g} = L_s . \tag{6}$$

The term $|\psi_a|/\rho g$ is defined as the sorptive length, and denoted by L_s. Using hydrological parameters believed to be appropriate for the Topopah Spring welded tuffs at

Yucca Mountain, and a more precise definition of sorptive length due to Philip (1987), Zimmerman et al. (1990) found a sorptive length of about 8 m. This means that gravity can be ignored in any matrix block whose diameter is much less than 8 m. Since fracture spacings in the Topopah Spring unit are thought to be on the order of tens of centimeters (Wang and Narasimhan, 1985), imbibition into matrix blocks will be dominated by capillary forces. Estimated sorptive lengths for some of the geological units at Yucca Mountain are given in Appendix B.

Each rock has its own set of ''characteristic functions'' that describe the relationships between S, ψ and k_r. Two sets of characteristic functions that are often used in modeling the hydraulic behavior of the volcanic tuffs at Yucca Mountain are those proposed by Brooks and Corey (1966), and Mualem (1976) and van Genuchten (1980). Although these two models use different equations for the two characteristic functions, the imbibition rates that result for the two cases are not very different, since imbibition rates are insensitive to the precise details of the characteristic curves. In Appendix F it is shown that if the parameters in the two models are chosen so as to have the $S(\psi)$ curves asymptotically coincide at low saturations, the resulting imbibition rates are nearly indistinguishable. Our dual-porosity model has therefore been developed under the assumption that the matrix blocks can be described by the van Genuchten characteristic curves, which are given by the following equations:

$$S(\psi) = S_r + (S_s - S_r)[1 + (\psi/\psi_a)^n]^{-m} \ , \tag{7}$$

$$k_r(\psi) = \frac{\{1 - (\psi/\psi_a)^{n-1}[1 + (\psi/\psi_a)^n]^{-m}\}^2}{[1 + (\psi/\psi_a)^n]^{m/2}} \ , \tag{8}$$

where ψ_a is a characteristic potential that has dimensions of [P], and m and n are

dimensionless parameters that are related by $m = 1 - 1/n$. The characteristic potential ψ_a is, in some rough sense, inversely proportional to the mean pore size of the rock. The parameter n is inversely related to the broadness of the pore-size distribution, in the sense that smaller values of n are associated with broader distributions, and vice versa. Although van Genuchten (1980) originally implied that n could in principle take on any value greater than 1, it has subsequently been argued on theoretical grounds by Fuentes et al. (1991) that n cannot be less than 2. Although soils often have values of n on the order of 6-12 (van Genuchten, 1980), the characteristic curves of Yucca Mountain tuffs tend to have very low values of n, in many cases $1 < n < 2$ (Rulon et al., 1986; Peters and Klavetter, 1988). This discrepancy can probably be explained by the fact that the experimental values of n are found from data taken at intermediate saturations, whereas the criterion $n > 2$ follows from considerations of the low saturation regime. S_r is the dimensionless residual water saturation, which is the value of S at which the liquid phase becomes immobile. S_s, which is usually very close to 1.0, is the saturation at which the matric potential goes to zero. Eqs. (7) and (8) express the saturation and the relative permeability as functions of the capillary potential. It is sometimes convenient to use the saturation as the independent variable, in which case the two characteristic functions would be written as

$$\psi(S) = \psi_a(\hat{S}^{-1/m} - 1)^{1/n} \quad , \tag{9}$$

$$k_r(S) = \hat{S}^{1/2}[1 - (1 - \hat{S}^{1/m})^m]^2 , \tag{10}$$

where $\hat{S} = (S - S_r)/(S_s - S_r)$ is the normalized saturation. Normalized characteristic curves for various values of n are shown in Figs. 1-3, using different combinations of independent and dependent variables. The relative permeability in each case drops off

monotonically with decreasing liquid saturation, although it does so more rapidly for larger values of n. The capillary pressure function varies rapidly at high and low saturations (i.e., near S_s and near S_r), and varies less drastically in the intermediate region.

Eq. (5) is essentially a nonlinear diffusion equation (see Brutsaert, 1976), with the conductance and capacitance related to the characteristic functions $k_r(\psi)$ and $S(\psi)$. This can be seen by using the chain rule to relate $\partial\psi/\partial x$ to $\partial S/\partial x$, and treating S as the independent variable, which leads to

$$\frac{\partial}{\partial x}\left[\frac{kk_r(S)}{\mu}\frac{d\psi}{dS}\frac{\partial S(x,t)}{\partial x}\right] = \phi\frac{\partial S(x,t)}{\partial t}\,. \tag{11}$$

This equation is now precisely in the form of a diffusion equation, with the combination of terms $kk_r(S)\psi'(S)/\mu\phi$ playing the role of a diffusion coefficient (see Hillel, 1980, p. 205), i.e.,

$$D(S) = \frac{kk_r(S)}{\mu\phi}\frac{d\psi}{dS}\,. \tag{12}$$

Since the diffusion coefficient varies with S, eq. (11) is typically very nonlinear, and in general cannot be solved in closed-form.

The governing differential equation (11) must be augmented by the appropriate boundary conditions and initial conditions in order to constitute a well-posed mathematical problem. Initially, the rock is at some partial saturation S_i, which corresponds through eq. (9) to some potential $\psi_i < 0$. At time $t = 0$ the potential at the $x = 0$ boundary of the block is raised to, say, $\psi = 0$. Mathematically, these conditions can be expressed as

$$\psi(x, t=0) = \psi_i \,, \tag{13}$$

$$\psi(x=0, t>0) = 0 \,, \tag{14}$$

$$\lim_{x\to\infty} \psi(x, t) = \psi_i \,. \tag{15}$$

The final condition, (15), expresses the fact that at any fixed time, the saturation must approach S_i infinitely far from the wetted boundary. In other words, the wetting front cannot travel infinitely far into the rock in a finite amount of time. In principle, eqs. (11-15) can be solved to find the potential profile $\psi(x,t)$. From this solution, the imbibition rate can be found by applying Darcy's law at the boundary:

$$q = -\frac{kA}{\mu}\left[\frac{\partial \psi}{\partial x}\right]_{x=0} . \tag{16}$$

As the dimensions of both k and A are $[L^2]$, the dimensions of μ are [PT], and the dimensions of $\partial\psi/\partial x$ are $[PT^{-1}]$, the flowrate q has dimensions of $[L^3T^{-1}]$.

Due to the mathematical structure of the governing equation (11), which contains one derivative with respect to t and two with respect to x, it can be shown (Bruce and Klute, 1956; Gardner and Mayhugh, 1958; see also Appendix A) that the imbibition rate at the boundary will always be proportional to $t^{-1/2}$, regardless of the precise details of the hydraulic diffusivity function. This fact led Philip (1955) to define the sorptivity σ by

$$q = \frac{A\sigma}{2t^{1/2}} \,, \tag{17}$$

where A is the wetted outer area of the block. The factor 2 is included so that the cumulative imbibition, which is obtained by integrating q with respect to t, is given by $Q = A\,\sigma t^{1/2}$. The sorptivity has dimensions of $[LT^{-1/2}]$, which corresponds to the square root of the dimensions of the diffusivity. If the diffusivity were independent of saturation, the sorptivity would be given exactly by (see Kutilek and Valentova, 1986)

$$\sigma = 2\phi(S_s - S_i)(D/\pi)^{1/2}. \tag{18}$$

For the case where the diffusivity varies with saturation, eq. (18) can be used to *define* the effective diffusivity, i.e.,

$$D_e = \frac{\pi\sigma^2}{4\phi^2(S_s - S_i)^2}. \tag{19}$$

Various methods have been proposed to estimate the sorptivities of unsaturated media, based on their characteristic functions. Many of the more commonly used methods are discussed by Kutilek and Valentova (1986) and Lockington (1993). Zimmerman and Bodvarsson (1989) used the Pohlhausen integral method (see Macey, 1959; Goodman, 1964) to find the following approximate expression for the sorptivity of a van Genuchten medium:

$$\sigma = \left[\frac{2nk\phi|\psi_a|(S_s - S_i)^{1+1/n}}{(n+1)\mu[m(S_s - S_r)]^{1/n}}\right]^{1/2}. \tag{20}$$

When compared with numerical solutions using the hydrological properties of the Topopah Spring welded tuff, this expression was found (Zimmerman and Bodvarsson,

1989) to have reasonable accuracy. Eq. (20) is in fact asymptotically accurate for large values of n, and for high initial saturations (see Zimmerman and Bodvarsson, 1991b), but it is not uniformly accurate over all ranges of possible conditions. Guided by the algebraic form of eq. (20), and utilizing numerical solutions of the Richards equation, it is possible to derive a much more accurate expression for the sorptivity. We start by rewriting eq. (20) in a more general form:

$$\sigma = \left[\frac{2k\phi|\psi_a|F(m)}{\mu(S_s - S_r)}\right]^{1/2}\left[\frac{S_s - S_i}{S_s - S_r}\right]^{\beta}, \tag{21}$$

where $F(m)$ is some function of m (or, equivalently, of n, since $m = 1 - 1/n$), and β is some parameter. These open functions/parameters can be found by fitting eq. (21) to numerically-computed sorptivities. The function $F(m)$ is found by fitting the numerically-computed sorptivities for an initial saturation of $S_i = S_r$. This procedure leads to the choice $F(m) = m^{4/3}$. By finding the best-fitting value of β at various values of m, and then performing a linear regression on the β–m pairs, we have found $\beta = 0.62 - 0.12m$. Hence, we arrive at the following expression for the sorptivity:

$$\sigma = \left[\frac{2m^{4/3}k\phi|\psi_a|}{\mu(S_s - S_r)}\right]^{1/2}\left[\frac{S_s - S_i}{S_s - S_r}\right]^{0.62 - 0.12m}. \tag{22}$$

The accuracy of eq. (22) can be tested by comparing its predictions to exact sorptivities found by direct integration of the Richards equation. This integration is performed by first transforming the Richards equation into a second-order ordinary differential equation, which is then written as a pair of first-order equations. These two equations are then solved using a fourth-order Runge-Kutta algorithm (see Press et al., 1992, pp. 704-708). This procedure is described in more detail in Appendix A. In

Fig. 4, these numerical values are compared to the values given by eq. (22); the agreement is fairly close, for all ranges of n and S_i. As n is theoretically restricted to values $n > 2$, and as the sorptivity curves are very insensitive to n when $n > 10$, Fig. 4 essentially covers all relevant cases.

As mentioned above, the Warren-Root-type model is not accurate at early stages of the imbibition process. Dykhuizen (1990,1991) attempted to improve upon the performance of a Warren-Root "quasi-steady-state" coupling term by using a different ordinary differential equation in the early stages of imbibition, which would correctly predict the $t^{-1/2}$ dependence of the infiltration rate. Zimmerman et al. (1993) used a similar approach which differs in that a single coupling equation is used, which in a sense contains Dykhuizen's two equations as special cases for small and large amounts of cumulative imbibition, respectively. This approach is based on an approximation to the pressure response of a spherical block subjected to a step-function increase in the pressure at its outer boundary, which was developed by Vermeulen (1953). This expression can be shown to satisfy the following ordinary differential equation:

$$\frac{d\bar{P}_m}{dt} = \alpha D_m \frac{[(P_f - P_i)^2 - (\bar{P}_m - P_i)^2]}{2(\bar{P}_m - P_i)}, \tag{23}$$

where P_i is the initial pressure in the matrix block, and α is the same shape factor that is used in the Warren-Root equation. When $\bar{P}_m$ is close to P_f, which is to say that the matrix and fractures are nearly in equilibrium with each other, it can be shown that eq. (23) reduces to eq. (4). At early times, when the fracture pressure is varying rapidly, and the matrix pressure has not yet had sufficient time to respond, eq. (23) can be shown to approximate the actual transient pressure response of the block with reasonable accuracy (see Zimmerman et al., 1993). For example, Fig. 5 shows the mean pressure $\bar{P}_m$ in a fully-saturated spherical matrix block whose outer boundary is

subjected to a step-change in the pressure from P_i to P_o, as predicted by eq. (23), by the Warren-Root equation (3), and by the exact solution (see Zimmerman et al., 1993). Eq. (23) predicts the mean pressure in the matrix block (which is equivalent to the cumulative flux into the block; see eq. (2)) very accurately, at both early and late times.

Zimmerman et al. (1993) utilized eq. (23) in place of the Warren-Root equation (4) as part of a modification to the TOUGH simulator for the special case of single-phase flow, and verified its accuracy. In conjunction with certain modifications (discussed below) to render the equation applicable to unsaturated flow, eq. (23) is the basic form we have used for the fracture/matrix coupling term. The question of determining the correct shape factor, α, to use in the fracture/matrix coupling equation is discussed in detail in Appendix D.

Dual-Porosity Simulator

We have implemented a Vermeulen-type expression for fracture/matrix flow as part of a module of subroutines that is compatible with the TOUGH code (Pruess, 1987). TOUGH is an integral finite difference code that can simulate the flow of liquid water, water vapor and air in porous or fractured media. Before describing the coupling procedure, and the structure of the new module, we will briefly review the structure and capabilities of TOUGH. Further details concerning TOUGH, along with sample problems, etc., can be found in the TOUGH User's Guide (Pruess, 1987).

TOUGH solves the equations that represent conservation of mass for water and for air, and conservation of energy, for water/air flow through porous media. The equations are solved using the "integral finite difference" approach (Edwards, 1972; Narasimhan and Witherspoon, 1976), in which the governing partial differential equations are first integrated over each gridblock, leading to first-order differences in space. Time is also discretized as a (forward) first-order finite-difference. All thermodynamic

variables that appear in the finite-difference equations therefore represent values that are averaged over the gridblock. The basic thermodynamic variables are usually taken to be temperature, pressure, and mass fraction of the air component. If the water is in a two-phase state, which would occur in regions of boiling near a waste canister, for example, the pressure and temperature would not be independent, and the third independent variable would be taken to be the vapor saturation of the water component; see Pruess (1987) for further details. As there are two mass conservation equations and one energy conservation equation to be solved, there are always only three independent variables, which are referred to within TOUGH as the "primary variables".

In passing from the known conditions at timestep t to the unknown conditions at timestep $t+\Delta t$, all properties, such as internal energy, etc., are evaluated at the values of the primary variables that obtain at time $t+\Delta t$. This is a so-called implicit approach, the use of which is required in order to avoid the numerical instabilities that occur when using an explicit method, in which all properties are evaluated at time t (Richtmyer and Morton, 1967, pp. 7-16; Rossen, 1977). Use of an implicit method causes the equations for the new values of the three primary variables to be coupled to each other. If there are N gridblocks, there will be $3N$ primary variables, and $3N$ coupled equations. Since internal energy, relative permeability, etc., vary nonlinearly with the primary variables, the $3N$ coupled equations are nonlinear, and are solved by Newton-Raphson iteration, which is essentially an iterative sequence of linearizations. Typically, about three or four iterations of the Newton-Raphson procedure are needed to solve (to within a certain required accuracy) the nonlinear equations in order to find the new values of the primary variables. Hence, the major computational burden of the TOUGH code is the solution of a sequence of $3N\times 3N$ systems of linear algebraic equations. In the version of TOUGH that we have used, these equations are solved using direct solution procedures; newer versions of TOUGH have options of using

other methods, such as conjugate gradient methods, etc., that may be more efficient for certain problems (see Moridis et al., 1994).

In order to demonstrate the computational approach used by TOUGH, without requiring the elaborate system of superscripts and subscripts that are needed for a complete formulation, for illustrative purposes we will consider the one-dimensional Richards equation, eq. (5). This is equivalent to ignoring the energy balance equation and the mass balance equation for air, as well as other factors such as diffusion of water vapor through the gaseous phase, etc., which are included in TOUGH. Consider three adjacent gridblocks in a one-dimensional system that is broken up into slab-like gridblocks of equal thickness, with their centroids located at points $x-\Delta x$, x, and $x+\Delta x$, and which are labelled $i-1, i,$ and $i+1$. The integrated form of the left-hand side of eq. (5) for gridblock i represents the net flux into that block, from the two adjacent blocks, and the integrated form of the right-hand side represents the change in the amount of water stored in that block. In integral finite difference format, this mass balance takes the form

$$\frac{\rho\overline{(kk_r/\mu)}_{i-1,i}A\,[\psi_{i-1}(t+\Delta t)-\psi_i(t+\Delta t)]\Delta t}{\Delta x}+\frac{\rho\overline{(kk_r/\mu)}_{i,i+1}A\,[\psi_{i+1}(t+\Delta t)-\psi_i(t+\Delta t)]\Delta t}{\Delta x}$$

$$+\,\rho q\,\Delta t\;=\rho\phi_i A\,\Delta x\,[S_i(t+\Delta t)-S_i(t)]\;, \qquad (24)$$

where A is the cross-sectional area perpendicular to the flow, ρ is the fluid density, and q, with dimensions of $[L^3T^{-1}]$, is a source/sink volumetric flux that is assumed to be instantaneously distributed throughout the gridblock. The terms with overbars represent some appropriate average transmissivity across the interface between adjacent blocks, the determination of which is discussed in the TOUGH User's Guide (Pruess, 1987). Eq. (21) can formally be solved for $S_i(t+\Delta t)$, which is the saturation in

gridblock i at time $t+\Delta t$. However, since the three potentials that appear on the left side of eq. (21) depend on the saturations at time $t+\Delta t$, the equation for the new value of S_i is *coupled* to those for S_{i-1} and S_{i+1}. In this way, the implicit method leads to a system of coupled nonlinear equations.

The TOUGH code utilizes the discretization method outlined above to derive a mass balance (water and air) equation, and an energy balance equation, for each gridblock. In each case, the sum of all the fluxes into a gridblock should exactly equal the change in the accumulation term. The difference between the flux and storage terms is known as the residual, which will vanish if the equations are satisfied. This set of equations is solved by Newton-Raphson iteration, which entails linearizing the equations about the current values of the primary variables, leading to a set of linear algebraic equations that can be solved by any number of standard methods. The Newton-Raphson method is iterated until all residuals are less than some specified accuracy. If this iterative process converges within fewer than a prescribed number of steps, usually taken to be four, Δt is doubled for the next timestep. This procedure allows the timesteps to grow rapidly and become large, which is desirable for diffusive-type processes, the rates of which usually decrease with time. However, the procedure of doubling the timestep does not account for the increase in the truncation error that is associated with approximating the time derivatives with first-order differences.

The TOUGH code contains provisions for sources/sinks of mass and heat, which are calculated in the subroutine QU. The sources/sinks are typically used to account for fluid that is injected or withdrawn from a borehole that penetrates one of the gridblocks. We have modified this subroutine so as to include a new type of source/sink, which represents liquid water flowing into (or out of) the fracture gridblock from the matrix blocks that are contained in a given fracture gridblock. The magnitude of the fracture/matrix flux for each fracture gridblock is computed using the following equation, which is found by combining eqs. (2,12,23):

$$q = \frac{\alpha V_m k_m k_r}{\mu} \frac{[(\psi_f - \psi_i)^2 - (\bar{\psi}_m - \psi_i)^2]}{2(\bar{\psi}_m - \psi_i)}. \tag{25}$$

This "generation" term represents the average flux q into a given fracture gridblock, over the time interval $[t, t+\Delta t]$. The volume V_m represents the total volume of matrix rock contained within the fracture gridblock; it is therefore related to the volume of the fracture gridblock by $V_m = (1-\phi_f)V_f$, where $\phi_f \ll 1$ is the fracture porosity. The relative permeability function k_r in eq. (25) refers to the relative permeability of the matrix block. As the imbibition rate is primarily controlled by the hydraulic conductivity of the matrix block *at the wetted boundary*, k_r is evaluated at the capillary pressure that exists at the outer boundary of the matrix block, which is to say at ψ_f, using eq. (8).

In order to make the calculation fully implicit, the flux is computed using the values of the variables at time $t+\Delta t$. The new value of $\bar{\psi}_m$ that exists in the matrix block at time $t+\Delta t$ must be consistent with the new average saturation. From a mass balance in the matrix block, the new average saturation at time $t+\Delta t$ is given by

$$\bar{S}_m(t+\Delta t) = \bar{S}_m(t) + \frac{q\Delta}{\phi_m V_m}. \tag{26}$$

The mean saturation $\bar{S}_m$ and the mean capillary pressure $\bar{\psi}_m$ are related to each other through eq. (7), using parameters appropriate for the matrix. At each TOUGH iteration, eqs. (7,25,26) are iterated (for each fracture element) to find a consistent set of values of $\{\bar{\psi}_m, \bar{S}_m, \text{and } q\}$. Once this is done, it is also necessary to calculate additional contributions to the Jacobian matrix, whose components are the partial derivatives of the energy, water and air residuals with respect to changes in the primary variables. For unsaturated flow, the primary variables are the liquid saturation, the gas phase

pressure, and the temperature. In our formulation, the possible presence of any dissolved air in the water that flows between the fracture elements and their associated matrix blocks is neglected. However, we do include the latent heat that is transported with the liquid, which is calculated by multiplying the mass flux given by eq. (25) by the liquid phase enthalpy.

Horizontal Flow Along a Single Leaky Fracture

One basic problem which has much relevance to understanding the behavior of the hydrological system at Yucca Mountain is that of water flowing along a fracture, with leakage into the adjacent matrix. This is also one of the simplest transient problems that involves flow in both fractures and matrix rock. If we consider a single, isolated fracture, the matrix must be modeled as being semi-infinite in extent, in each direction. The solution to this problem, and its relevance to the hydrological behavior of Yucca Mountain, has been discussed by Travis et al. (1984), Martinez (1987), and Nitao and Buscheck (1991). A schematic diagram of this problem is shown in Fig. 6. Flow into the fracture is driven by the imposed potential at the $y = 0$ boundary. Water flows along the fracture, while at the same time slowly leaking off laterally into the matrix rock. Due to the symmetry of the problem, only one of the two matrix regions needs to be included in the computational grid.

For the matrix blocks, we use the hydrological parameters that have been estimated for the Topopah Spring Member of the Paintbrush Tuff (Miocene) at Yucca Mountain (Rulon et al., 1986), which are $k = 3.9 \times 10^{-18}\,\mathrm{m}^2$, $\psi_a = -0.8718 \times 10^5\,\mathrm{Pa}$, $\phi = 0.14$, $S_s = 0.984$, $S_r = 0.318$, and $n = 3.04$. More recently-measured values are given by Flint and Flint (1994); however, as our present purpose is merely to compare the semi-analytical simulation method to MINC-type simulations, it is only necessary that the numerical values of the parameters be roughly similar to those for the rocks at Yucca Mountain. Very little experimental data exists for determining the appropriate

characteristic curves for single fractures, at Yucca Mountain or elsewhere. In the studies conducted by Martinez (1987) and Nitao and Buscheck (1991), the fracture was assumed to be bounded by two smooth, parallel walls that are separated by a distance b. The absolute permeability for this type of fracture can be exactly calculated to be $b^2/12$ (Bear, 1972, p. 164). The capillary pressure function $S(\psi)$ and the relative permeability function for a smooth-walled fracture of aperture b are represented by unit-step functions located at some value ψ_c (see Martinez, 1987, Fig. 3). The value of ψ_c is related to b and to the surface tension properties of the rock/water/air system through the equation (Martinez, 1987, p. 15)

$$\psi_c = \frac{-2\gamma\cos\theta}{b} , \tag{27}$$

where γ, which has dimensions of $[MT^{-2} = PL]$, is the surface tension between water and air, and θ is the (dimensionless) contact angle of the water/rock interface. At room temperature, $\gamma \approx 0.076\,\text{N/m}$.

The experimental evidence that currently exists seems to indicate that fractures can be described by the same type of characteristic functions that are used to model three-dimensional porous media (Persoff and Pruess, 1993; Reitsma and Kueper, 1994). For the fracture, we will use the characteristic curves that were derived by Pruess et al. (1988) using a mathematical model of a fracture as a rough-walled channel. Although these curves are not based on direct measurements, the parameters in the model were to some extent conditioned by data from Yucca Mountain. The values of the hydrological parameters for the fracture are taken to be $k = 5.5\times10^{-11}\,\text{m}^3$ (per fracture), $S_s = 1.0$, $S_r = 0.0$, $\psi_a = -1.65\times10^3\,\text{Pa}$, and $n = 2.89$. If the permeability $b^2/12$ of a smooth-walled channel is modified to account for fracture roughness and contact area (see Kumar et al., 1991; Zimmerman et al., 1991c,1992), this single-

fracture permeability is seen to be consistent with a fracture whose aperture is on the order of 100 μm. The volumes of the fracture elements were chosen to correspond to an aperture of 800 μm, however. This relatively large aperture was chosen so as to accentuate the early-time regime of the solution, in which matrix imbibition is not yet of much consequence, so as to clearly verify whether or not the new method is capable of capturing the transition between the two regimes (see below).

In our simulations, the fracture was discretized into 45 elements, with the length of the n–th element given by $L_n = (1.2)^{n-1}$ m; *i.e.*, the element lengths were 1.0 m, 1.2 m, 1.44 m, etc. Relatively small fracture gridblocks are needed near the surface in order to accurate model the diffusive front, particularly at small times. The temperature was taken to be 20°C, and the initial capillary pressure was taken to be -1.013×10^5 Pa. This capillary pressure corresponds, through the capillary pressure functions, to an initial matrix saturation of 0.6765, and an initial fracture saturation of 0.0004. For the fractures and matrix blocks to be in equilibrium at the start of the process, their capillary pressures must be equal. In general, this will lead to different saturations in the fractures and matrix. Since the average fracture aperture is typically much larger than the average pore diameter in the matrix block (Nitao and Buscheck, 1989), the magnitude of the van Genuchten capillary scaling parameter ψ_a will be much larger in the matrix than in the fracture. For equal capillary pressures, the matrix will have a much smaller value of ψ/ψ_a, and therefore a higher saturation. A capillary suction that is sufficient to almost completely dry out the fracture will consequently cause only moderate drying of the matrix.

We have solved this problem using TOUGH with the new dual-porosity module to perform the fracture/matrix interaction calculations, and also using TOUGH without the source/sink expressions, but with explicit discretization of the matrix rock adjacent to the fracture. When solving the problem with explicit discretization of the fracture and matrix regions, the matrix elements must be extended sufficiently far into the the

formation so as to effectively simulate a semi-infinite region. This distance will depend on the total elapsed time of the simulation. In the example simulation, which covered an elapsed time of 10^8 s (about 3 years), the matrix elements were extended about 20 m away from the fracture. This was achieved using 20 matrix gridblocks in the direction transverse to the fracture, with the thickness of the n–th gridblock given by $L_n = (2.0)^n \times 10^{-5}$ m. The total length of matrix gridblocks in the direction normal to the fracture was therefore equal to 21.97 m. Note that very small matrix gridblocks are needed near the fracture in order to accurately resolve the saturation fronts in the matrix at small times.

The instantaneous flowrate of liquid into the fracture at the $y = 0$ inlet, as a function of time, is shown in Fig. 7. At early times, no appreciable leakage has taken place into the relatively impermeable matrix, and the flow field is essentially that of diffusive flow along the fracture. In this regime, the flux into the fracture at the inlet decays as $t^{-1/2}$. As time progresses, the wetted interface area between the fracture and the matrix rock increases, and the effect of leakage becomes more important. The overall flowrate into the fracture gradually changes from a $t^{-1/2}$ variation to a $t^{-1/4}$ variation, as was predicted theoretically by Nitao and Buscheck (1991). The saturation profiles in the fracture are plotted in Fig. 8, at elapsed times of 10^4 s, 10^6 s, and 10^8 s. At each time, there is very close agreement between the saturation profile predicted by the semi-analytical method, and that predicted using a discretized matrix.

The amounts of CPU time needed for the simulations, performed on a Solbourne (Series 5) computer, are shown in Table 1. In each case the simulation was carried out to 10^8 s, starting with an initial timestep of 0.01 s, and with no restrictions placed on the timestep growth. The semi-analytical solution required about 70% fewer timesteps than did the fully-discretized solution, which is to say it allowed, on the average, timesteps that were about 3.38 times larger. The total number of Newton-Raphson iterations needed by the fully-discretized simulation was about 3.04 times

greater than that needed by the semi-analytical method. The savings in CPU time for the semi-analytical method was about 96%, which corresponds to a 25-fold increase in speed. This reflects both an increased speed per iteration, and a need for a fewer total number of iterations to reach the desired total simulation time of 10^8 s.

Table 1. CPU times for the problem of horizontal infiltration into a single fracture located in a permeable formation. Both simulations were conducted with TOUGH running on a Solbourne (Series 5) computer.

	Fully-Discretized	Semi-Analytical
# fracture elements	45	45
# matrix elements	45×20=900	0
Total # elements*	946	46
Timesteps	624	185
Iterations	3205	1053
CPU time (s)	20901	823

* Includes one boundary element

Vertical Infiltration into a Formation Containing Parallel Fractures

Another idealized hydrological problem that is relevant to the site characterization process at Yucca Mountain is that of infiltration of liquid water into a formation containing an array of parallel fractures, under the influence of both capillary and gravitational forces (see Fig. 9). Such infiltration can occur under conditions of either constant pressure at the surface, or constant flux. We will consider infiltration that occurs under constant pressure conditions; in particular, we will consider the "barely-ponded" case, in which there is a very small positive potential at the surface, caused by a small depth of standing water. The effect of a positive potential of magnitude ψ_s at the surface will have a negligible effect on imbibition compared to the capillary forces, as long as $|\psi_s| \ll |\psi_a|$. Since a ponded head of depth h causes a surface potential of magnitude $\rho g h$, the effect of ponding will be negligible as long as $h \ll \psi_a / \rho g = L_s$, where L_s is the sorptive length of the fracture (see Appendix B). For the parameters used in this example, the sorptive length is 0.17 m, or 17 cm, so the case of negligible ponded head is physically realistic. Therefore, in order to simplify the interpretation of the results, we take the ponded head to be zero. The type of infiltration modeled in this problem would occur, for example, after a brief but intense rainfall event. Assuming uniform properties in the horizontal plane, the imbibition can be modeled as a one-dimensional problem, similar to the leaky-fracture problem discussed in the previous section. The only differences in the simulations are the inclusion of a gravitational gradient, and the use of a finite size for the matrix blocks. TOUGH allows for the gravitational gradient to be set equal to zero, or to its actual value of 9.81 m/s^2, or to any other value, as specified in the input file.

For this problem the fracture continuum was discretized into 50 elements, with the length of the n–th element given by $L_n = (1.2)^{n-1}$ m. This is a similar gridding scheme as was used for the horizontal flow problem, except that five additional grid-blocks were needed to insure that the front did not reach the end of the grid within

10^8 s. Fourteen matrix gridblocks were placed normal to each fracture gridblock, with their lengths given by $L_n = (2.0)^n \times 10^{-5}$ m. These matrix gridblocks therefore extend a total distance of 0.3277 m away from the fracture, which corresponds to a spacing between fractures of $2L = 0.6554$ m. This spacing is in the range that was reported by Wang and Narasimhan (1985). The matrix blocks in this problem are therefore slabs of length $2L$. The proper shape factor for a slab of thickness $2L$, which is needed for the semi-analytical simulation, is given by $\alpha = \pi^2/(2L)^2 = 22.98$ (see Appendix D). The equivalent-continuum fracture permeability was taken to be 3.357×10^{-14} m^2, and the fracture gridblock volumes were again chosen to correspond to an aperture of 800 μm.

Fig. 10 shows the saturation profiles in the fractures, as a function of depth below the surface, after elapsed infiltration times of 10^6 s, 10^7 s, and 10^8 s. Gravity causes the liquid front to extend much farther down into the formation than would have been the case under the influence of capillarity alone (compare Figs. 10 and 7). The agreement between the fully-discretized TOUGH solution and the solution obtained with our new source/sink method is again quite close. Fig. 11 shows the infiltration rate into the formation as a function of time. The initial downward-sloping region that exists for $t < 10^3$ s reflects the influence of capillarity, which is important only at small times. After the effect of capillarity diminishes, the volumetric flux tends towards the value $q = \rho g k_f / \mu$, which would be the infiltration rate into the fractured formation of permeability k_f, if the matrix blocks were impermeable. In this problem, $\rho g k_f / \mu = 3.29 \times 10^{-7}$ m/s. Eventually, at times that are sufficiently large that the matrix blocks near the surface are full, the infiltration rate re-stabilizes at $q = \rho g k_f / \mu$. However, as predicted analytically by Nitao and Buscheck (1989,1991), there is an intermediate regime, during which the the matrix blocks near the surface are in the process of being filled, when the infiltration rate rises somewhat above $\rho g k_f / \mu$. The infiltration rate calculated using the semi-analytical approach displays this qualitative feature, whereas the fully-discretized solution in fact shows a slight decrease below

this infiltration rate. Although these effects are relatively small (the two infiltration rates never differ by more than 20%), and do no not seem to have any simple physical explanation, it nevertheless seems that the semi-analytical method can more readily discern this subtle aspect of the solution; presumably, a finer gridding of the matrix blocks would enable the fully-discretized solution to predict this effect.

Table 2 shows the computational details of the two simulations. The number of timesteps needed to reach 10^8 s was about 27% less for the semi-analytical simulation than for the fully-discretized case. The ratio of CPU times between the two simulations was about 6:1. Note that in the case of horizontal infiltration, the flowrate into the first fracture element continually decreases, whereas for vertical infiltration, the flux is more or less constant in time. Recall that TOUGH will allow the timestep to grow if the Newton-Raphson iterations converge within, say, four iterations. Our simulations have generally shown that one of the factors that controls the ease of convergence is that the total volumetric flux through any given gridblock in one timestep cannot exceed about 10^4 pore volumes. If the flowrate decreases, the maximum allowable timestep will grow at a rate such that $q\,\Delta t \approx 10^4(\phi V)_{\min}$. Hence the timestep can grow continually in the vertical flow problem, but will not grow beyond some fixed value during vertical flow. This accounts for the fact that both methods required less timesteps for the horizontal flow problem as for the vertical problem. In either case, the maximum timestep will be controlled by the size of the smallest gridblock. In the fully-discretized horizontal flow problem, the smallest gridblock was a matrix element adjacent to the first fracture element; the elimination of this element in the grid that was used in the semi-analytical simulation had the effect of allowing larger timesteps to be taken. This is an additional advantage afforded by the new method.

Table 2. CPU times for the problem of vertical infiltration into a formation consisting of a set of parallel, equally-spaced fractures. Both simulations utilize TOUGH running on a Solbourne (Series 5) computer.

	Fully-Discretized	Semi-Analytical
# fracture elements	50	50
# matrix elements	50×14=700	0
Total # elements*	946	46
Time steps	970	705
Iterations	5082	4785
CPU time (s)	20508	3431

* Includes one boundary element

Conclusions

This report has described a new semi-analytical dual-porosity model for unsaturated flow in fractured/porous media. The model is based on a lumped-parameter formulation, in which the mean liquid potential in each matrix block is represented by a single value. Fluid flow from the fracture network into the matrix blocks is modeled by a nonlinear equation, with an effective transmissivity that depends on the hydrological properties of the matrix rock, the geometry of the matrix blocks, as well as on the mean saturation of the matrix blocks. This expression for fracture/matrix flow has been incorporated into a module that is compatible with the TOUGH simulator to act as a source/sink term for the fracture elements. The modified code has been tested on the problem of flow along a single horizontal fracture, as well as vertical infiltration into a fractured formation under constant-head boundary conditions. In both cases the new method gives very close agreement with simulations carried out by explicitly discretizing the matrix blocks, while yielding a substantial savings in CPU time. Since the new method permits an order of magnitude decrease in the number of computational cells, the process of creating the grid and the input file for the TOUGH simulations is greatly simplified. Both of these factors will allow for much more efficient simulation of unsaturated flow processes in fractured/porous formations, such as, in particular, the unsaturated zone at Yucca Mountain, Nevada. The new dual-porosity module described in this report is currently being used, in conjunction with the three-dimensional site-scale model of the unsaturated zone at Yucca Mountain that has been developed by scientists at Lawrence Berkeley Laboratory and the U. S. Geological Survey (Wittwer et al., 1994), to conduct transient simulations of infiltration processes at Yucca Mountain.

Acknowledgments

This work was carried out under U.S. Department of Energy Contract No. DE-AC03-76SF00098, administered by the DOE Nevada Office, in cooperation with the United States Geological Survey, Denver. The authors thank Yvonne Tsang and Joe Wang of LBL, Bob Lewis and Martha Mustard of the USGS, and Ron Linden of the DOE, for reviewing this report.

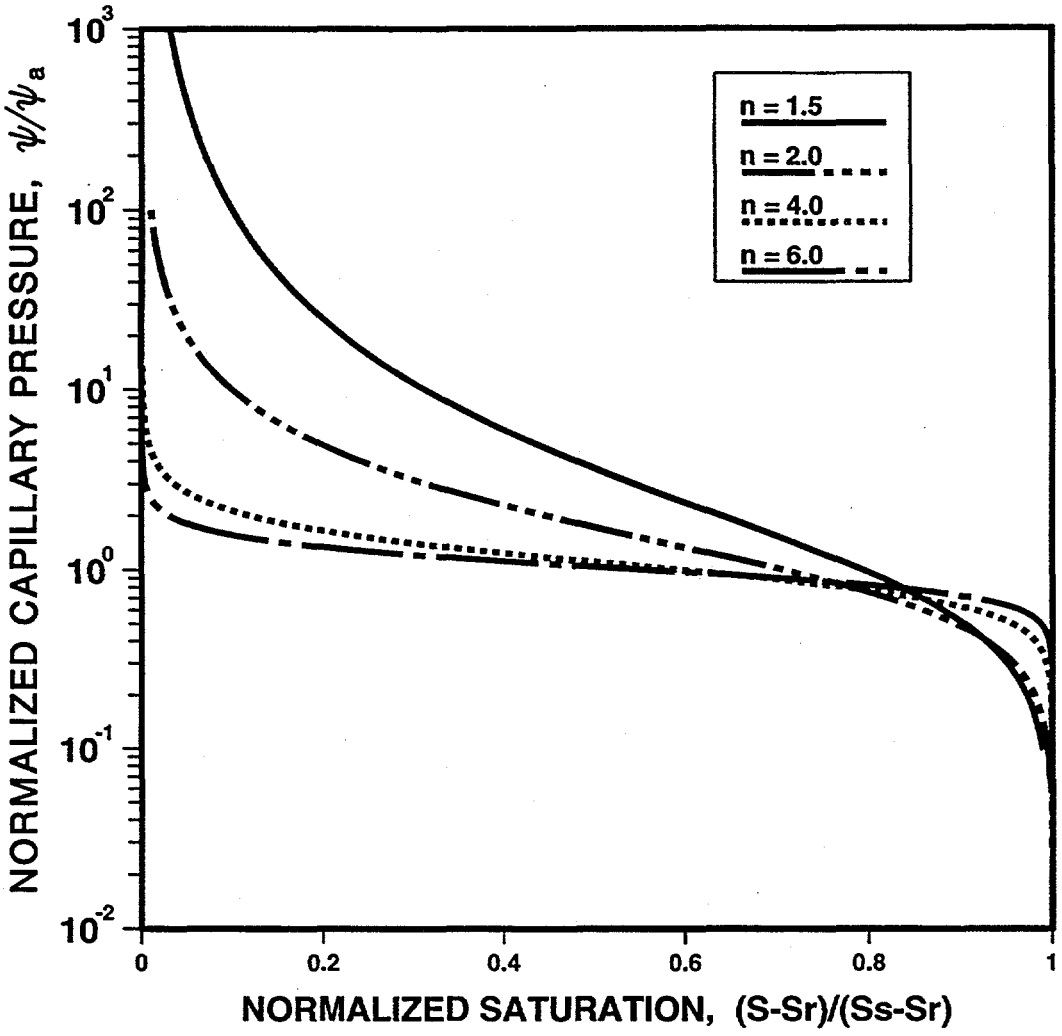

Fig. 1. Normalized capillary pressure curves of Mualem - van Genuchten media, as functions of normalized saturation. The parameters n and m are related by $n = 1/(1-m)$. The equation of the curves, and the definition of normalized saturation, are given by eq. (9), and the adjoining text.

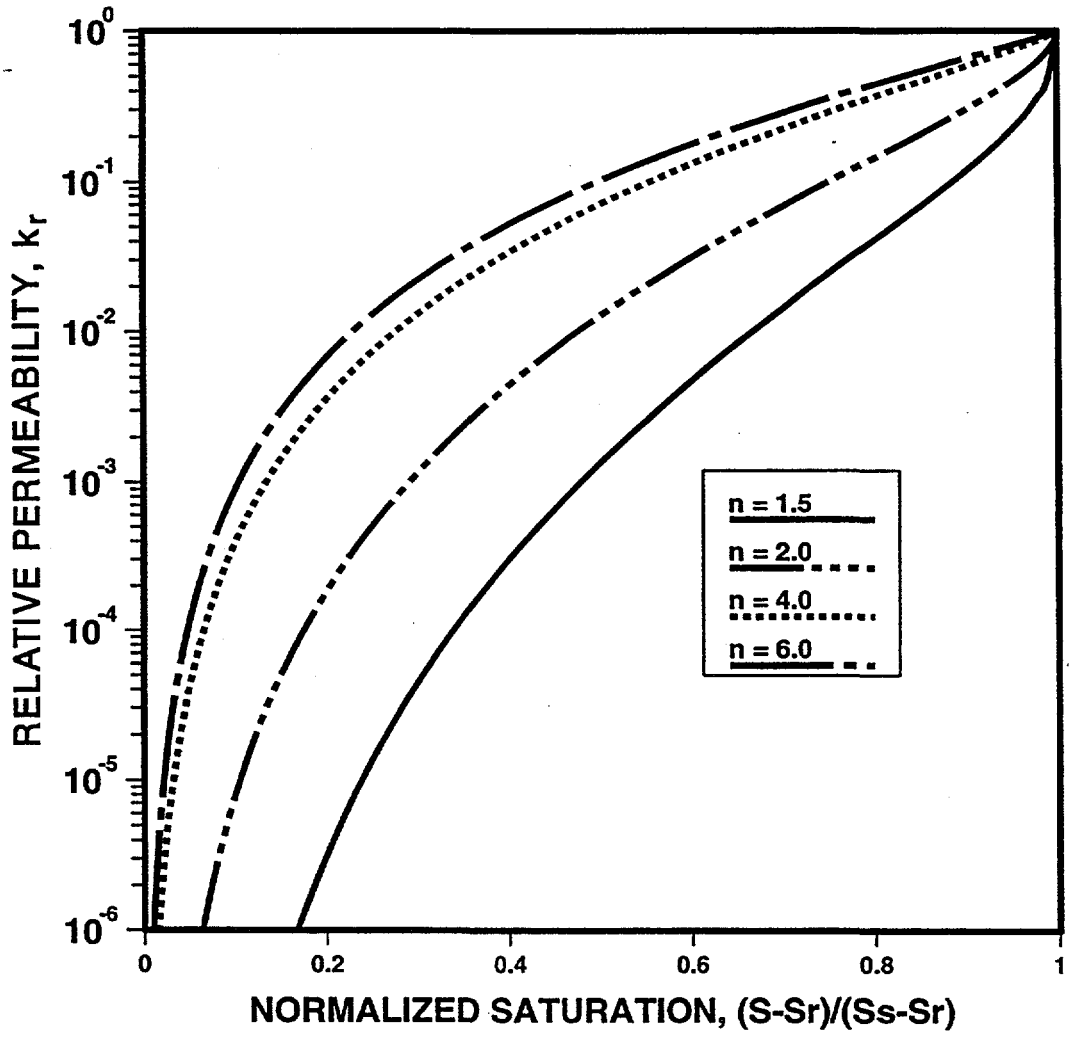

Fig. 2. Relative permeability curves of Mualem - van Genuchten media, as functions of normalized saturation. The parameters n and m are related by $n = 1/(1-m)$. The equation of the curves, and the definition of normalized saturation, are given in eq. (10), and the adjoining text.

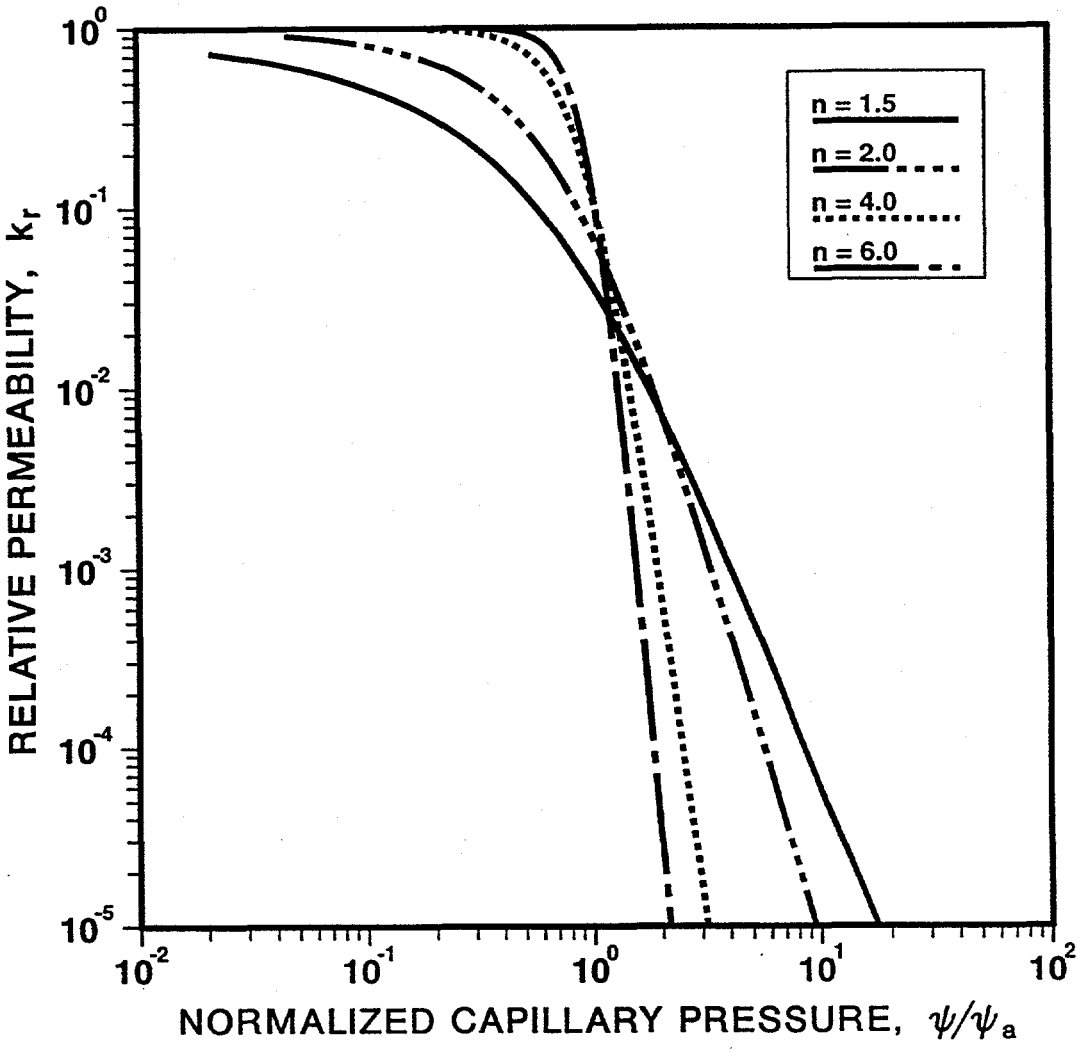

Fig. 3. Relative permeability curves of Mualem - van Genuchten media, as functions of normalized capillary potential. The parameters n and m are related by $n = 1/(1-m)$. The equation of the curves is given by eq. (8).

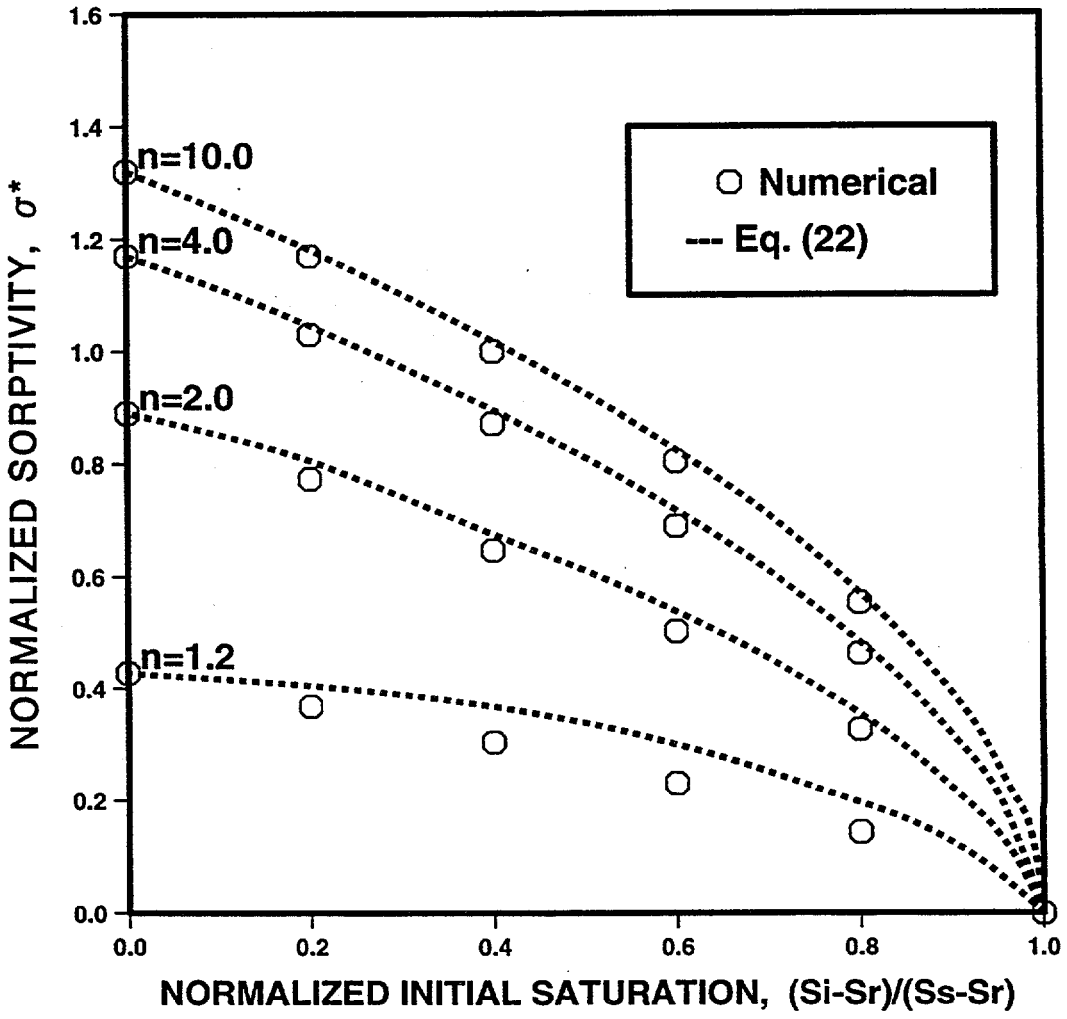

Fig. 4. Normalized sorptivity $\sigma^* = \sigma[\mu(S_s - S_r)/k\phi|\psi_a|]^{1/2}$ of a van Genuchten medium, as calculated exactly by numerical integration of eq. (5), and from the approximate expression (22).

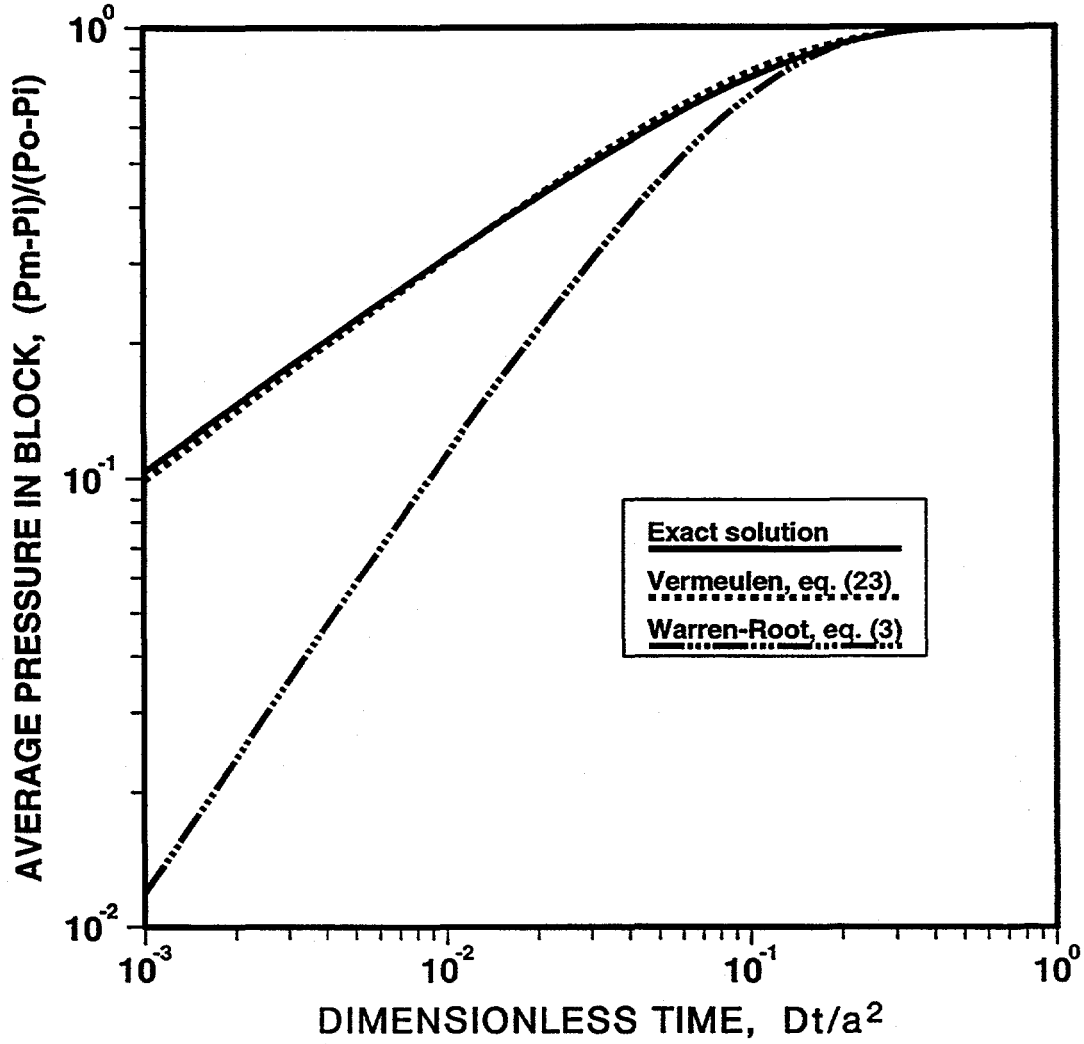

Fig. 5. Normalized mean pressure $\bar{P}_m$ in a saturated spherical matrix block of radius a subject to a step-function change in the pressure at its outer boundary from P_i to P_o, according to eq. (23), the Warren-Root equation (3), and the exact solution (see Zimmerman et al., 1993). The diffusion coefficient is $D = k/\phi\mu c$, and the shape factor for a sphere is $\alpha = \pi^2/a^2$.

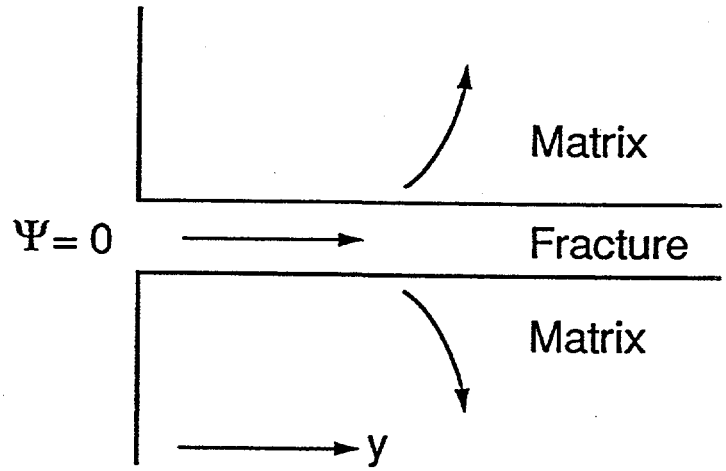

XBL 894-7532
T.I.D. Claris CAD
4/4/89

Fig. 6. Schematic diagram of flow along a single horizontal fracture, from a constant-pressure inlet, with transverse leakage into the matrix.

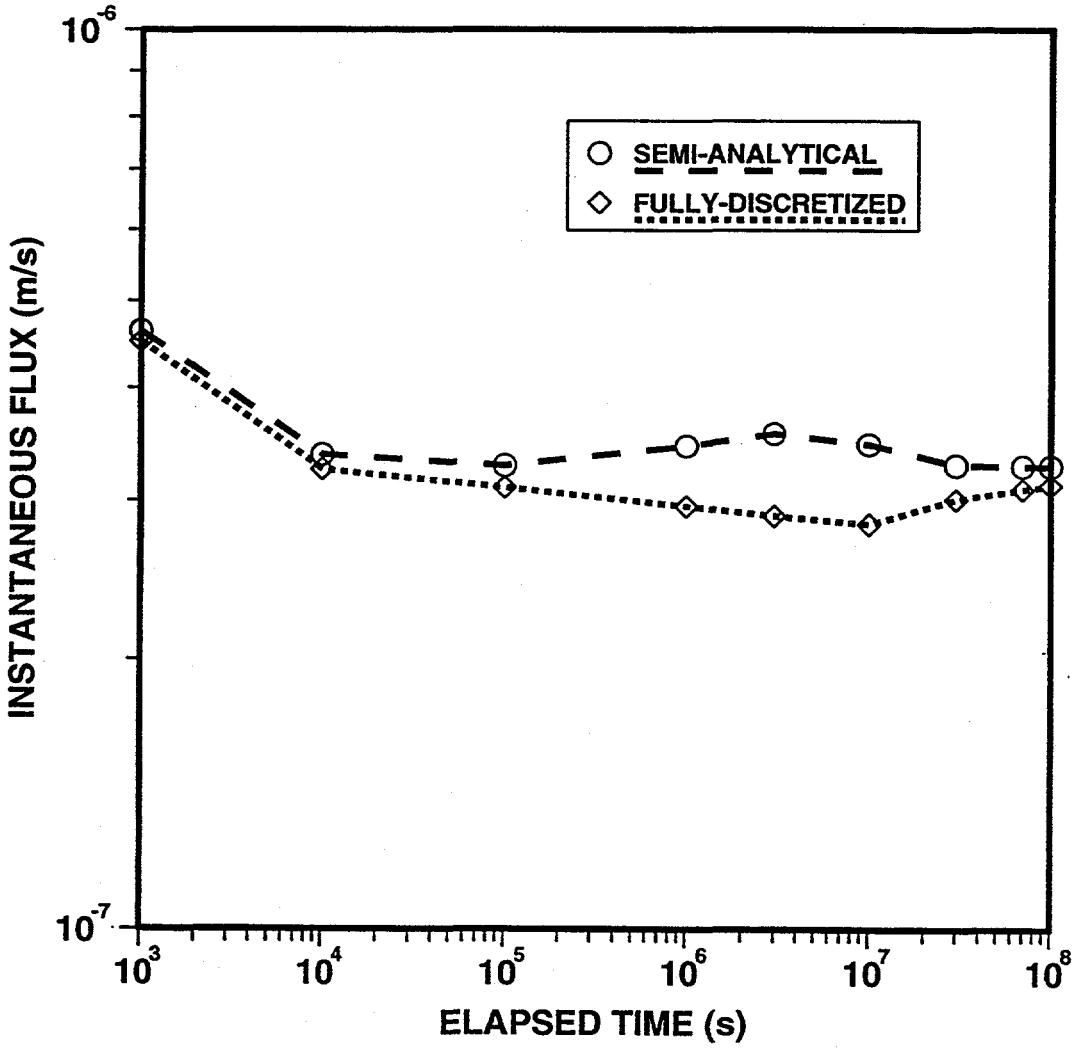

Fig. 7. Instantaneous flux into the fracture, per unit depth perpendicular to the page in Fig. 6, for the horizontal fracture flow problem.

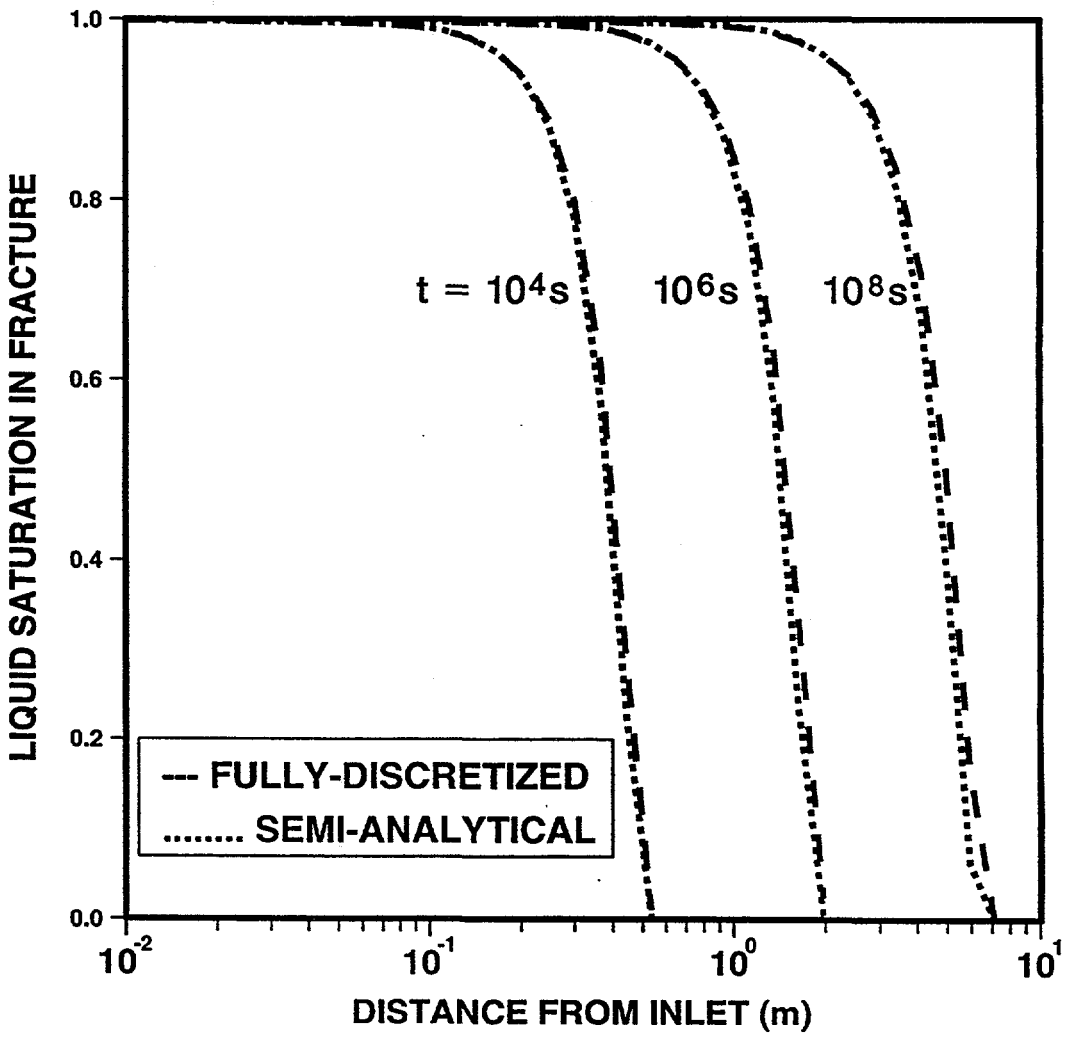

Fig. 8. Saturation profile in the fracture, during flow along a single horizontal fracture, after elapsed times of 10^4 s, 10^6 s, and 10^8 s. Parameters used in the simulations are listed in the text.

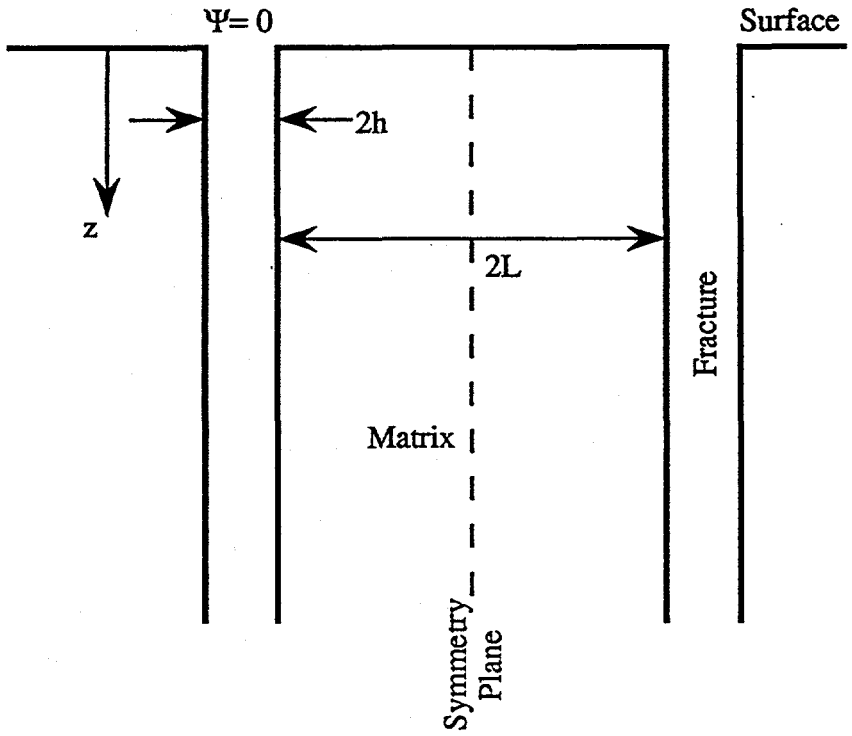

Fig. 9. Schematic diagram of vertical infiltration into a medium containing a set of parallel, equally-spaced of fractures of aperture $2h$ and spacing distance $2L$.

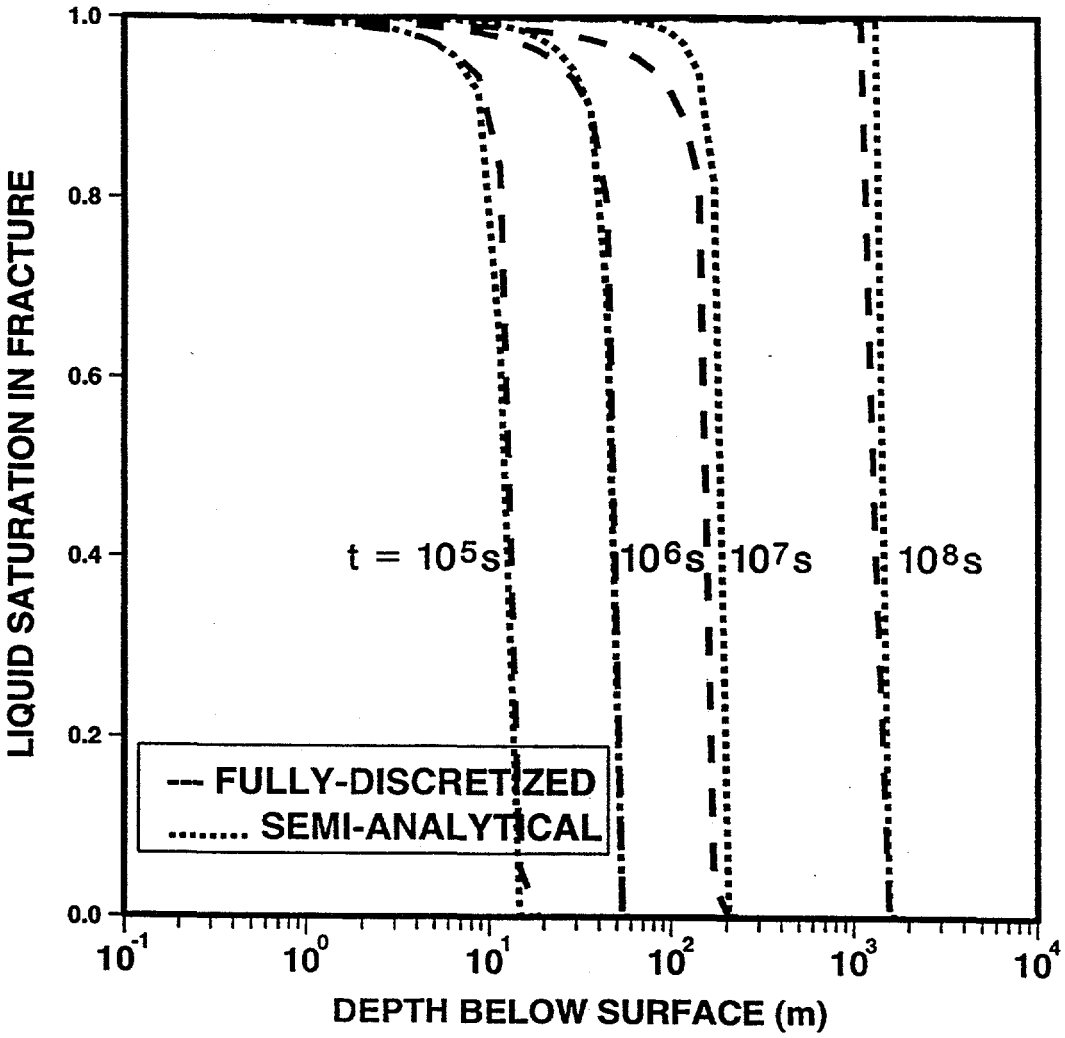

Fig. 10. Saturation profile in the fracture network, during vertical infiltration into a fractured formation, after elapsed times of 10^5 s, 10^6 s, 10^7 s and 10^8 s. Parameters used in the simulations are listed in the text.

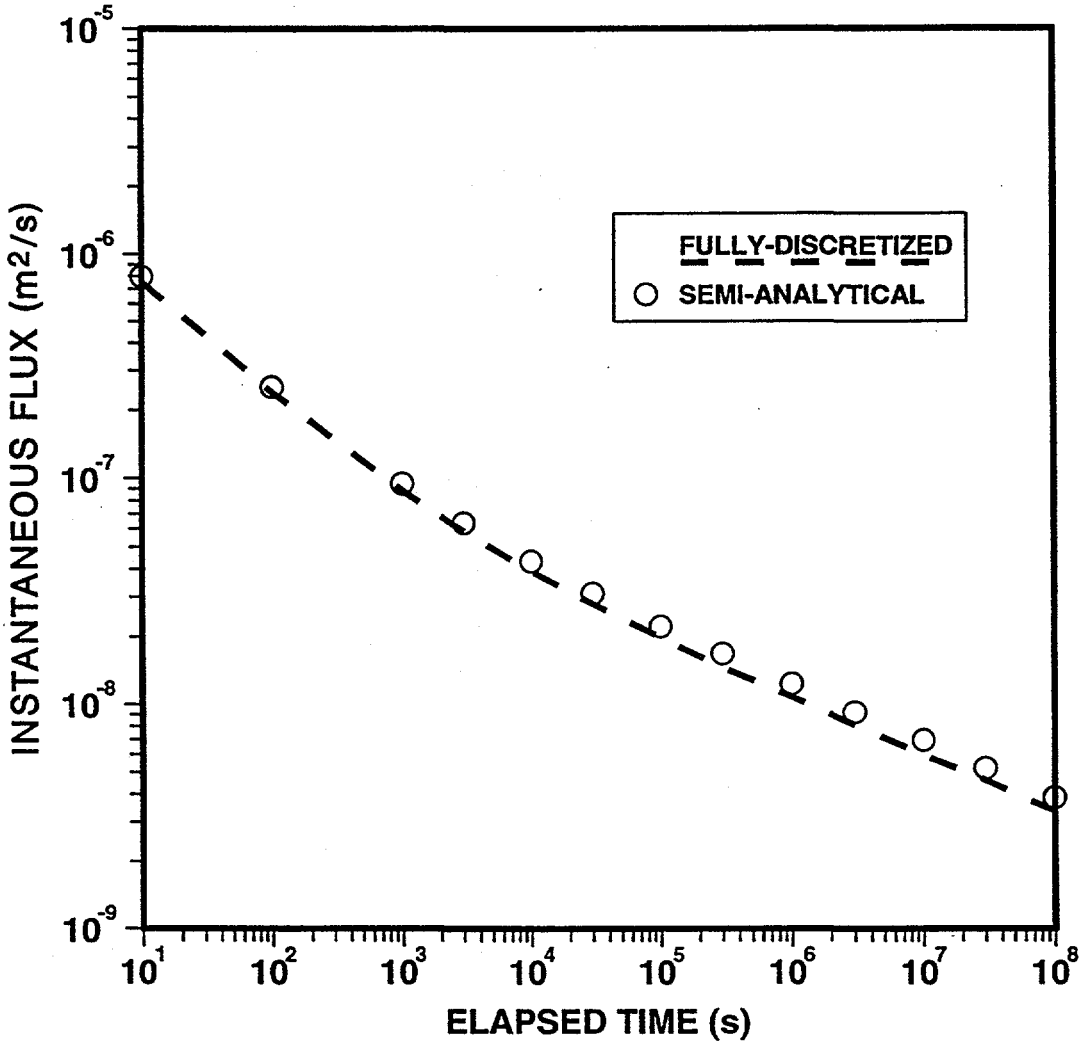

Fig. 11. Instantaneous flux at the surface of the fractured/porous formation, for the vertical infiltration problem.

Appendix A: Numerical Solution of the Richards Equation

The Richards equation is a second-order, nonlinear partial differential equation in two variables, x and t. However, because of its mathematical form, which contains two derivatives with respect to x and one derivative with respect to t, a Boltzmann "similarity" transformation can be used (see Hillel, 1980, p. 208) to transform it into a second-order ordinary differential equation. This second-order ordinary differential equation can then be written as a pair of first-order differential equations, which can then be solved numerically using standard methods. This approach is more efficient and more accurate than a numerical solution of the original partial differential equation, due to the reduction in the number of independent variables from two to one.

For a van Genuchten medium, the Richards equation (without gravity) takes the form (see eq. (4))

$$\frac{\partial}{\partial x}\left[\frac{k k_r(\psi)}{\mu\phi}\,\frac{\partial \psi(x,t)}{\partial x}\right] = \frac{\partial S(x,t)}{\partial t}\ , \tag{A1}$$

where the characteristic functions are given by

$$S(\psi) = S_r + (S_s - S_r)[1 + (\psi/\psi_a)^n]^{-m}\ , \tag{A2}$$

$$k_r(\psi) = \frac{\{1 - (\psi/\psi_a)^{n-1}[1 + (\psi/\psi_a)^n]^{-m}\}^2}{[1 + (\psi/\psi_a)^n]^{m/2}}\ . \tag{A3}$$

The boundary and initial conditions for the problem are

$$\psi(x, t=0) = \psi_i\ , \tag{A4}$$

$$\psi(x=0, t>0) = 0, \tag{A5}$$

$$\lim_{x\to\infty} \psi(x,t) = \psi_i . \tag{A6}$$

Guided by the approximate solution developed by Zimmerman and Bodvarsson (1989a), we define the dimensionless potential $\hat{\psi}$ by

$$\hat{\psi} = \frac{\psi}{\psi_a}, \tag{A7}$$

the normalized saturation by

$$\hat{S} = \frac{S - S_r}{S_s - S_r}, \tag{A8}$$

and the dimensionless similarity variable by

$$\eta = \left[\frac{\mu\phi(S_s - S_r)x^2}{2|\psi_a|kt}\right]^{1/2}. \tag{A9}$$

As ψ will be negative in the unsaturated zone, and $\psi_a < 0$, the normalized capillary potential $\hat{\psi}$ will be positive. In terms of these dimensionless variables, the Richards equation is transformed into

$$\frac{d}{d\eta}\left[k_r(\hat{\psi})\frac{d\hat{\psi}}{d\eta}\right] + \eta\hat{S}'(\hat{\psi})\frac{d\hat{\psi}}{d\eta} = 0, \tag{A10}$$

where the normalized characteristic functions are given by

$$\hat{S}(\hat{\psi}) = [1+\hat{\psi}^n]^{-m}\,, \tag{A11}$$

$$k_r(\hat{\psi}) = \frac{\{1-\hat{\psi}^{n-1}[1+\hat{\psi}^n]^{-m}\}^2}{[1+\hat{\psi}^n]^{m/2}}\,. \tag{A12}$$

and the symbol $'$ denotes differentiation. The three boundary/initial conditions, eqs. (A4-6), collapse into the following two boundary conditions:

$$\hat{\psi}(0) = 0\,, \tag{A13}$$

$$\lim_{\eta\to\infty} \hat{\psi}(\eta) = \hat{\psi}_i\,. \tag{A14}$$

Eqs. (A10-14) form a second-order ordinary differential equation two-point boundary-value problem. To solve these equations numerically, we first transform eq. (A10) into a pair of first-order differential equations. This is done by defining two independent variables

$$\hat{\psi}_1 = \hat{\psi}\,, \tag{A15}$$

$$\hat{\psi}_2 = \frac{d\hat{\psi}}{d\eta}\,. \tag{A16}$$

Using the product rule to expand out the derivative of the bracketed term, eq. (A10)

can be written as a pair of first-order equations:

$$\frac{d\hat{\psi}_1}{d\eta} = \hat{\psi}_2, \tag{A17}$$

$$\frac{d\hat{\psi}_2}{d\eta} = -\frac{k_r'(\hat{\psi}_1)}{k_r(\hat{\psi}_1)}(\hat{\psi}_2)^2 - \frac{\eta\hat{S}'(\hat{\psi}_1)}{k_r(\hat{\psi}_1)}\hat{\psi}_2, \tag{A18}$$

where, as before, the symbol $'$ denotes differentiation. The two boundary conditions (A13,14) now apply to the dependent variable $\hat{\psi}_1$. The derivatives $k_r'(\hat{\psi})$ and $S'(\hat{\psi})$ are found by differentiating eqs. (A11,12).

After the potential profile $\hat{\psi}(\eta)$ is found, the volumetric flux into the medium can be found from Darcy's law (eq. (13)), as follows:

$$\frac{q}{A} = -\frac{k}{\mu}\left[\frac{\partial\psi}{\partial x}\right]_{x=0} = -\frac{k}{\mu}\frac{d\psi}{d\hat{\psi}}\frac{d\hat{\psi}}{d\eta}\frac{d\eta}{dx}$$

$$= -\frac{k}{\mu}\psi_a\frac{d\hat{\psi}}{d\eta}\left[\frac{\mu\phi(S_s - S_r)}{2|\psi_a|kt}\right]^{1/2}$$

$$= \left[\frac{|\psi_a|\phi k(S_s - S_r)}{2\mu t}\right]^{1/2}\left[\frac{d\hat{\psi}}{d\eta}\right]_{\eta=0}. \tag{A19}$$

Comparing this expression with the definition of sorptivity, eq. (14), we see that

$$\sigma = \left[\frac{2|\psi_a|\phi k(S_s - S_r)}{\mu}\right]^{1/2}\left[\frac{d\hat{\psi}}{d\eta}\right]_{\eta=0}. \tag{A20}$$

If we define the normalized sorptivity $\hat{\sigma}$ as in Fig. 4, we have

$$\hat{\sigma} = \left[\frac{d\hat{\psi}}{d\eta}\right]_{\eta=0} . \tag{A21}$$

The normalized sorptivity is therefore equal to the value of $\hat{\psi}_2$ at $\eta=0$.

The initial condition for $\hat{\psi}$ is always taken to be 0. The relationship shown in eq. (A21) shows that if we take the sorptivity to be known, we could integrate eqs. (A15,16) to solve for the potential at infinity, which is $\hat{\psi}_i$; this is equivalent to solving for the initial saturation $\hat{S}_i$. This integration could be performed using any standard integration technique for a system of ordinary differential equations, such as a Runge-Kutta algorithm, or a simple first-order Euler algorithm (see Press et al., 1992, pp. 702-708). The integration would begin at $\eta=0$, and end when $\hat{\psi}_2$ has essentially reached zero, and $\hat{\psi}_1$ has leveled off to some asymptotic value $\hat{\psi}_i$. For the purposes of generating a plot of the sorptivity as a function of the initial saturation, as in Fig. 4, this procedure would be sufficient.

If, on the other hand, it was desired to find the sorptivity for a given value of $\hat{\psi}_i$, the following iterative approach could be used. The sorptivity could be guessed, thereby supplying a value for $\hat{\psi}_2$ at $\eta=0$, and the integration carried out to yield some value $\hat{\psi}_1^{\infty}$. This value $\hat{\psi}_1^{\infty}$ will essentially be a function of $\hat{\sigma}$. Conversely, $\hat{\sigma}$ will be a function of $\hat{\psi}_1^{\infty}$, although instead of being given as an explicit function, the functional relationship is a result of the numerical integration. Aside from this seeming complication, the problem has been reduced to a one-variable root-finding problem, i.e.,

$$\hat{\psi}_1^{\infty}(\hat{\sigma}) = \hat{\psi}_i , \tag{A22}$$

where $\hat{\psi}_i$ is the initial capillary potential, and $\hat{\psi}_1^{\infty}$ is the value found as a result of numerical integration using a certain value $\hat{\sigma}$ for the potential gradient at $\eta = 0$ (see eq. A21). Hence any standard iterative method, such as bisection or Newton-Raphson iteration (see Press et al., 1992, pp. 355-360) could be used to converge to the value of $\hat{\sigma}$ that yields the correct value of $\hat{\psi}_i$.

As an example of the use of the similarity transformation for solving the one-dimensional Richards equation without gravity, consider the problem of horizontal imbibition into a slab of Topopah Spring tuff whose initial liquid saturation is 0.65, from a saturated boundary that is held at zero capillary pressure. The physical parameters for this rock are taken from Rulon et al. (1986), and are listed in Table A1. This problem was solved using the Boltzmann transformation method outlined above, and also using TOUGH. In the TOUGH simulations, the potential at the inlet is held constant by means of a very large boundary block that is connected to the first gridblock (see Fig. A2). This "source" gridblock has the same characteristic functions as the slab, but a volume of $10^{50}\,m^3$. Initially, this source block is at a pressure of $10^5\,Pa$, and has a liquid saturation of 0.984. At this saturation, the capillary pressure is zero (see Table A1), so the liquid phase pressure is also $10^5\,Pa$. As the liquid in the slab of tuff is initially at a saturation of 0.65, its capillary pressure is $-1.062\times10^5\,Pa$, its air phase pressure is $1.0\times10^5\,Pa$, and so the liquid phase pressure is $\psi_l = \psi_v + \psi_c = 1.0\times10^5 - 1.062\times10^5 = -0.062\times10^5 Pa$. Hence, there is a pressure gradient in the liquid phase that drives water into the slab from the source block. The volume of the source block is sufficiently large that the loss of fluid into the slab will not cause any noticeable drop in its pressure.

In order to mimic the physical situation modeled by the Richards equation, the air phase is allowed to "short-circuit" out of the block. This is accomplished (see Pruess, 1987) by connecting each tuff gridblock to a large "sink" block, also of volume $10^{50}\,m^3$. The characteristic functions of this sink block are chosen so that there is no

capillary pressure effect, which implies that the air and liquid in the sink block are always at the same pressure. The sink block is initially fully saturated with air at a pressure of 10^5 Pa. As there is no capillary pressure effect, the water potential in the sink block is also at 10^5 Pa, which is higher than that of the water in the slab; hence, water will not enter the sink block from the slab of tuff. As water enters the slab from the source block, it slightly compresses the air ahead of it, raising its pressure above 10^5 Pa, thereby driving air into the sink block.

In one TOUGH simulation the mesh consisted of 20 gridblocks, each of 0.05 m thickness, and in the other there were 100 gridblocks, each of 0.01 m thickness. For comparison with the TOUGH results, the similarity solution can be expressed in terms of the distance from the inlet, x, and the elapsed time, t, by using eq. (A9). The results of the three simulations, after an elapsed time of 10^7 s, are shown in Figs. A3 and A4. The TOUGH simulations show a certain amount of broadening of the wetting front, due to numerical dispersion (see Moridis and Pruess, 1992, pp. 4-8). Since the discretization error in the integral finite difference method is proportional to the square of the gridblock thickness (Moridis and Pruess, 1992, pp. 81-82), the fine-grid simulation is more accurate than the coarse-grid results. The numerical dispersion, which is an artifact of the solution method, can also be limited by using midpoint-weighting instead of upstream weighting for the inter-block transmissivities. The saturation profile and liquid potential profile computed with the fine grid lie very close to those computed using the Boltzmann transformation. Since TOUGH has already been validated for one-dimensional imbibition problems (see Pruess, 1987, pp. 50-52), this example serves in a sense to validate the solution method described in this appendix.

Table A1. Physical properties and parameters used in solution of one-dimensional imbibition problem into a slab of Topopah Spring welded tuff. Rock property values are taken from Rulon et al. (1986).

Property	Symbol	Value	Units
Porosity	ϕ	0.14	-
Permeability	k	3.9×10^{-18}	[m^2]
Air-entry pressure	ψ_a	-8.72×10^{4}	[Pa]
van Genuchten parameter	n	3.04	-
Viscosity*	μ	0.001	[Pa s]
Satiated saturation	S_s	0.984	-
Residual saturation	S_r	0.318	-
Initial saturation	S_i	0.650	-

* This value is used in the similarity solution; TOUGH uses pressure-dependent values computed from equations of state. At the simulation temperature of 293 °K, there is very little difference between the pressure-dependent values and the value 0.001 Pa s.

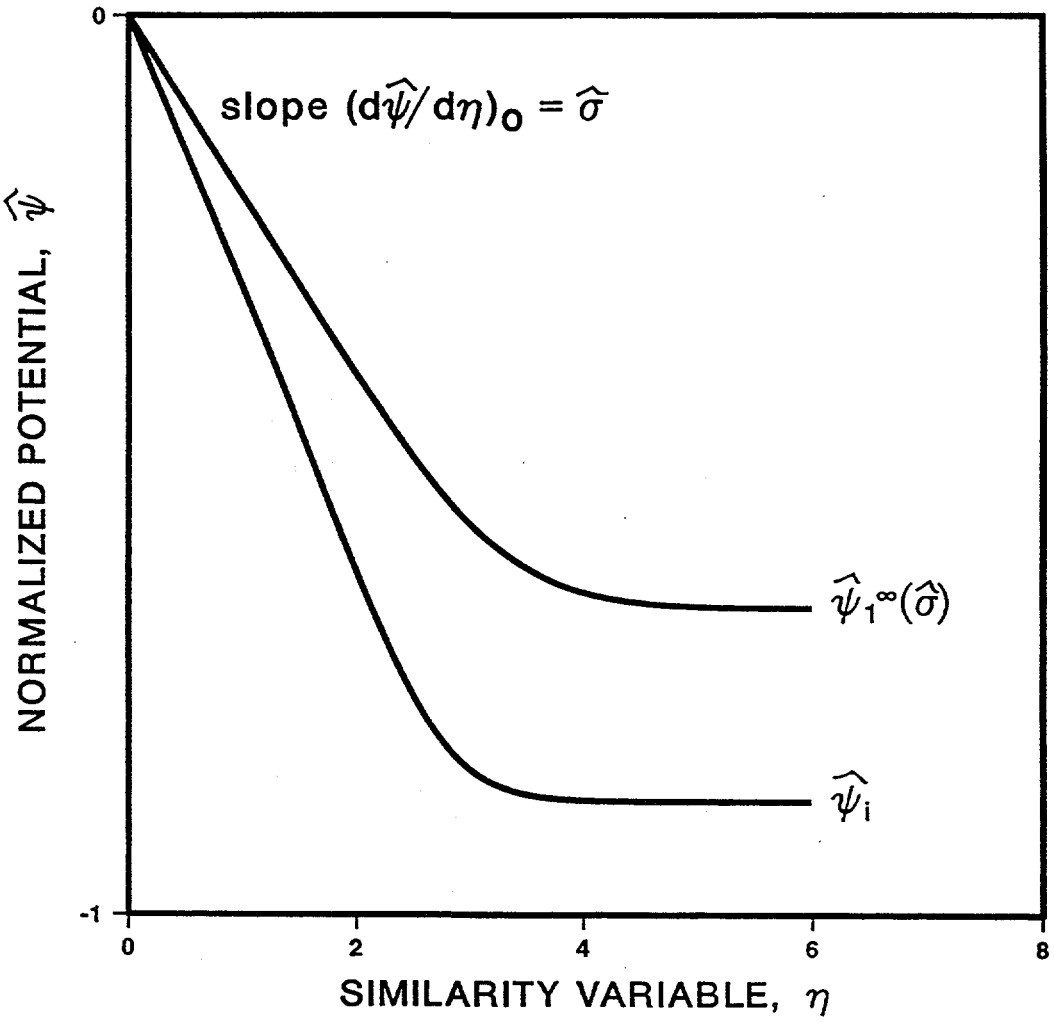

Fig. A1. Schematic diagram of solution procedure for Richards equation. The initial slope $d\hat{\psi}/d\eta$ at $\eta=0$ is equal to the normalized sorptivity, $\hat{\sigma}$. Different choices of $\hat{\sigma}$ will lead to different asymptotic values of $\hat{\psi}^{\infty}$. Only one choice of $\hat{\sigma}$ will lead to the correct asymptotic potential, $\hat{\psi}^{\infty}=\hat{\psi}_i$.

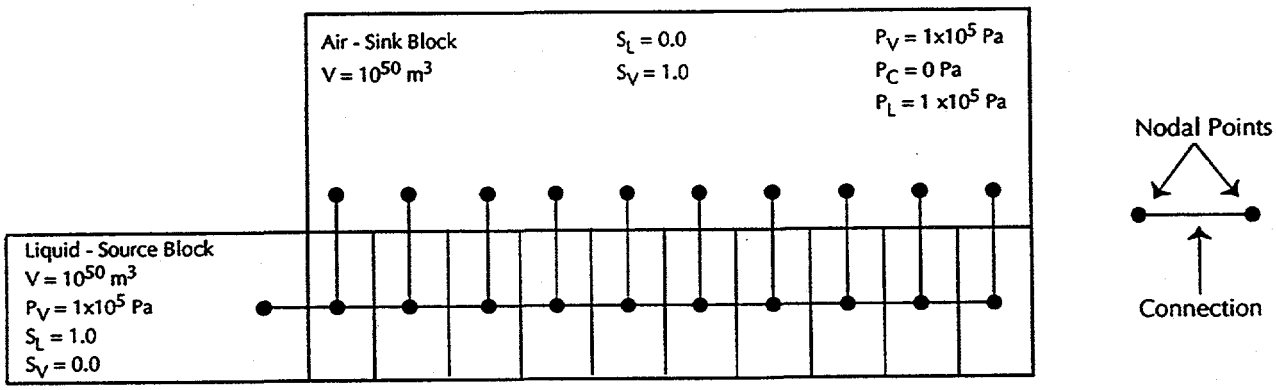

Fig. A2. Schematic diagram of the computational grid used in the TOUGH simulations. The 1 m long slab is broken up into either 20 or 100 equally-sized gridblocks, each with a cross-sectional area of $1\,m^3$. The large boundary gridblock at the left serves as a source of liquid water at 1×10^5 Pa pressure, and zero capillary pressure, while the large sink block serves as a sink for air, as described in the text.

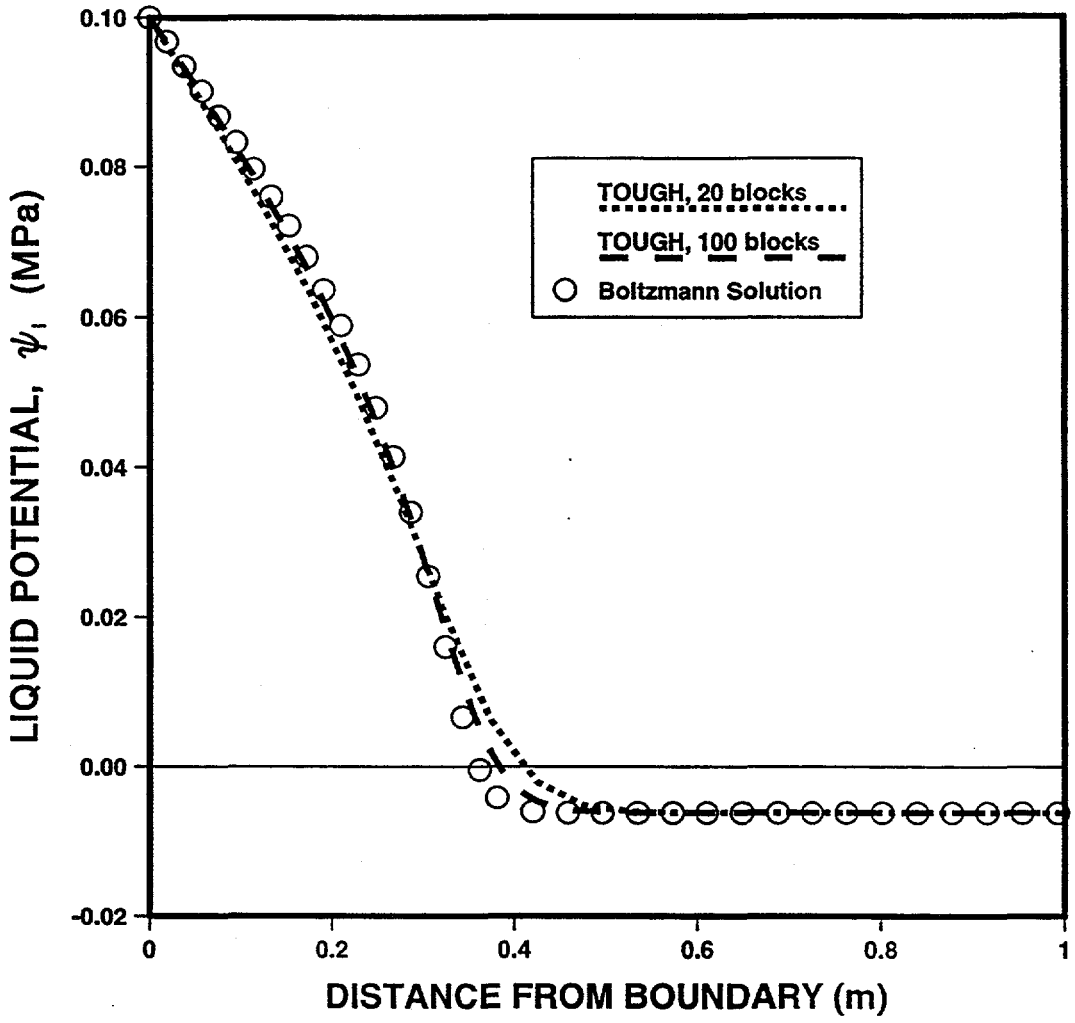

Fig. A3. Potential profiles computed for one-dimensional absorption of water into a slab of Topopah Spring welded tuff. Properties and parameters are listed in Table A1. The elapsed time is 10^7 s.

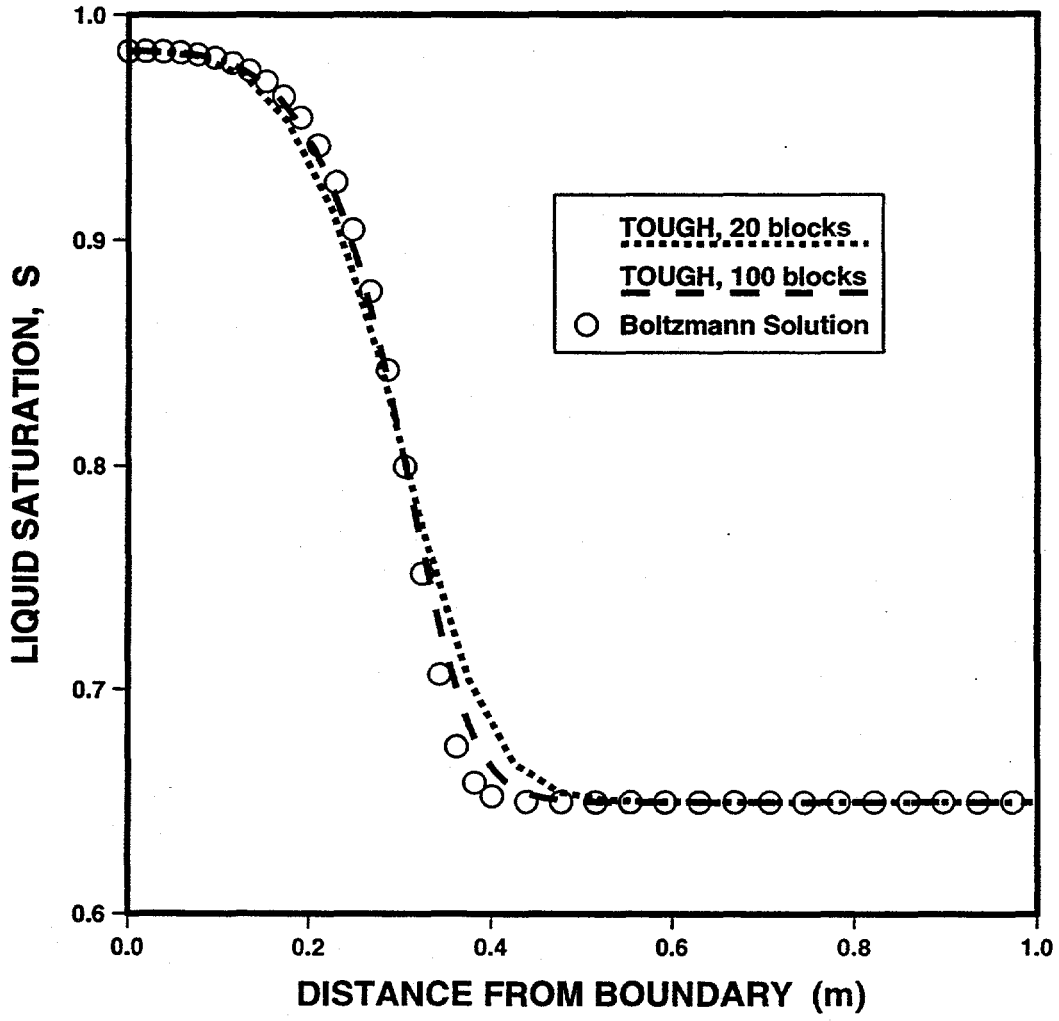

Fig. A4. Saturation profiles computed for one-dimensional absorption of water into a slab of Topopah Spring welded tuff. Properties and parameters are listed in Table A1. The elapsed time is 10^7 s.

Appendix B: Sorptive Lengths of Yucca Mountain Tuffs

The sorptive length L_s is a characteristic length in an unsaturated porous media at which the capillary and gravitational forces are of roughly the same magnitude. For lengths scales much less than L_s, capillary forces will dominate gravitational forces, whereas for length scales much larger than L_s, gravity will be the dominant force. If the diameter δ_m of a matrix block is much less than the sorptive length for that block, the gravitational term in the Richards equation can be ignored, and imbibition into the block can be assumed to be governed by capillary forces alone. The sorptive length is also of importance in other processes in which there is a combined influence of capillary suction and gravity. For example, consider the phenomenon of fingering, in which an initially uniform downward-moving imbibition front breaks up into one or more narrow fingers that travel at a much faster rate. This is an instability phenomenon which is caused when gravitational forces overtake capillary forces. The diameter of these finger-like flow perturbations can be shown to be, aside from a dimensionless multiplicative constant, equal to the sorptive length (Selker et al., 1992). Hence, if a matrix block is sufficiently small (i.e., $\delta_m \ll L_s$) so that gravity can be neglected in the Richards equation, the possibility of fingering within that block can also be ignored.

To derive a simple expression for the sorptive length, consider the full Richards equation for one-dimensional flow in the downward vertical direction, including both the capillary and gravitational gradients in the term for the flux (Hillel, 1980):

$$\frac{\partial}{\partial z}\left[\frac{kk_r(\psi)}{\mu\phi}\frac{\partial}{\partial z}\left(\psi(z,t)-\rho g z\right)\right] = \frac{\partial S(z,t)}{\partial t}, \qquad \text{(B1)}$$

where ρ is the density of the pore water, g is the gravitational acceleration, and the coordinate z points in the downward direction. The gradient that drives the flux of

water consists of two terms, the capillary pressure gradient, $\partial\psi/\partial z$, and the gravitational gradient, $\partial(\rho g z)/\partial z$. The order of magnitude of the capillary gradient within the matrix block can be estimated as $|\psi_a|/L$, where ψ_a is the characteristic potential that appears in the van Genuchten functions, and L is a characteristic length of the matrix block (in the vertical direction). The gravitational gradient is uniform throughout the block, and is equal to ρg. Equating the magnitudes of these two gradients leads to eq. (5), which states that

$$L_s = \frac{|\psi_a|}{\rho g}. \tag{B2}$$

According to this analysis, the sorptive length will depend on the hydrological properties of the rock, but not on the initial saturation.

A more careful analysis given by Philip (1987), which accounts for the variation of the capillary pressure gradient with saturation, yields the following expression for the sorptive length:

$$L_s = \frac{1}{\rho g\,[k_r(0) - k_r(\psi_i)]} \int_{\psi_i}^{0} k_r(\psi)\, d\psi. \tag{B3}$$

By this definition, the sorptive length depends on the initial saturation of the medium, through ψ_i. Division of both terms in eq. (B3) by ψ_i shows that eq. (B3) generalizes eq. (B2) by replacing ψ_a by the ratio of the average value of k_r over the range from 0 to ψ_i to the mean slope of k_r over this range of potentials. In the special case where $k_r = \exp(-\psi/\psi_a)$, the sorptive length given by eq. (B3) would agree with the simpler approximation given by eq. (B2). For a van Genuchten medium, Philip's expression takes the form

$$L_s = \frac{1}{\rho g\,[1-k_r(\psi_i)]} \int_{\psi_i}^{0} \frac{\{1-(\psi/\psi_a)^{n-1}[1+(\psi/\psi_a)^n]^{-m}\}^2}{[1+(\psi/\psi_a)^n]^{m/2}}\, d\psi\,. \qquad \text{(B4)}$$

This expression can be simplified slightly by utilizing the normalized capillary pressure, as defined in Appendix A,

$$\hat{\psi} = \frac{\psi}{\psi_a}\,, \qquad \text{(B5)}$$

in which case eq. (B4) can be written as

$$L_s = \frac{|\psi_a|}{\rho g\,[1-k_r(\hat{\psi}_i)]} \int_{0}^{\hat{\psi}_i} \frac{\{1-(\hat{\psi})^{n-1}[1+(\hat{\psi})^n]^{-m}\}^2}{[1+(\hat{\psi})^n]^{m/2}}\, d\hat{\psi}\,. \qquad \text{(B6)}$$

The integral appearing in eq. (B6) can be evaluated numerically for various values of $\hat{\psi}_i$, each of which correspond to a particular value of the initial saturation, through the capillary pressure equation, eq. (6). Note that L_s does not depend on the absolute permeability, the porosity, or the viscosity of the pore fluid.

Table B1 shows the computed sorptive lengths of various Yucca Mountain tuffs, along with their characteristic capillary pressures, ψ_a (taken from Rulon et al., 1986). The sorptive lengths were calculated by evaluating eq. (B6) numerically at two different saturations, and also by using the simpler expression (B2). In these calculations, the pore fluid density is taken to be $1000\,\mathrm{kg/m^3}$, and the gravitational aceleration is $g = 9.81\,\mathrm{m/s^2}$. For the three Yucca Mountain tuffs discussed in Table B1, Eqs. (B2) and (B3) give reasonably close values for L_s in the range of saturations that is probably of most interest at Yucca Mountain. Fig. B1 shows the sorptive length as a function of initial saturation, for various values of the van Genuchten n parameter,

normalized with respect to the approximate value $|\psi_a|/\rho g$; the curves therefore reflect the discrepancy between eqs. (B3) and (B6). For a broad range of initial saturations from about 0.30-0.90, the two methods give the same order-of-magnitude estimate for L_s, with the discrepancy increasing at very high or very low initial saturations. However, the purpose of calculating the sorptive length is to decide whether or not the gravitational term in the Richards equation can be neglected during matrix block imbibition. As the gravitational term can be ignored if $\delta_m \ll L_s$, a precise value for L_s is not needed. It therefore can be concluded from Table B1 and Fig. B1 that gravitational forces are negligible in any matrix block at Yucca Mountain which has a diameter less than about one meter.

Table B1. Sorptive lengths of various Yucca Mountain tuffs, at two different initial saturations. The van Genuchten parameters are taken from Rulon et al. (1986). The sorptive lengths at the two different initial saturations are calculated by evaluating eq. (B5) numerically. The last column contains the approximate sorptive length, computed from eq. (B1), which is independent of the initial saturation.

Rock type	$-\psi_a$ (Pa)	n	$S_i = 0.6$	$S_i = 0.8$	eq. (B1)
Paintbrush nonwelded	2.74×10^4	2.250	2.61 m	1.96 m	2.80 m
Topopah Spring welded	8.72×10^4	3.040	8.27 m	5.74 m	8.89 m
Calico Hills vitric	7.30×10^4	2.345	8.96 m	7.74 m	7.44 m

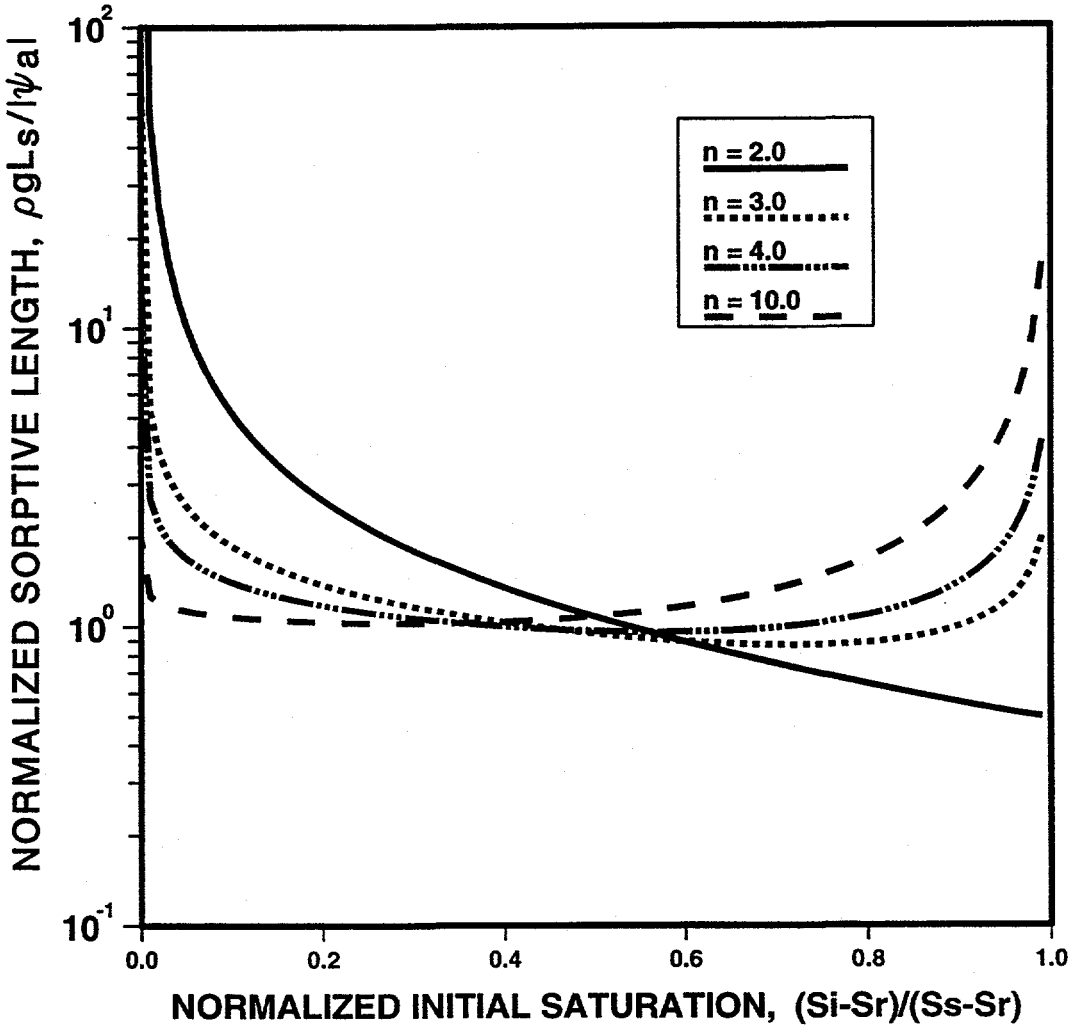

Fig. B1. Sorptive length of a van Genuchten medium, as a function of the initial saturation and the van Genuchten n parameter, normalized with respect to the approximate value $|\psi_a|/\rho g$. The curves are found from numerical integration of eq. (B6).

Appendix C: Matrix Equilibration Times for Yucca Mountain Tuffs

The main criterion for deciding if a fractured rock mass can be treated as an equivalent porous medium is whether or not the times scales of interest are long or short compared to the characteristic time scale of matrix imbibition. If the time scales of interest are long, then the matrix blocks will have sufficient time to equilibrate with their surrounding fractures, and the rock formation will behave as an equivalent porous medium. For shorter time scales, the pressures in the fractures and matrix blocks will not be equal, and transient interflow will be taking place. For these situations, dual-porosity simulations would be needed. In order to decide which of these two cases obtains, it is necessary to know the characteristic matrix equilibration times.

Zimmerman et al. (1990) derived approximate expressions for the time needed for sheet-like, cylindrical and spherical matrix blocks to fully saturate with water, under conditions where the boundary potential abruptly increases from ψ_i to 0. A scaling law was then proposed to extend this result to irregularly-shaped blocks. This scaling law involved a characteristic length scale of the matrix block, which was defined to be the ratio of the volume of the block V to its outer surface area A. For three-dimensional blocks, they found that the time needed for the matrix block to (essentially) achieve full saturation is given by (Zimmerman et al., 1990, eqs. 38-42, Fig. 7)

$$t_e = \frac{4n\mu\phi[m(S_s - S_r)]^{1/n}(V/A)^2(S_s - S_i)^m}{(n+1)|\psi_a|k}, \qquad \text{(C1)}$$

where the subscript e denotes the "equilibration" time, and the rock properties are those of the matrix block, not of the fractures.

As it will suffice to know merely the correct order of magnitude of the equilibration time, this expression can be simplified. First note that as it is generally the case that $S_s \approx 1$ and $S_r \approx 0$, and $n > 2$, the term $(S_s - S_r)^{1/n}$ can be ignored. Furthermore,

since $m = 1 - 1/n$, the term $m^{1/n}$ will always be close to unity, and so it too can be ignored. This is also true for the ratio $n/(n+1)$. Finally, as long as S_i is not too close to S_s (which is true almost by definition in the unsaturated zone), the term $(S_s - S_i)^m$ will also be of order one, which leaves

$$t_e \approx \frac{4\mu\phi(V/A)^2}{|\psi_a|k}. \tag{C2}$$

Eq. (C2) shows that the equilibration time is proportional to the porosity of the rock and the viscosity of the pore fluid, although this latter parameter will not vary substantially. It is inversely proportional to the permeability of the matrix rock, and inversely proportional to ψ_a, which measures the strength of the capillary suction. The equilibration time is proportional to the square of the characteristic size of the matrix block, V/A.

Another simple way to derive an expression for the matrix block equilibration time is to utilize a Warren-Root type equation for matrix imbibition. The admissibility of this procedure rests on the fact that although the Warren-Root equation is not accurate at early stages of imbibition, it does correctly predict the time eventually needed for the matrix block to equilibrate with the fractures (see Zimmerman et al., 1993). For unsaturated flow into a spherical matrix block of radius a, the Warren-Root equation (3) can be written as

$$\frac{d\psi_m}{dt} = \frac{\pi^2 D}{a^2}\psi_m, \tag{C3}$$

where we use the fact that $\psi_f = 0$ in the fractures that surround the matrix block. The unsaturated hydraulic diffusivity of the matrix can be related to the sorptivity as in eq.

(16):

$$D = \frac{\pi\sigma^2}{4\phi^2(S_s - S_i)^2}, \tag{C4}$$

and the sorptivity can be estimated from eq. (19) as

$$\sigma = \left[\frac{2m^{4/3}k\phi|\psi_a|}{\mu(S_s - S_r)}\right]^{1/2}\left[\frac{S_s - S_i}{S_s - S_r}\right]^{0.62-0.12m}. \tag{C5}$$

The initial condition for imbibition is that $\psi_m = \psi_i$ when $t = 0$, so the solution to eq. (C3) is

$$\psi_m(t) = \psi_i e^{-\pi^2 Dt/a^2}, \tag{C6}$$

where D is given through eqs. (C4,5). The time needed for the potential to decay to about 1% of its initial value can be found by setting the argument of the exponential to 4.6, since $e^{-4.6} \approx 0.01$. This procedure gives

$$t_e = \frac{9.2\mu\phi a^2(S_s - S_i)^{0.76+0.24m}(S_s - S_r)^{2.24-0.24m}}{\pi^3 m^{4/3} k|\psi_a|}. \tag{C7}$$

Again eliminating parameter-dependent terms that are of order one, we can simplify this to

$$t_e \approx \frac{9.2\mu\phi a^2(S_s - S_i)^{0.76+0.24m}}{\pi^3 k|\psi_a|}. \tag{C8}$$

We can generalize this result to non-spherical blocks by recognizing that $V/A = a/3$, and then replacing a^2 with $9(V/A)^2$. Ignoring the resulting numerical constant, which is $82.8/\pi^3 \approx 1$, we find

$$t_e \approx \frac{\mu\phi(V/A)^2(S_s - S_i)^{0.76+0.24m}}{|\psi_a|k} . \tag{C9}$$

Finally, we again assume that S_i is not too close to S_s, in which the saturation-dependent term can also be ignored, leaving

$$t_e \approx \frac{\mu\phi(V/A)^2}{|\psi_a|k} . \tag{C10}$$

Except for the factor 4, this expression agrees with that given in eq. (C2). For a conservative estimate of the equilibration time, eq. (C2) can be used.

Although the spherical matrix block is a useful mathematical idealization that allows the imbibition equation to be reduced to one variable, a cube is actually a more realistic model of a matrix block. If the spacing between successive fractures is L, then the matrix block volume would be L^3, the outer surface area would be $6L^2$, and so $(V/A)^2 = L^2/36$. In this case eq. (C2) can be written as

$$t_e \approx \frac{\mu\phi L^2}{9|\psi_a|k} . \tag{C11}$$

As the pore fluid viscosity μ does not depend on the properties of the matrix rock, and ϕ will usually be equal to 0.10, to within at most one order of magnitude, we see that the parameters that have the greatest effect on the matrix equilibration time are fracture

spacing, permeability, and the characteristic capillary pressure ψ_a.

The fact that both methods of estimating t_e led to nearly the same expression provides some evidence that the results are reasonable. Eq. (C11) can also be derived using dimensional analysis and simple physical arguments. We start by listing the dimensioned variables that are involved in the problem, and their dimensions in an [MPLT] system, in which mass, pressure, length and time are the basic dimensions: t_e [T]; μ [PT]; L [L]; k [L^2]; and ψ_a [P]. Since there are five variables and three dimensions (P, L, and T; M does not appear), the Buckingham pi theorem (Collins, 1990, p. 240) shows that two independent dimensionless ''pi-groups'' can be formed. Using the standard procedure, we find

$$\Pi_1 = \frac{t_e |\psi_a|}{\mu}, \tag{C12}$$

$$\Pi_2 = \frac{L^2}{k}. \tag{C13}$$

Hence there exists some functional relationship of the form $\Pi_1 = f(\Pi_2)$, or

$$\frac{t_e |\psi_a|}{\mu} = f(L^2/k). \tag{C14}$$

We now note that since the Richards equation is invariant under the transformation $\{t \rightarrow ct, k \rightarrow c^{-1}k\}$, for any constant c (as can be verified by direct substitution), t_e must depend inversely on k. [To prove this, consider that t_e is a function of k, i.e., $t_e = f(k)$. Now let $t \rightarrow ct$ and $k \rightarrow c^{-1}k$, which leaves solution to the imbibition problem unaltered, in which case $t_e \rightarrow ct_e$, and $ct_e = f(c^{-1}k)$. Since this holds for any

value of c, we can pick $c = k$, in which case we get $kt_e = f(1)$. But $f(1)$ is by definition a single constant, hence $kt_e = constant$.] The relationship between the two dimensionless groups in eq. (C14) must therefore be a linear relationship, i.e.,

$$\frac{t_e |\psi_a|}{\mu} = \tilde{C}\frac{L^2}{k}, \tag{C15}$$

where $\tilde{C}$ is some dimensionless constant. Finally, we note that, all other parameters being constant, the equilibration time should be proportional to the porosity. This can be proven, starting from eq. (5), by using reasoning similar to that used above to show that $t_e \approx 1/k$. This implies $\tilde{C} = C\phi$, in which case we can solve eq. (C15) to find

$$t_e = \frac{C\mu\phi L^2}{|\psi_a| k}. \tag{C16}$$

The preceding arguments give the same form for t_e as did the more detailed quantitative analyses, except that the value of the dimensionless constant C is not specified.

The estimated matrix block equilibration times for several Yucca Mountain tuffs are listed in Table C1, as calculated from eq. (C11). The pore fluid viscosity is taken to be 0.001 Pa s, which corresponds to a temperature of 20 °C. Fracture spacings of 0.1 m and 1.0 m are chosen for the calculations. The fracture spacings estimated by Wang and Narasimhan (1985) were about 0.2 m, which would lead to equilibration times four times larger than those calculated for $L = 0.1$ m.

Table C1. Matrix equilibration times (t_e) for various Yucca Mountain tuffs, calculated from eq. (C11), for different fracture spacings. The hydrological parameters are taken from Rulon et al. (1986). For ease of interpretation, times are not given in SI units (i.e., seconds), but in the unit most closely corresponding to the magnitude of t_e.

Rock type	ϕ	k (m^2)	$-\psi_a$ (Pa)	$L = 0.1$ m	$L = 1$ m
Paintbrush nonwelded	0.46	1.0×10^{-15}	2.74×10^{4}	5.2 hours	21.6 days
Topopah Spring welded	0.14	3.9×10^{-18}	8.72×10^{4}	5.3 days	1.45 years
Calico Hills vitric	0.37	5.0×10^{-16}	7.30×10^{4}	3.1 hours	13.0 days

Appendix D: Matrix Block Shape Factors

The general forms of both the Warren-Root and Vermeulen equations contain a parameter α that has dimensions of $[L^{-2}]$. It is therefore inversely proportional to the square of some suitably-defined characteristic length scale of the matrix block. Even for the case of a constant diffusion coefficient, which has received the most study, the proper choice of this parameter has been the source of controversy. Barenblatt et al. (1960), Warren and Root (1963), and Moench (1984) suggested leaving α as an open parameter whose value is found by fitting field data to the predictions of the dual-porosity model. One difficulty with this approach is that, if the matrix blocks are distributed over different sizes and shape classes, the overall behavior of a formation will *not* be characterizable by a single value of α (Hayot and Lafolie, 1993). It would therefore be useful to be able to determine the correct values of α corresponding to matrix blocks having specific sizes and shapes.

For cubical matrix blocks of length L, Warren and Root (1963) proposed the value $\alpha = 60/L^2$. Their derivation was somewhat ad hoc, however, and cannot be generalized to other shapes. A more extensive discussion of the relationship between α and block geometry was given by deSwaan (1990). He suggested choosing the value of α so that the Warren-Root equation correctly predicts the time at which the imbibition process is 50% complete. In other words, the exact solution and the Warren-Root solution were forced to agree at one, arbitrarily chosen, point in time. This approach has the effect of making the Warren-Root method relatively accurate for some intermediate time regime, for the particular case of a step-function change in the fracture pressure. The asymptotic quasi-steady-state flux will, however, be off by some multiplicative constant.

One simple and reasonable criterion that can be imposed on the choice of α is that the appropriate value of α should lead to the correct imbibition rate in the long-time, quasi-steady-state regime. This approach was proposed by van Genuchten and

Dalton (1986); see also Barker (1985). They found the long-time asymptotic behavior for flow into spherical, cylindrical, and sheet-like matrix blocks by examining the behavior of the step-function response in Laplace-space, for small values of the Laplace parameter s. The relationship between the large-time behavior of a function and the behavior of its Laplace transform for small values of s is discussed by Latta (1974, p. 639) and Chen and Stone (1993). The relationship between α and matrix block geometry can be analyzed in the time domain, rather than the Laplace domain, as follows. Start with the pressure-diffusion equation in the form

$$\nabla^2 \psi(\mathbf{x}, t) = \frac{1}{D} \frac{\partial \psi}{\partial t}, \tag{D1}$$

where $\mathbf{x}$ is the position vector of a generic point in the block, and D is the diffusivity. To make this problem tractable, we assume that the diffusion coefficient is constant. This should cause no loss in generality, as the shape factor α is a geometric property of the matrix block, and does not depend on the hydrological properties of the rock. The boundary and initial conditions are

$$\psi(\mathbf{x}, t = 0) = \psi_i , \tag{D2}$$

$$\psi(\mathbf{x} \in \Gamma, t > 0) = 0 , \tag{D3}$$

where Γ denotes the outer boundary of the block. Using the method of separation of variables, we search for solutions to eq. (D1) that have the form $\psi(\mathbf{x}, t) = F(\mathbf{x})G(t)$. The standard procedure (see Dettman, 1962, pp. 108-116) then leads to

$$\frac{\nabla^2 F(\mathbf{x})}{F(\mathbf{x})} = \frac{1}{D}\frac{G'(t)}{G(t)} = -\lambda, \tag{D4}$$

where λ must be a constant that does not depend on $\mathbf{x}$ or t. The functions $F(\mathbf{x})$ must therefore satisfy the equation

$$\nabla^2 F(\mathbf{x}) = -\lambda F(\mathbf{x}), \tag{D5}$$

along with the boundary condition

$$F(\mathbf{x}) = 0 \quad \text{for all } \mathbf{x} \in \Gamma. \tag{D6}$$

The values of λ are therefore the eigenvalues of the Laplacian operator for the region interior to Γ, with Dirichlet-type boundary conditions. Only for geometrically simple shapes can the eigenvalues be found explicitly. Nevertheless, there will always be an infinite set of eigenvalues λ_n, each corresponding to one or more eigenfunctions $F_n(\mathbf{x})$. For a finite-sized body, the eigenvalues will be discrete and positive, and can be labeled as $\lambda_1 < \lambda_2 < \cdots$ (see Dettman, 1962, pp. 110). In certain cases an eigenvalue can have more than one independent eigenfunction associated with it. This possibility is of no importance in finding the α parameter, so we ignore it. From eq. (D4) the functions $G_n(t)$ can be found to be $\exp(-\lambda_n D t)$. Hence the general solution to eq. (D1) can be written as

$$\psi(\mathbf{x}, t) = \sum_{n=0}^{\infty} C_n F_n(\mathbf{x}) e^{-\lambda_n D t}, \tag{D7}$$

where the C_n are constants. The C_n are found from the initial conditions, although

their precise values are not relevant to the determination of α.

The important point is that, for large times, the term involving λ_1 will dominate the series, since the other terms, corresponding to higher eigenvalues, will be exponentially smaller. The long-time behavior of the matrix block is therefore dominated by the smallest eigenvalue, $\lambda_1 \equiv \lambda_{min}$. Comparison of eq. (D7) with eqs. (3) and (C3) shows that, in order to give the correct long-time behavior, the parameter α should be chosen to equal λ_{min}. These minimum eigenvalues can be found for various simple shapes from the solutions compiled by Crank (1975) and Carslaw and Jaeger (1959). For example, $\alpha = \pi^2/a^2$ for a sphere of radius a; $\alpha = \pi^2/L^2$ for a thin sheet of thickness L; $\alpha = 3\pi^2/L^2$ for a cubical block of length L; and $\alpha = z_1^2/a^2$ for a long cylinder of radius a, where $z_1 = 2.405$ is the first positive root of the Bessel function $J_o(z)$.

For more general shapes, for which the minimum eigenvalue λ_{min} cannot be found explicitly, it would be useful to have an approximate rule-of-thumb for estimating α. Zimmerman et al. (1990) suggested the following procedure. For a spherical block of radius a, the volume/area ratio V/A is equal to $a/3$. Hence so $a = 3V/A$, and the parameter $\alpha = \pi^2/a^2$ can be written as

$$\alpha = \frac{\pi^2/9}{(V/A)^2}. \qquad \text{(D8)}$$

Eq. (D8) can be used for arbitrarily-shaped blocks, provided the appropriate value of V/A is used. It is of course necessary to examine the extent to which this approximation holds for realistically-shaped blocks. Whereas soils, for example, may contain very irregularly-shaped microporous aggregate particles which play the role of matrix blocks (van Genuchten and Dalton, 1986), the matrix blocks at Yucca Mountain are most likely three-dimensional polygons (see Wang and Narasimhan, 1985). Although we cannot test this approximation for arbitrarily-shaped polygons, we can test it for

blocks that are shaped like rectangular parallelepipeds, which will be the case if the fracture sets are orthogonal. In this case we can compare the proposed approximation (D8) to the exact known result (Carslaw and Jaeger, 1959, p. 187):

$$\alpha_{exact} = \lambda_{\min} = \pi^2 \left[\frac{1}{L_1^2} + \frac{1}{L_2^2} + \frac{1}{L_3^2} \right], \tag{D9}$$

where L_1, L_2, and L_3 are the lengths of the three sides of the matrix block. The volume of the matrix block is $L_1 L_2 L_3$, and its outer surface area is $2(L_1 L_2 + L_2 L_3 + L_3 L_1)$, so the approximation (D8) yields

$$\alpha_{apprx} = \frac{4\pi^2}{9} \left[\frac{1}{L_1} + \frac{1}{L_2} + \frac{1}{L_3} \right]^2. \tag{D10}$$

The ratio of the approximate value of α to the exact value is

$$\frac{\alpha_{app}}{\alpha_{exa}} = \frac{4(L_1 L_2 + L_2 L_3 + L_3 L_1)^2}{9[(L_1 L_2)^2 + (L_2 L_3)^2 + (L_3 L_1)^2]}. \tag{D11}$$

The ratio in eq. (D11) takes on maximum or minimum values when the ratios of the three lengths take on their limiting values, i.e., $L_1 = L_2 \gg L_3$, etc. Table D1 summarizes these extreme cases, along with one arbitrarily chosen example. The table shows that the approximation (D8) is reasonably accurate; in particular, in no case does it grossly underpredict or overpredict the value of α. Since these cases cover a large range of aspect ratios of the matrix blocks, from sheets to cubes to long prisms, it seems reasonable to use expression (D8) in the general case, when the fracture sets

might not be orthogonal.

Another possible method of estimating α would be to utilize certain upper and lower bounds that have been established for λ_{min}. These bounds are expressed in terms of geometric parameters such as the block volume, the radius of the largest sphere that can be inscribed within the block, etc. Knowledge of the value of the outer surface area A cannot be used to calculate bounds on λ_{min}, as λ_{min} is not greatly affected by A. This can be explained as follows. The amount of surface area is very sensitive to roughness of the fracture surfaces, whereas the volume of the matrix block will not be affected by roughness. In fractal models, for example, a block that has a finite volume may in fact have an infinite surface area (Korvin, 1992). But the equilibration time for a matrix block should depend on its gross geometry, and not on its superficial roughness (see Fig. D1). Hence, A is not a parameter that can appear in rigorous bounds on λ_{min}. Two potentially useful bounds on λ_{min} are the following (Garabedian, 1964, Chapter 11):

$$\frac{\pi^2}{r_{eq}^2} \leq \lambda_{min} \leq \frac{\pi^2}{r_{in}^2} , \tag{D12}$$

where r_{in} is the radius of the largest sphere that can be inscribed within the block (see Fig. D2), and r_{eq} is the radius of the sphere that has the same volume as the block, i.e.,

$$r_{eq} = \left[\frac{3V}{4\pi}\right]^{1/3} . \tag{D13}$$

It is also true that π^2/r_{ex}^2 provides a lower bound to λ_{min}, where r_{ex} is the smallest sphere that can be superscribed around the block (see Fig. D2). However, as r_{ex}

cannot be less than r_{eq}, this lower bound is not as restrictive as the one given in eq. (E12), and is therefore not as useful.

As an example of the use of the bounds given in eq. (D12), consider a cube of length L. The volume of the cube is L^3, and the largest sphere that can be inscribed in the cube has radius $L/2$, so eqs. (D12,13) yield

$$\left[\frac{4\pi}{3}\right]^{2/3}\frac{\pi^2}{L^2} = \frac{2.60\pi^2}{L^2} \le \lambda_{\min} = \frac{3\pi^2}{L^2} \le \frac{4\pi^2}{L^2}. \tag{D14}$$

In this case, the bounds are reasonably close. In fact, the arithmetic mean of the two bounds would narrow down the estimate of $\lambda_{\min}$ to

$$\lambda_{\min} = (3.30 \pm 0.70)\frac{\pi^2}{L^2}, \tag{D15}$$

which is a maximum possible error (assuming that the correct value was unknown) of only 26%. The actual error incurred by using the arithmetic mean of the bounds, however, is only 10% in this case. Unfortunately, these bounds become very far apart for sheet-like or prismatic blocks, for instance. Consider a long cylindrical block of radius a and length L, where $L \to \infty$. The largest sphere than can be inscribed inside the cylinder would also have radius a. As $L \to \infty$, the volume of the block becomes infinite, and subsequently r_{eq} would become infinite; eq. (D12) would then give

$$0 \le \lambda_{\min} = \frac{(2.405)^2}{a^2} = \frac{5.78}{a^2} \le \frac{\pi^2}{a^2} = \frac{9.87}{a^2}, \tag{D16}$$

where, as mentioned above, 2.405 is the first positive root of the Bessel function $J_o(z)$.

The upper bound overestimates λ_{min} by 71%, whereas the lower bound is trivial and contains no information. The scaling law described by eq. (D8), however, yields an estimate of $4.39/a^2$, which is only 24% less than the actual value. We conclude from this and similar examples that whereas eq. (D8) is not a rigorous approximation in any strict sense, it will generally yield reasonably accurate estimates of λ_{min}.

Table D1. Relationship between geometry of the matrix block and the value of the α parameter. The matrix blocks are parallelepipeds with sides of length L_1, L_2, and L_3. The exact value of α is computed from eq. (D9), and the approximate value is computed from eq. (D10). The approximate expression is always within about a factor of two of the exact value.

Fracture spacing	Block shape	α(exact)	α(approx)	$\alpha_{app}/\alpha_{exa}$
$L_1=L_2=L_3$	cube	$\frac{3\pi^2}{L_3^2}$	$\frac{4\pi^2}{L_3^2}$	4/3
$L_1=L_2\gg L_3$	sheet	$\frac{\pi^2}{L_3^2}$	$\frac{4\pi^2}{9L_3^2}$	4/9
$L_1\gg L_2=L_3$	long prism	$\frac{2\pi^2}{L_3^2}$	$\frac{16\pi^2}{9L_3^2}$	8/9
$L_1=2L_2=3L_3$	arbitrary example	$\frac{14\pi^2}{9L_3^2}$	$\frac{16\pi^2}{9L_3^2}$	8/7

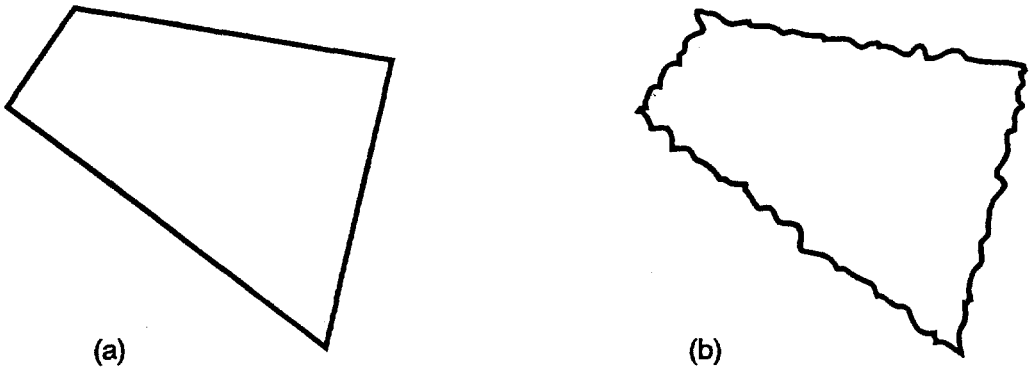

Fig. D1. The two blocks shown above have the same volume, and have essentially the same macroscopic shape. It can be proven, using the bounding methods described in the text and in Fig. D2, that their shape factors will be nearly equal. However, block (b) has a much larger surface area, if measured on a micro-scale. Hence, when using approximations such as eq. (D8) to estimate shape factors, a ''smoothed-out'' surface area should be used; this is equivalent to replacing block (b) with block (a) before calculating the surface area. If the surface area estimates are based on measured distances between fractures, this problem will not arise.

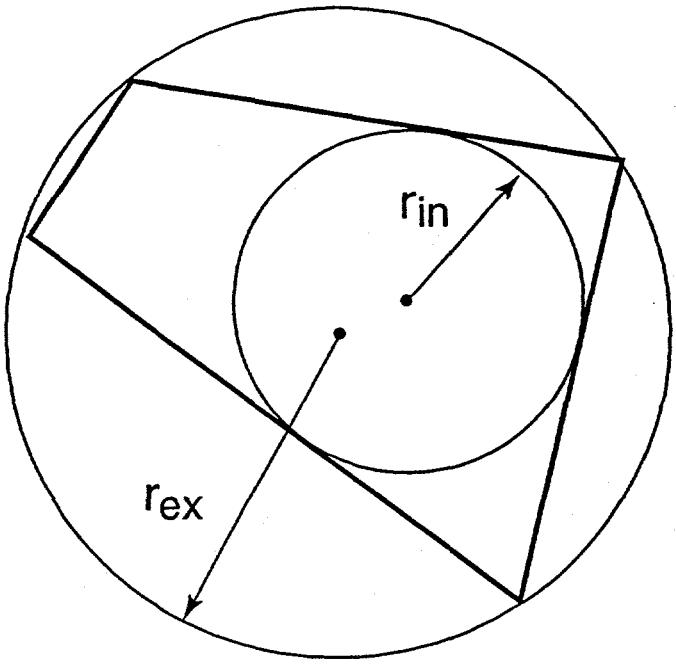

ESD-9404-0003

Fig. D2. An arbitrarily-shaped matrix block, along with the largest sphere that can be inscribed within it, and the smallest sphere that can be superscribed around it. The radii of these two spheres, r_{in} and r_{ex}, can be used to provide bounds on the shape factor for the matrix block: $\pi^2/r_{in}^2 < \alpha < \pi^2/r_{ex}^2$.

Appendix E: Effect of Air on Imbibition of Water

The question of whether or not air will impede the imbibition of water into an initially unsaturated rock has been the subject of much study (cf., Adrian and Franzini, 1966; Phuc and Morel-Seytoux, 1972; Constantz et al., 1988). Before attempting to answer this question, it is necessary to formulate it more precisely. Physically, those portions of the void space of a rock or soil lying above the water table that are not occupied by water will be occupied by air. It is the existence of the two components, water and air, along with the interface between them, that gives rise to the capillary pressure phenomena, the negative pressure in the water phase, and thus the driving force needed in order for water to be imbibed by suction into the rock. Furthermore, those portions of the void space that are initially filled with air provide the space to accommodate the water as it imbibes into the rock. As this occurs, of course, the air must somehow flow out of these regions of the pore space. Nevertheless, it is clear that the entire process of water imbibition into a matrix block cannot occur without the presence of the air component.

In order to ask whether or not air impedes the imbibition process, one must specify an alternative process to be used for comparison. Since, almost by definition, imbibition in the unsaturated zone does not occur in the absence of air, in a certain sense the question is not physically meaningful. However, it is meaningful in the following mathematical sense. As mentioned in the main text, and in Appendix A, the flow of water is usually modeled by assuming that the air phase is infinitely mobile, and at a uniform pressure. This leads to the Richards equation as the governing equation for the saturation and pressure of the water component. The question can then be raised as to whether or not solutions to the Richards equation will accurately reflect the imbibition process. Alternatively, the question can be raised as to the relation between the solutions to the Richards equation and the solutions to the full pair of coupled equations describing the motion of the water and air components. This is what is

actually meant by the question of whether or not air impedes the imbibition of water into a matrix block.

Simultaneous flow of water and air in a porous medium is usually thought to be described by the following equations:

$$\frac{\partial}{\partial x}\left[\frac{kk_{rl}(\psi_l)}{\mu\phi}\frac{\partial\psi_l}{\partial x}\right] = \frac{\partial S_l(x,t)}{\partial t}, \tag{E1}$$

$$\frac{\partial}{\partial x}\left[\frac{kk_{rv}(\psi_v)}{\mu\phi}\frac{\partial\psi_v}{\partial x}\right] = \frac{\partial S_v(x,t)}{\partial t}, \tag{E2}$$

where the subscript l denotes the liquid phase (water), and the subscript v denotes the vapor phase (air). These equations are coupled through the relations (see de Marsily, 1986, p. 215)

$$S_l + S_v = 1, \tag{E3}$$

which reflects the fact that no other components are assumed to be present, and

$$\psi_l - \psi_v = \psi_c(S_l), \tag{E4}$$

in which the capillary pressure function $\psi_c(S_l)$ is described by an equation such as that of van Genuchten (1980), Brooks and Corey (1966), etc. If the air pressure is assumed to be constant, then $\partial\psi_l/\partial x = \partial\psi_c/\partial x$, and eq. (E1) will be equivalent to eq. (5). In this approximation, the mass balance equation for the air, (E2), is not quite satisfied, since the term $\partial\psi_v/\partial x$ will be zero, whereas the term $\partial S_v/\partial t$ will be nonzero.

However, it is customary to ignore eq. (E2) in this approximation. The TOUGH simulator (Pruess, 1987) in effect solves both eq. (E1) and eq. (E2), since they represent conservation of mass for the two components. TOUGH also solves an energy balance equation, although this equation is essentially superfluous in isothermal flow problems. This is because, since internal energy depends strongly on temperature, but only weakly on pressure, extremely small temperature changes are needed to balance out the changes in energy that accompany the variations in pressure.

Although the Richards model is widely used, different physical interpretations have been given for the approximations embodied in it. The common explanation is that the air is infinitely mobile, and will flow instantaneously in response to the smallest of pressure gradients (McWhorter, 1971; Touma and Vauclin, 1986). de Marsily (1986), on the other hand, interprets the Richards model as assuming that the air phase is *immobile*, in which case eq. (E2) is *automatically* satisfied. This is in some ways a more consistent interpretation for our purposes, as we assume that no air from the matrix enters the fracture network, and the fracture/matrix interflow consists only of water. In order to use this interpretation, however, we must ignore the fact that an immobile gas, when forced into a smaller volume, will undergo a pressure increase, thus invalidating the assumption of constant pressure in the air phase. Hence it seems that no interpretation is free from inconsistencies. Moreover, the existing experimental and theoretical evidence concerning the air-impedance effect seems to be contradictory and inconclusive.

In order to test whether or not eqs. (E4) can be ignored during an imbibition process, we have used TOUGH to run a pair of imbibition simulations for a matrix block comprised of Topopah Spring welded tuff. One of the outer boundaries of the matrix block is connected to a very large source block that initially has an air-phase pressure of 1.0×10^5 Pa, and a capillary presssure of zero. The other boundary is impermeable, which models the effect of a no-flow symmetry boundary in a finite-sized matrix

block. The gridblocks that represent the slab of tuff are initially at an air phase pressure of 1.0×10^5 Pa, but at a liquid saturation of 0.65. This saturation corresponds, through the capillary pressure function, to a capillary pressure of -1.062×10^5 Pa, which implies a liquid phase pressure of $1.0-1.062=-0.062\times10^5$ Pa. Hence, there is a pressure gradient in the liquid phase that drives water into the slab from the source block. In one of the simulations, each gridblock is connected to a very large sink gridblock that has an initial air-phase pressure of 1×10^5 Pa, a liquid saturation of 0.0, and has a value of $\psi_a=0$, i.e., no capillary pressure effect. Hence, the potential of water in the sink block would be 1.0×10^5 Pa, in which case water will not flow from the slab into the sink block. The air-phase pressure gradient, however, will be such that air will flow from each slab gridblock into the sink block. This has the effect of short-circuiting the air flow out of the slab, and maintaining the air at a uniform pressure. This case essentially corresponds to solving the Richards equation. Comparison of the imbibition rates in the two cases described above provides an estimate of the extent to which the air ''impedes'' the flow of water.

The parameters used in the simulations are listed in Table A1. They are taken from Rulon et al. (1986), and represent a welded tuff from the Topopah Spring unit at Yucca Mountain. The computed pressure profiles for the water and air components are shown in Figs. E1 and E2. The liquid phase pressure profiles are similar, although they diverge somewhat as time progresses. In the simulation in which the air is ''short-circuited'' out of the slab, the air phase pressure is nearly uniform at 1.0×10^5 Pa. In the other simulation, the air is compressed slightly ahead of the liquid imbibition front, creating a gradient that drives some air into the slab, and some air out of the slab in a counter-flow direction to the liquid. The induced air-phase pressures are relatively small, since, due to the low viscosity of air, only a small gradient is needed drive the air out of the block. The computed liquid imbibition rates are shown in Fig. E3, which shows that the air has only a slightly inhibiting effect on liquid

imbibition. These results, which should not depend in any qualititave way on on the geometry of the matrix block, seem to show that as long as the flow process is governed by the usual continuum field equations, and as long as the liquid-phase pressure is not greater than the air-phase pressure, the use of the Richards equation will not lead to appreciable errors in the predicted imbibition rates.

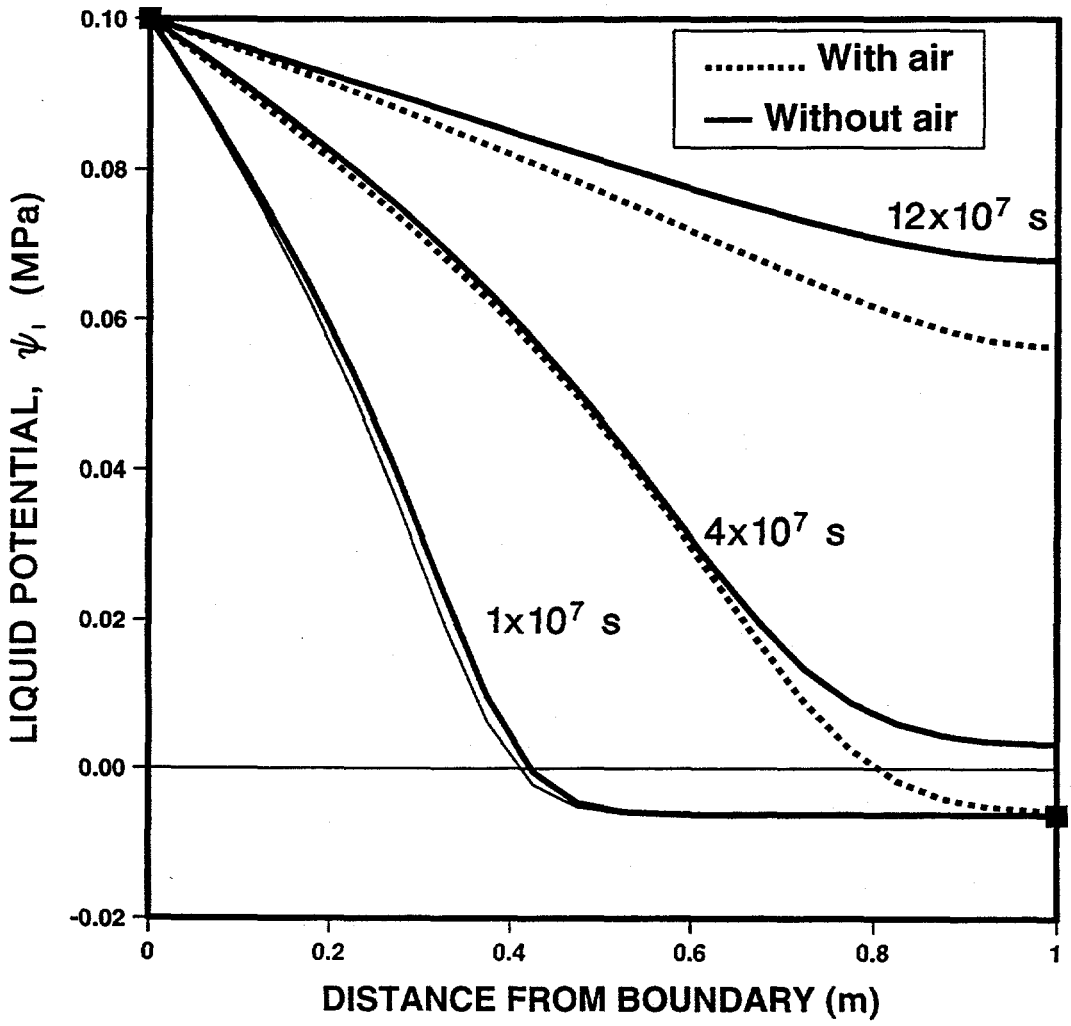

Fig. E1. Pressure profile in the liquid phase, during one-dimensional horizontal imbibition into a slab of Topopah Spring welded tuff. The parameters, initial conditions, etc., are shown in Table A1. There is a no-flow boundary at $x = 1.0$ m, which models simultaneous imbibition from both faces into a 2.0 m–thick slab. The individual gridblocks are each of width 5 cm. In one simulation the air-phase pressure is maintained at 1.0×10^5 Pa, as described in the text.

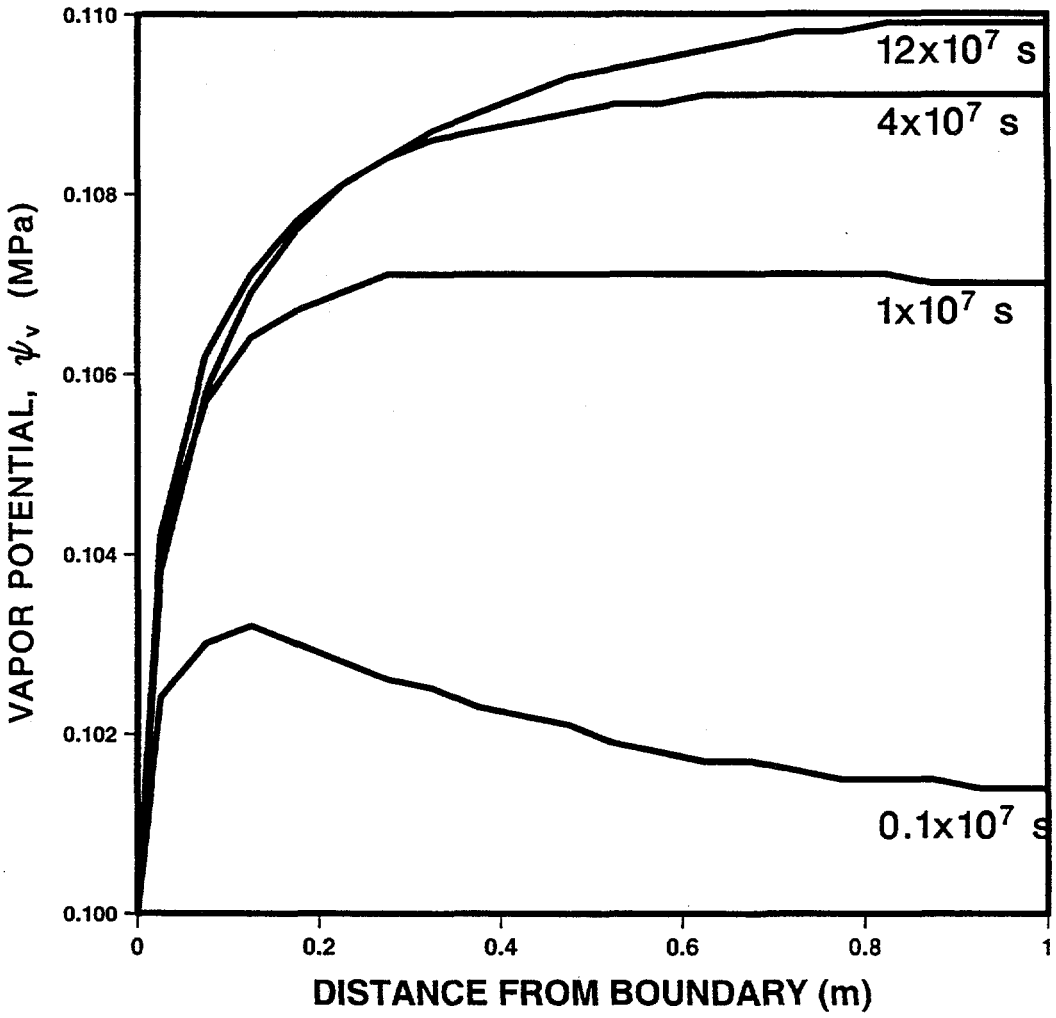

Fig. E2. Pressure profile in the air phase, for same problem as shown in Fig. E1. For the case in which the air is allowed to escape from each gridblock, the air phase pressure is essentially constant at 1.0×10^5 Pa. Note that the air phase pressure reaches its maximum value at a point slightly ahead of the location of the wetting front (compare Figs. E1 and E2).

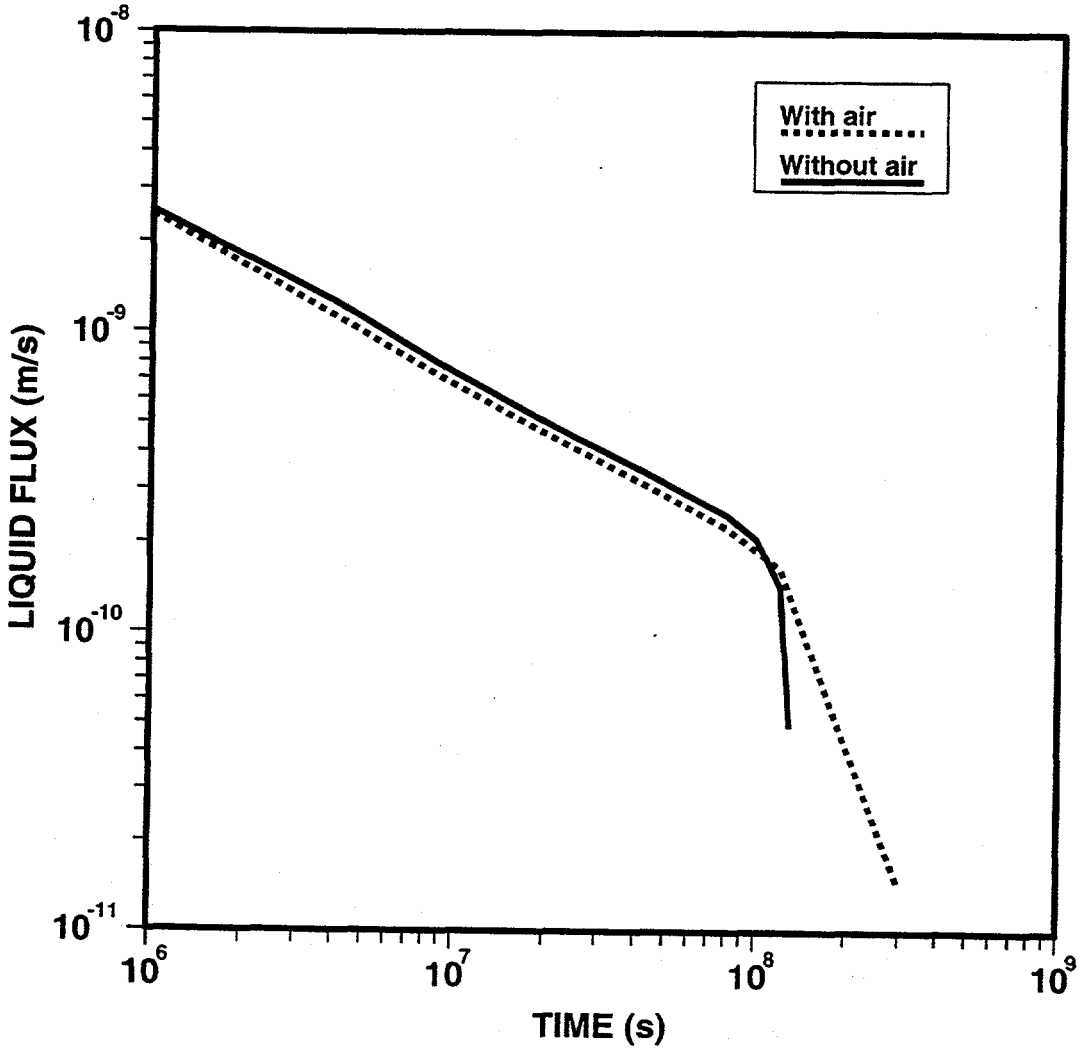

Fig. E3. Imbibition rates of liquid into the slab, for the two cases described in text and Figs. E1 and E2. At early times, the imbibition rate are proportional to $t^{-1/2}$, as described in Appendix G. At later times, as the block fills with water, the imbibition rate declines to zero. Except at very large times, the presence of air has a minimal effect on the liquid imbibition rate.

Appendix F: Comparison of van Genuchten and Brooks-Corey Sorptivities

The sorptivity is defined by eq. (17) as a measure of the rate of imbibition into a one-dimensional unsaturated porous medium. The medium is assumed to be initially at a uniform saturation, and is then abruptly subjected to a capillary potential of zero at its outer boundary. The governing differential equation and the boundary conditions for this problem are given by eqs. (11-15). These equations must be supplemented by specific algebraic forms for the capillary pressure and relative permeability functions, in order to find an actual solution. As the imbibition rate will be proportional to $t^{-1/2}$, and to the wetted surface area A, the sorptivity σ is defined by eq. (17), which is repeated here for convenience:

$$q = \frac{A\sigma}{2t^{1/2}}. \tag{F1}$$

Two commonly used forms for the characteristic functions of an unsaturated medium are those that have been proposed by Brooks and Corey (1966), and by Mualem (1976) and van Genuchten (1980). They differ mainly in that the Brooks-Corey capillary pressure curve exhibits a finite air-entry pressure, whereas the van Genuchten capillary pressure curve gives the capillary pressure as a continuous function of saturation. According to the van Genuchten model, any negative suction will allow a certain amount of air to enter the rock, causing the liquid saturation to fall below 100%. According to the Brooks-Corey functions, air cannot enter the rock until the suction reaches a certain threshold value, known as the air-entry pressure, ψ_{ae}. If we adhere to the convention that $\psi<0$ in the unsaturated region, then ψ_{ae} will also be negative. The van Genuchten functions are given by eqs. (7,8), which are repeated here for convenience:

$$\hat{S}(\psi) = [1+(\psi/\psi_a)^n]^{-m} \ , \tag{F2}$$

$$k_r(\psi) = \frac{\{1-(\psi/\psi_a)^{n-1}[1+(\psi/\psi_a)^n]^{-m}\}^2}{[1+(\psi/\psi_a)^n]^{m/2}} \ , \tag{F3}$$

where the normalized saturation is given by $\hat{S} = (S - S_r)/(S_s - S_r)$. The Brooks-Corey functions can be written as (see Brooks and Corey, 1966; Zimmerman and Bodvarsson, 1991a)

$$\hat{S}(\psi) = \begin{cases} 1 & \text{if} \quad (\psi/\psi_{ae}) \le 1 \\ (\psi/\psi_{ae})^{-\lambda} & \text{if} \quad (\psi/\psi_{ae}) > 1 \, , \end{cases} \tag{F4}$$

$$k_r(\psi) = \begin{cases} 1 & \text{if} \quad (\psi/\psi_{ae}) \le 1 \\ (\psi/\psi_{ae})^{-3\lambda+2} & \text{if} \quad (\psi/\psi_{ae}) > 1 \, . \end{cases} \tag{F5}$$

Although the capillary pressure curves predicted by the two models differ qualitatively in the region of low capillary pressures, they both predict a power-law relation between $\hat{S}$ and ψ at very large capillary pressures. This makes it possible to match the two models in the low saturation region, as shown by Wang (1992). First consider the van Genuchten capillary pressure function in the limit of large negative values of ψ:

$$\hat{S}(\psi) = [1+(\psi/\psi_a)^n]^{-m} \approx (\psi/\psi_a)^{-mn} = (\psi/\psi_a)^{-(n-1)} , \tag{F6}$$

where we use the fact that $m = 1 - 1/n$ in the van Genuchten model. Comparison of eqs. (F4) and (F6) shows that the two models agree if we set

$$\psi_{ae} = \psi_a \,, \tag{F7}$$

$$\lambda = n - 1 \,. \tag{F8}$$

Note that although the parameter ψ_a in the van Genuchten model does not have the same physical interpretation as does the air-entry pressure ψ_{ae} in the Brooks-Corey model, they both play a similar role as scaling factors for the capillary pressure. Also, if the parameters of the functions are found by fitting the curves to water retention data, it seems reasonable that the resulting parameters would satisfy conditions (F7) and (F8). We will therefore assume that these relations hold, and will write the Brooks-Corey functions in terms of ψ_a and n. Note also that although relations (F7,8) cause the capillary pressure curves to agree at low saturations, the relative permeability curves do not quite coincide. Figs. F1 and F2 show comparisons between the characteristic curves of the two models, assuming that eqs. (F7,8) hold.

The sorptivities associated with the Brooks-Corey and van Genuchten models can be found by numerically integrating the Richards equation, as described in Appendix A. The results are shown in normalized form in Fig. F3, for the case $n = 3, \lambda = 2$. For simplicity, we assume that $S_s = 1$ and $S_r = 0$ in this example. The normalized sorptivity σ^* is defined by

$$\sigma^* = \left[\frac{2|\psi_a|\phi k}{\mu} \right]^{-1/2} \sigma \,, \tag{F9}$$

as in eq. (A20). As might be expected, the qualitatively different forms of the two capillary pressure curves in the high-saturation region causes the two sorptivity curves to behave differently near $S_i = 1$. However, this is difficult to see in Fig. F3, since the different behavior is highly localized near $S_i = 1$. Approximate analytical methods (see Parlange et al., 1991,1992; Zimmerman and Bodvarsson, 1991a,1991b) tend to show that the Brooks-Corey sorptivity varies as $(1-S_i)^{1/2}$ in the high-saturation region, whereas the Van Genuchten sorptivity varies as $(1-S_i)^{1/2+1/2n}$. The exponents agree as $n \to \infty$, but differ somewhat at the lower values of n that are typical of Yucca Mountain tuffs (see Wang, 1992). However, this range of high initial saturations does not seem to be of much importance for the unsaturated zone at Yucca Mountain, where initial matrix block saturations are probably in the range of $0.4-0.8$ (Wittwer et al., 1993).

The interesting aspect of the results plotted in Fig. F3 is that at intermediate and lower initial saturations, the Brooks-Corey and van Genuchten sorptivities converge. From this, we conclude that although the two models yield different predictions for the characteristic curves, they will yield very similar predictions for the sorptivity, which is the parameter that most closely controls the rate of fluid exchange between the fractures and the matrix blocks. This is particularly true in the range of initial saturations that are of most interest at Yucca Mountain.

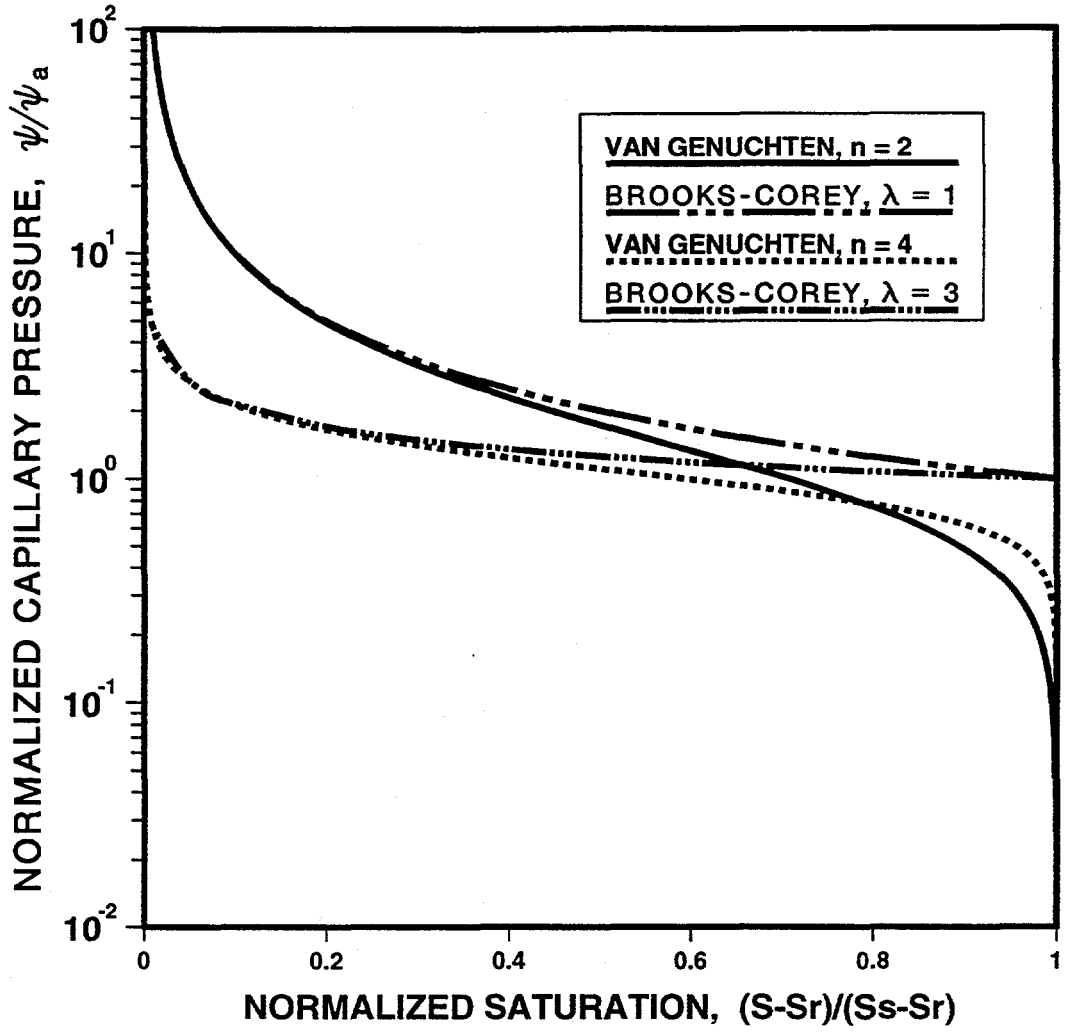

Fig. F1. Normalized capillary pressure curves of the van Genuchten and Brooks-Corey type. The Brooks-Corey curves exhibit an abrupt air-entry pressure at $\psi = \psi_a$, whereas the van Genuchten curves are continuous functions of ψ. If the van Genuchten n parameter and the Brooks-Corey λ parameter are related by $\lambda = n - 1$, the curves will coincide asymptotically at low saturations.

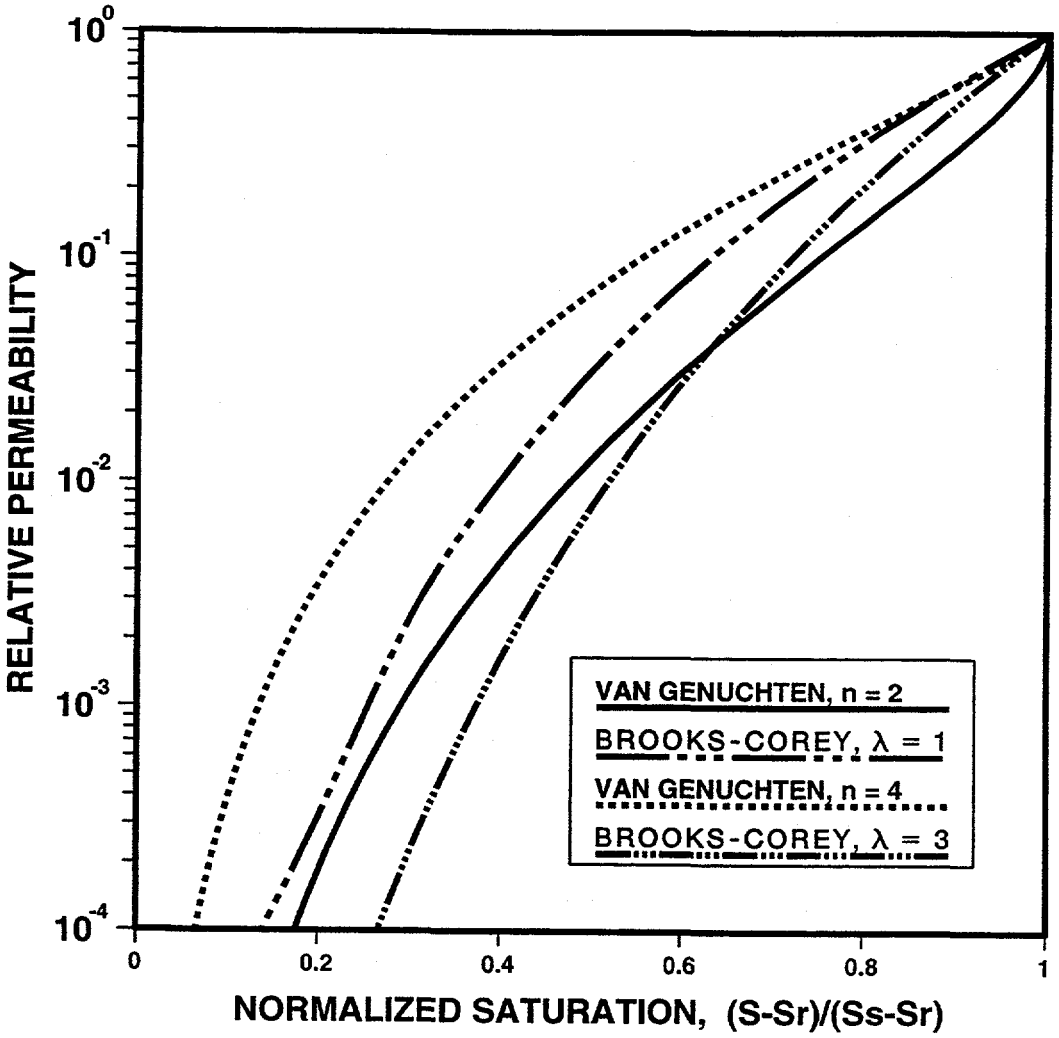

Fig. F2. Relative permeability curves of the van Genuchten and Brooks-Corey type. The choice $\lambda = n - 1$, which causes the capillary pressure curves to agree at low saturations, does not cause the relative permeability curves to coalesce.

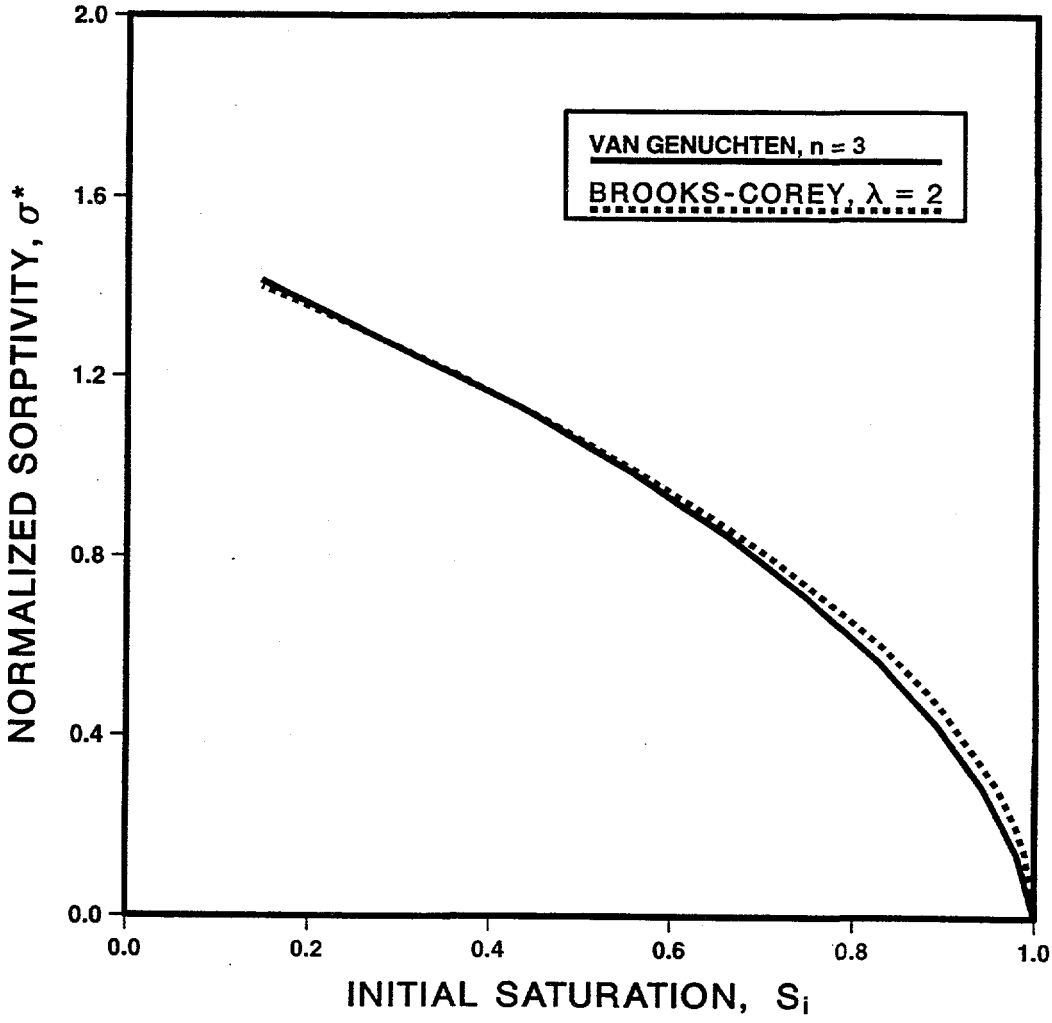

Fig. F3. Normalized sorptivities of van Genuchten and Brooks-Corey media, computed using the Boltzmann transformation method described in Appendix A. Normalized sorptivity is defined by eq. (F9). By choosing $\lambda = n - 1$, the sorptivities agree closely, particularly at low-to-moderate values of the initial saturation. At high initial saturations, where the sorptivities are very low, the two curves have different power-law behaviors.

Nomenclature

Roman letters

a radius of cylinder or sphere, half-thickness of slab [m]

A surface area of block; gridblock interface area [m^2]

b fracture aperture [m]

c compressibility [Pa^{-1}]

C dimensionless constant in expression for equilibration time (Appendix C)

$\tilde{C}$ dimensionless constant in expression for equilibration time (Appendix C)

C_n constants in solution to diffusion equation [Pa] (Appendix D)

D diffusivity [$m^2\,s^{-1}$]

D_e effective diffusivity of unsaturated rock [$m^2\,s^{-1}$]

F function of m appearing in sorptivity expression

F_n eigenfunction of Laplacian operator (Appendix D)

g gravitational acceleration [$m\,s^{-2}$]

h ponding depth [m]

k absolute permeability [m^2]

k_r relative permeability to liquid phase

k_{rl} relative permeability to liquid phase (Appendix E)

k_{rv} relative permeability to vapor phase (Appendix E)

L characteristic vertical dimension of block; fracture spacing [m]

L_s sorptive length [m] (Appendix A)

m van Genuchten parameter, $= 1 - 1/n$

n van Genuchten parameter

P pressure [Pa]

P_f pressure in fracture [Pa]

P_m mean pressure in matrix block [Pa]

q instantaneous liquid flux [$m\,s^{-1}$]

Q cumulative liquid flux [m^3]

r_{in} radius of largest sphere inscribed within matrix block [m] (Appendix D)

r_{eq} radius of sphere with same volume as matrix block [m] (Appendix D)

r_{ex} radius of smallest sphere superscribed about matrix block [m] (Appendix D)

S liquid saturation

S_i initial liquid saturation

S_l liquid saturation (Appendix E)

S_r residual liquid saturation

S_s liquid saturation at zero potential

S_v vapor/air saturation (Appendix E)

$\hat{S}$ normalized liquid saturation, $=(S-S_r)/(S_s-S_r)$

t time since start of process [s]

t_e time for matrix block to equilibrate with fractures [s]

V volume of block [m^3]

x horizontal coordinate [m]

$\mathbf{x}$ vector of generic location within matrix block [m] (Appendix D)

y horizontal coordinate along fracture [m]

z vertical coordinate [m]

Greek letters

α matrix block shape factor in fracture/matrix interflow equations [m^{-2}]

β saturation exponent in sorptivity equation

δ_m diameter (or characteristic length) of matrix block [m]

η Boltzmann similarity variable (Appendix A)

γ surface tension at the rock/water interface [$kg\,s^{-2}$]

Γ boundary of matrix block (Appendix D)

λ Brooks-Corey parameter (Appendix F)

λ eigenvalue of Laplacian operator [m^{-2}] (Appendix D)

λ_{min} smallest eigenvalue of Laplacian operator [m^{-2}] (Appendix D)

μ viscosity of pore water [Pa s]

ρ density of water [$kg\,m^{-3}$]

ϕ porosity

ϕ_f fracture porosity

ϕ_m matrix porosity

Π dimensionless pi group (Appendix C)

ψ potential [Pa]

ψ_a scaling factor in van Genuchten function [Pa]

ψ_{ae} Brooks-Corey air-entry pressure [Pa] (Appendix F)

ψ_c capillary potential, $=\psi_l - \psi_v$ [Pa] (Appendix E)

ψ_i initial potential [Pa]

ψ_l potential in liquid phase [Pa] (Appendices A,E)

ψ_m mean potential in matrix block [Pa]

ψ_s potential at surface of block [Pa]

ψ_v potential in vapor phase [Pa] (Appendices A,E)

$\hat{\psi}$ dimensionless potential, $=\psi/\psi_a$

$\hat{\psi}_1$ same as $\hat{\psi}$ (Appendix A)

$\hat{\psi}_2$ derivative of $\hat{\psi}$, $=d\psi/d\eta$ (Appendix A)

σ sorptivity, $= Q/A\sqrt{t}$ [$\mathrm{m\,s^{-1/2}}$]

σ^* dimensionless sorptivity, $= [2|\psi_a|\phi k(S_s - S_r)/\mu]^{-1/2}\sigma$ (Appendix F)

θ contact angle of water-rock interface

References

Adrian, D. D., and Franzini, J. B. (1966). Impedance to infiltration by pressure build-up ahead of the wetting front, *J. Geophys. Res.*, **71,** 5857-5862.

Barenblatt, G. I., Zheltov, Y. P., and Kochina, I. N. (1960). Basic concepts in the theory of seepage of homogeneous liquids in fissured rocks, *J. Appl. Math. Mech., Engl. Transl.*, **24,** 1286-1303.

Barker, J. A. (1985). Block-geometry functions characterizing transport in densely fissured media, *J. Hydrology,* **77,** 263-279.

Bear, J. (1988). *Dynamics of Fluids in Porous Media,* Dover Publications, New York.

Brooks, R. H., and Corey, A. T. (1966). Properties of porous media affecting fluid flow, *Proc. Amer. Soc. Civ. Eng.,* **92(IR2),** 61-88.

Bruce, R. R., and Klute, A. (1956). The measurement of soil moisture diffusivity, *Soil Sci. Soc. Amer. Proc.,* **20,** 458-462.

Brutsaert, W. (1976). The concise formulation of diffusive sorption of water in a dry soil, *Water Resour. Res.,* **12,** 1118-1124.

Carslaw, H. S., and Jaeger, J. C. (1959). *Conduction of Heat in Solids*, Clarendon Press, Oxford.

Chen, C. S., and Stone, W. D. (1993). Asymptotic calculation of Laplace inverse in analytical solutions of groundwater problems, *Water Resour. Res.,* **29,** 207-209.

Collins, R. E. (1990). *Flow of Fluids Through Porous Materials*, Research and Engineering Consultants, Englewood, Colo.

Constantz, J., Herkelrath, W. N., and Murphy, F. (1988). Air encapsulation during infiltration, *Soil Sci. Soc. Amer. J.,* **52,** 10-16.

Crank, J. (1975). *The Mathematics of Diffusion, 2nd ed.,* Oxford University Press, New York.

de Marsily, G. (1986). *Quantitative Hydrogeology,* Academic Press, San Diego.

deSwaan, A. (1990). Influence of shape and skin of matrix-rock blocks on pressure transients in fractured reservoirs, *Soc. Pet. Eng. Form. Eval.,* **5,** 344-352.

Dettman, J. W. (1962). *Mathematical Methods in Physics and Engineering,* McGraw-Hill, New York.

Douglas, J., and Arbogast, T. (1990). Dual porosity models for flow in naturally fractured reservoirs, *Dynamics of Fluids in Hierarchical Porous Media,* J. H. Cushman, ed., Academic Press, San Diego, pp. 177-221.

Duguid, J. O., and Lee, P. C. Y. (1977). Flow in fractured porous media, *Water Resour. Res.,* **13,** 558-566.

Dykhuizen, R. C. (1990). A new coupling term for dual-porosity models, *Water Resour. Res.,* **26,** 351-356.

Dykhuizen, R. C. (1991). Reply to Comment by Maloszewski and Zuber, *Water Resour. Res.,* **27,** 2153.

Edwards, A. L. (1972). TRUMP: A computer program for transient and steady state temperature distribution in multidimensional systems, *Rep. UCRL-14754, Rev. 3,* Lawrence Livermore National Laboratory, Livermore, Calif.

Elsworth, D. (1989). Thermal permeability enhancement of blocky rocks: one-dimensional flows, *Int. J. Rock Mech.,* **26,** 329-339.

Flint, A. L., and Flint, L. E. (1994). Spatial distribution of potential near-surface moisture flux at Yucca Mountain, *Proceedings of the 5th International High-Level Radioactive Waste Management Conference*, American Nuclear Society, pp. 2352-2358.

Fuentes, C., Haverkamp, R., Parlange, J.-Y., Brutsaert, W., Zayani, K., and Vachaud, G. (1991). Constraints on parameters in three soil-water capillary retention equations, *Transp. Porous Media,* **6,** 445-450.

Garabedian, P. R. (1964). *Partial Differential Equations,* John Wiley & Sons, New York.

Gardner, W. R., and Mayhugh, M. S. (1958). Solutions and tests of the diffusion equation for the movement of water in soil, *Soil Sci. Soc. Amer. Proc.,* **22,** 197-201.

Gerke, H. H., and van Genuchten, M. T. (1993). Evaluation of a first-order water transfer term for variably saturated dual-porosity flow models, *Water Resour.*

Res., **29,** 1225-1238.

Goodman, T. R. (1964). Application of integral methods to transient nonlinear heat transfer, *Adv. Heat Transf.*, **1,** 51-122.

Green, W. H., and Ampt, C. A. (1911). Studies on soil physics, 1, Flow of air and water through soils, *J. Agri. Sci.*, **4,** 1-24.

Hayot, C., and Lafolie, F. (1993). One-dimensional solute transport modelling in aggregated porous media, Part 2: Effects of aggregate size distribution, *J. Hydrol.*, **143,** 85-107.

Hestir, K. and Long, J. C. S. (1990). Analytical expressions for the permeability of random 2-dimensional Poisson fracture networks based on regular lattice percolation and equivalent media theories, *J. Geophys. Res.*, **95,** 21565-21581.

Hillel, D. (1980). *Fundamentals of Soil Physics,* Academic Press, San Diego, Calif.

Korvin, G. (1992). *Fractal Models in the Earth Sciences,* Elsevier, Amsterdam.

Kumar, S., Zimmerman, R. W., and Bodvarsson, G. S. (1991). Permeability of a fracture with cylindrical asperities, *Fluid Dyn. Res.*, **7,** 131-137.

Kutilek, M., and Valentova, J. (1986). Sorptivity approximations, *Transp. Porous Media,* **1,** 57-62.

Lai, C. H., Bodvarsson, G. S., and Pruess, K. (1985). On the accuracy of the MINC approximation, *Report LBL-21025,* Lawrence Berkeley Laboratory, Berkeley, Calif.

Latta, G. E., (1974). Transform methods, in *Handbook of Applied Mathematics,* C. E. Pearson, ed., Van Nostrand Reinhold, New York, pp. 585-644.

Lockington, D. (1993). Estimating the sorptivity for a wide range of diffusivity dependence on water content, *Transp. Porous Media,* **10,** 95-101.

Long, J. C. S., and Witherspoon, P. A. (1985). The relationship of the degree of interconnection to permeability in fracture networks,

Matthews, C. S., and Russell, D. G. (1967). *Pressure Buildup and Flow Tests in Wells,* Society of Petroleum Engineers, Dallas.

Macey, R. I. (1959). A quasi-steady-state approximation method for diffusion problems, 1, Concentration dependent diffusion coefficients, *Bull. Math. Biophys.*, **21,**

19-32.

Martinez, M. J. (1987). Capillary-driven flow in a fracture located in a porous medium, *Rep. SAND84-1697,* Sandia National Laboratory, Albuquerque, N.M.

McWhorter, D. B. (1971). Infiltration affected by flow of air, *Hydrology Paper 49,* Colorado State University, Fort Collins, Colo.

Moench, A. F. (1984). Double-porosity models for a fissured groundwater reservoir with fracture skin, *Water Resour. Res.,* **20,** 831-846.

Moridis, G. J., and Pruess, K. (1992). TOUGH simulations of Updegraff's set of fluid and heat flow problems, *Report LBL-32611,* Lawrence Berkeley Laboratory, Berkeley, Calif.

Moridis, G. J., Pruess, K., and Antunuez, E. (1994). T2CGI: A package of preconditioned conjugate gradient solvers for TOUGH2, *Report LBL-35518,* Lawrence Berkeley Laboratory, Berkeley, Calif.

Mualem, Y. (1976). A new model for predicting the hydraulic conductivity of unsaturated porous media, *Water Resour. Res.,* **12,** 513-522.

Najurieta, H. L. (1980). Theory for pressure transient analysis of naturally fractured reservoirs, *J. Pet. Tech.,* **32,** 1241-1250.

Narasimhan, T. N., and Witherspoon, P. A. (1976). An integrated finite-difference method for analyzing fluid flow in porous media, *Water Resour. Res.,* **12,** 57-64.

Niemi, A., and Bodvarsson, G. S. (1988). Preliminary capillary hysteresis simulations in fractured rocks, Yucca Mountain, Nevada, *J. Contam. Hydrol.,* **3,** 277-291.

Nitao, J. J., and Buscheck, T. A. (1989). Movement of a liquid front in an unsaturated, fractured porous medium, 1, Physical theory, *Report UCRL-101005,* Lawrence Livermore National Laboratory, Livermore, Calif.

Nitao, J. J., and Buscheck, T. A. (1991). Infiltration of a liquid front in an unsaturated, fractured porous medium, *Water Resour. Res.,* **27,** 2099-2112.

Odling, N. E., and Webman, I. (1991). A "conductance" mesh approach to the permeability of natural and simulated fracture patterns, *Water Resour. Res.,* **27,** 2633-2643.

Parlange, J.-Y., Godaliyadda, G., Fuentes, C., and Haverkamp, R. (1991). Comment on "An approximate solution for one-dimensional absorption in unsaturated porous media" by R. W. Zimmerman and G. S. Bodvarsson, *Water Resour. Res.,* **27,** 2159-2150.

Parlange, J.-Y., Barry, D. A., and Haverkamp, R. (1992). A simple approximate solution for horizontal infiltration in a Brooks-Corey medium - Comment, *Transp. Porous Media,* **9,** 297-301.

Persoff, P., and Pruess, K. (1993). Flow visualization and relative permeability measurements in rough-walled fractures, *Proceedings of the 4th International High-Level Radioactive Waste Management Conference*, American Nuclear Society, pp. 2033-2041.

Peters, R. R., and Klavetter, E. A. (1988). A continuum model for water movement in an unsaturated fractured rock mass, *Water Resour. Res.,* **24,** 416-430.

Philip, J. R. (1955). Numerical solution of equations of the diffusion type with diffusivity concentration-dependent, *Trans. Faraday Soc.,* **51,** 885-892.

Philip, J. R. (1987). The quasilinear analysis, the scattering analog, and other aspects of infiltration and seepage, in *Proceedings, International Conference on Infiltration Development and Application,* University of Hawaii at Manoa, pp. 1-27.

Phuc, L. V., and Morel-Seytoux, H. J. (1972). Effect of soil air movement and compressibility on infiltration rates, *Soil Sci. Soc. Amer. J.,* **36,** 237-241.

Press, W. H., Flannery, B. P., Teukolsky, S. A., and Vetterling, W. T. (1992). *Numerical Recipes in FORTRAN, 2nd ed.,* Cambridge University Press, New York.

Pruess, K. (1987). TOUGH user's guide, *Report LBL-20700,* Lawrence Berkeley Laboratory, Berkeley, Calif.

Pruess, K., and Narasimhan, T. N. (1985). A practical method for modeling fluid and heat flow in fractured porous media, *Soc. Petrol. Eng. J.,* **25,** 14-26.

Pruess, K., and Wu, Y. S. (1993). A new semianalytical method for numerical simulation of fluid and heat flow in fractured reservoirs, *SPE Adv. Tech. Ser.,* **1,** 63-72.

Pruess, K., Wang, J. S. Y., and Tsang, Y. W. (1988). Effective continuum approximation for modeling fluid and heat flow in fractured porous tuff, *Report LBL-20778,* Lawrence Berkeley Laboratory, Berkeley, Calif.

Reitsma, S., and Kueper, B. H. (1994). Laboratory measurement of capillary pressure-saturation relationships in a rock fracture, *Water Resour. Res.,* **30,** 865-878.

Richards, L. A. (1931). Capillary conduction of liquids through porous mediums, *Physics,* **1,** 318-333.

Richtmyer, R. D., and Morton, K. W. (1967). *Difference Methods for Initial-Value Problems*, Interscience, New York.

Rossen, R. H. (1977). Simulation of naturally fractured reservoirs with semi-implicit source terms, *Soc. Pet. Eng. J.,* **17,** 201-210.

Rulon, J., Bodvarsson, G. S., and Montazer, P. (1986). Preliminary numerical simulations of groundwater flow in the unsaturated zone, Yucca Mountain, Nevada, *Report LBL-20553,* Lawrence Berkeley Laboratory, Berkeley, Calif.

Selker, J., Parlange, J.-Y., and Steenhuis, T. (1992). Fingering flow in two-dimensions, 2: Predicting finger moisture profile. *Water Resour. Res.,* **28,** 2523-2528.

Snow, D. T. (1965). Anisotropic permeability of fractured media, *Water Resour. Res.,* **5,** 1273-1289.

Streltsova, T. D. (1983). Well pressure behavior of a naturally fractured reservoir, *Soc. Pet. Eng. J.,* **23,** 769-780.

Touma, J. and Vauclin, M. (1986). Experimental and numerical analysis of two-phase infiltration in a partially saturated soil, *Trans. Porous Media,* **1,** 27-55.

Travis, B. J., Hodson, S. W., Nuttall, H. E., Cook, T. L., and Rundberg, R. S. (1984). Preliminary estimates of water flow and radionuclide transport in Yucca Mountain, *Report LA-UR-84-40,* Los Alamos National Laboratory, Albuquerque, N.M.

Updegraff, C. D., Lee, C. E., and Gallegos, D. P. (1991). DCM3D, a dual-continuum, three-dimensional, ground-water flow code for unsaturated, fractured, porous media, *Report SAND90-7015,* Sandia National Laboratories, Albuquerque, N.M.

U.S. Department of Energy (1986). Final environmental assessment - Yucca Mountain site, Nevada Research and Development Area, Nevada, *Rep. DOE/RW-0012,* Office of Civilian Radioactive Waste Management, Washington, D.C.

van Genuchten, M. Th. (1980). A closed-form equation for predicting the hydraulic conductivity of unsaturated soils, *Soil Sci. Soc. Amer. J.,* **44,** 892-898.

van Genuchten, M. Th., and Dalton, F. N. (1986). Models for simulating salt movement in aggregated field soils, *Geoderma,* **38,** 165-183.

Vermeulen, T. (1953). Theory of irreversible and constant-pattern solid diffusion, *Ind. Eng. Chem.,* **45,** 1664-1670.

Wang, J. S. Y. (1992). Variations of hydrological parameters of tuff and soil, in *Proceedings of the 3rd International High-Level Radioactive Waste Management Conference*, American Nuclear Society, pp. 727-731.

Wang, J. S. Y., and Narasimhan, T. N. (1985). Hydrologic mechanisms governing fluid flow in a partially saturated, fractured, porous medium, *Water Resour. Res.,* **21,** 1861-1874.

Warren, J. E., and Root, P. J. (1963). The behavior of naturally fractured reservoirs, *Soc. Petrol. Eng. J.,* **3,** 245-255.

Wilson, L. G., and Luthin, J. N. (1963). Effect of air flow ahead of the wetting front on infiltration, *Soil Sci.,* **96,** 136-143.

Wittwer, C. S., Bodvarsson, G. S., Chornack, M. P., Flint, A. L., Flint, L. E., Lewis, B. D., Spengler, R. W., and Rautman, C. A. (1992). Design of a three-dimensional site-scale model for the unsaturated zone at Yucca Mountain, Nevada, *Proceedings of the 3th International High-Level Radioactive Waste Management Conference*, American Nuclear Society, pp. 263-271.

Youngs, E. G., and Peck, A. J. (1964). Moisture profile development and air compression during water uptake by bounded porous bodies, *Soil Sci.,* **98,** 290-294.

Zimmerman, R. W., and Bodvarsson, G. S. (1989a). An approximate solution for one-dimensional absorption in unsaturated porous media, *Water Resour. Res.,* **25,** 1422-1428.

Zimmerman, R. W., and Bodvarsson, G. S. (1991a). A simple approximate solution for horizontal infiltration in a Brooks-Corey medium, *Transp. Porous Media,* **6,** 195-205.

Zimmerman, R. W., and Bodvarsson, G. S. (1991b). Reply to ''Comment on "An approximate solution for one-dimensional absorption in unsaturated porous media" by R. W. Zimmerman and G. S. Bodvarsson'' by Parlange et al., *Water Resour. Res.*, **27,** 2161-2162.

Zimmerman, R. W., Bodvarsson, G. S., and Kwicklis, E. M. (1990). Absorption of water into porous blocks of various shapes and sizes, *Water Resour. Res.*, **26,** 2797-2806.

Zimmerman, R. W., Chen, D. W., and Cook, N. G. W. (1992). The effect of contact area on the permeability of fractures, *J. Hydrol.*, **139,** 79-96.

Zimmerman, R. W., Chen, G., Hadgu, T., and Bodvarsson, G. S. (1993). A numerical dual-porosity model with semi-analytical treatment of fracture/matrix flow, *Water Resour. Res.*, **29,** 2127-2137.

Zimmerman, R. W., Kumar, S., and Bodvarsson, G. S. (1991c). Lubrication theory analysis of the permeability of rough-walled fractures, *Int. J. Rock Mech.*, **28,** 325-331.